

TECHNISCHE UNIVERSITÄT MÜNCHEN

Department Chemie

The effect of posttranslational modifications on biochemical and structural characteristics of Prion Protein variants and the SMN Tudor domain

Nam Ky Chu

Vollständiger Abdruck der von der Fakultät für Chemie der Technischen Universität München zur Erlangung des akademischen Grades eines Doktors der Naturwissenschaften genehmigten Dissertation.

Vorsitzende: Univ.-Prof. Dr. Sevil Weinkauf
Prüfer der Dissertation: 1. Univ.- Prof. Dr. Christian F.W. Becker
2. Univ.- Prof. Dr. Michael Sattler

Die Dissertation wurde am 10.05.2013 bei der Technischen Universität München eingereicht und durch die Fakultät für Chemie am 15.07.2013 angenommen.

For my family

1. Index

1. Index	- 0 -
2. Summary.....	- 5 -
3. Zusammenfassung.....	- 7 -
4. Introduction	- 9 -
4.1 Prion diseases.....	- 9 -
4.2 The cellular prion protein, PrP ^C	- 10 -
4.2.1 The prion protein gene, <i>Prnp</i>	- 10 -
4.2.2 Biosynthesis of PrP ^C	- 10 -
4.2.3 Structure of PrP ^C	- 11 -
4.2.4 PrP ^C trafficking to the cell surface	- 13 -
4.2.5 Endocytosis of PrP ^C and its implication in the conversion of PrP ^C to PrP ^{Sc} ..	- 14 -
4.2.6 Possible physiological roles of PrP ^C	- 16 -
4.3 Conversion of PrP ^C to PrP ^{Sc}	- 17 -
4.3.1 Comparison PrP ^C and PrP ^{Sc}	- 17 -
4.3.2 <i>In vitro</i> conversion analysis	- 18 -
4.3.3 Role of ordered lipid domains (rafts) in PrP ^{Sc} formation.....	- 21 -
4.3.4 GPI anchor in the PrP ^{Sc} formation	- 22 -
4.4 Semisynthesis of membrane-associated prion protein variants	- 23 -
4.4.1 Native chemical ligation	- 23 -
4.4.2 Expressed protein ligation.....	- 23 -
4.4.2 Semisynthesis of membrane-anchored prion proteins.....	- 29 -
5. Objectives	- 32 -
6. Materials and methods	- 34 -
6.1. Materials.....	- 34 -
6.1.1 Chemicals.....	- 34 -
6.1.2 Molecular biology materials.....	- 34 -
6.2 General methods	- 34 -
6.2.1 SDS-polyacrylamide gel electrophoresis (SDS-PAGE) and Western blot ...	- 34 -

6.2.2 CD spectroscopy	- 36 -
6.3. Semisynthesis of lipidated PrP constructs and biochemical assays of PrP-lipid interactions	- 36 -
6.3.1. Cloning work.....	- 37 -
6.3.2 Expression and purification of recombinant PrP containing a C-terminal thioester	- 38 -
6.3.3 Peptide synthesis	- 40 -
6.3.4 Expressed protein ligation (EPL) reactions	- 41 -
6.3.5 Screening folding condition of PrP.....	- 41 -
6.3.6 Folding of lipidated rPrP proteins.....	- 42 -
6.3.7 Preparation of phospholipid small unilamellar vesicles (SUVs).....	- 42 -
6.3.8 Incubation of PrP with phospholipid vesicles	- 44 -
6.3.9 Flootation assay	- 44 -
6.3.10 Proteinase K (PK) digestion.....	- 45 -
6.3.11 Preparation of calcein-containing vesicles (Cal-SUVs).....	- 45 -
6.3.12 Calcein release.....	- 46 -
6.3.13 NBD fluorescence quenching	- 46 -
6.3.14 Tryptophan fluorescence.....	- 47 -
6.3.15 Tryptophan fluorescence quenching.....	- 47 -
6.4 Construction of plasmids for soluble expression of PrP-Mxe intein in <i>E. coli</i>	- 48 -
6.4.1 Plasmid construction	- 48 -
6.4.2 Protein expression and purification.....	- 49 -
6.4.3 Protease cleavage reactions.....	- 50 -
6.4.4 Preparation of ASP fusion protein containing a C-terminal α -thioester.....	- 50 -
6.4.5 Synthesis of NBD-labeled peptide	- 50 -
6.4.6 Expressed protein ligation.....	- 51 -
6.4.7 Aggregation assays.....	- 51 -
6.5 Semisynthesis of SMN-sDMA proteins	- 51 -
6.5.1 Plasmid construction	- 51 -

6.5.2 Expression and purification of ^{15}N - ^{13}C labeled SMN Tudor-Mxe intein fusion protein	52 -
6.5.3 Synthesis of sDMA peptides	52 -
6.5.4 Expressed protein ligation and purification of SMN-SDMA proteins	53 -
6.5.5 NMR spectroscopy	53 -
7. Results and discussions	54 -
7.1. Semisynthesis of C-terminally lipidated prion protein variants (PrPs) and the effect of a C-terminal membrane anchor on the interactions of PrP with membranes	54 -
7.1.1 PrP constructs	54 -
7.1.2 Preparation of PrP- α thioesters	55 -
7.1.3 Synthesis and purification of membrane anchor peptide	57 -
7.1.4 Expressed protein ligation (EPL) and HPLC purification of lipidated PrP proteins	59 -
7.1.5 Folding of PrP variants	62 -
7.1.6 Flootation assays	64 -
7.1.7 Proteinase K resistance	68 -
7.1.8 Fluorescence-based analysis of PrP interactions with vesicles.....	70 -
7.1.9 Cryo electron microscopy (EM).....	80 -
7.1.10 PrP conformation and membrane interaction.....	81 -
7.1.11 Characterizing the interactions of PrP variants with membranes via tryptophan fluorescence	84 -
7.1.12 Discussion	90 -
7.1.13 Future works	95 -
7.2 Recombinant expression of soluble prion protein for C-terminal modification....	95 -
7.2.1 Introduction.....	95 -
7.2.2 Construction, expression, and purification of DnaK-PrP fusion protein.....	97 -
7.2.3 Cleavage of DnaK from DnaK-PrP	97 -
7.2.4 Removal of SBD from DnaK-PrP.....	98 -
7.2.5 High yield production of soluble PrP(90-231) from ASP construct.....	100 -
7.2.6 Synthesis of NBD-labeled peptide	101 -

7.2.7 Preparation of soluble PrP containing a C-terminal α -thioester.....	102 -
7.2.8 Conclusion	105 -
7.3 Covalently linking the Tudor domain of SMN protein and its low affinity ligand sDMA for structural studies.....	106 -
7.3.1 Introduction	106 -
7.3.2 Expression and purification of SMN Tudor- <i>Mxe</i> intein-6xHis.....	108 -
7.3.3 Synthesis of sDMA peptides	109 -
7.3.4 Expressed protein ligation of SMN Tudor and sDMA peptides.....	111 -
7.3.5 Comparative NMR analysis of SMN Tudor-sDMA proteins and SMN Tudor that was fully saturated with high excess of free sDMA	115 -
7.3.6 Conclusion	119 -
8. Abbreviations	120 -
9. References	123 -
Declaration.....	141 -
Publications.....	142 -
Curriculum vitae.....	143 -
Acknowledgements	144 -

2. Summary

Membrane attachment via a C-terminal GPI anchor is a prerequisite for conversion of PrP^C into PrP^{Sc}, therefore its effect(s) on PrP structure and function needs to be deciphered. To this end, PrP variants (PrPs) including full length PrP (residues 23-231, FL_PrP), N-terminally truncated PrP (residues 90-231, T_PrP) and PrP missing its central hydrophobic region (Δ 105-125, Δ CR_PrP) were equipped with a C-terminal membrane anchor via a semisynthesis strategy. This strategy has so far suffered from insoluble expression of PrP-intein fusion constructs in *E. coli* and low folding efficiencies. Here, the solubility of PrP-intein fusion protein was improved by fusing the ATPase domain of the *E. coli* DnaK chaperone to its N-terminus. This fusion construct provides a straightforward and efficient way to generate soluble PrP variants containing C-terminal modifications with overall yields 5 times higher than in previous studies using PrP folded from inclusion bodies.

Interactions of the lipidated PrP variants with lipid bilayers were analyzed. Flootation assays indicated binding of lipidated PrPs to two different kinds of phospholipid vesicles conferred by their C-terminal lipid anchor. In conformational analysis of PrPs in the presence of anionic POPG vesicles, CD measurements revealed that non-lipidated PrPs changed their conformations into β -sheet-enriched structures while lipidated PrPs still remained predominantly α -helical or converted into random coils. Additionally, in the presence of POPG vesicles non-lipidated FL_PrP became resistant to proteinase K (PK) digestion, whereas lipidated FL_PrP remained PK sensitive. In contrast to non-lipidated FL_PrP, no PK resistance of T_PrP and Δ CR_PrP constructs was observed. Thus, electrostatic (weak in T_PrP) and hydrophobic (lacking in Δ CR_PrP) interactions seem to be involved in binding of PrP to POPG vesicles. Tryptophan fluorescence of PrP variants was measured to analyze the interaction of PrP N-termini with lipid membranes. No difference between lipidated and non-lipidated PrPs was observed. Nevertheless, comparative tryptophan fluorescence quenching experiments proved that the lipid anchor changes binding of this region to the membrane. These results demonstrated that the C-terminal membrane attachment leads to interaction of PrP with membrane that is distinct from non-lipidated PrPs and influences the biochemical and conformational characteristics of PrPs. On the other hand, several fluorescence-based techniques were employed to further analyze the interaction of PrPs with lipid vesicles such as calcein release and NBD fluorescence quenching. These analyses revealed a potential pore formation of lipidated Δ CR_PrP,

which is known to be a highly neurotoxic PrP in transgenic mice and to induce spontaneous ionic currents in cell-based studies.

SMN protein is involved in the assembly of snRNPs with a relatively weak interaction of its Tudor domain and symmetrically dimethylated arginine (sDMA) residues in the C-terminal tails of Sm proteins. In order to stabilize such weak interaction for structural studies, the second semisynthesis strategy was aimed at producing SMN Tudor with a C-terminal attachment of sDMA. This study is collaboration with the group of Prof. Dr. Michael Sattler (TU München). Here, the sDMA residue was incorporated in peptides with glycine linkers of different length and an N-terminal cysteine for the ligation with SMN Tudor carrying a C-terminal α -thioester. Initially, all efforts to generate SMN α -thioester for subsequent ligation reactions were unsuccessful because of formation of a highly stable thiolactone that prevented any ligation with sDMA peptides. To overcome this challenge, a one-pot ligation procedure was developed, in which preincubation of the SMN-intein fusion protein with the sDMA-containing peptide was followed by the addition of ethanethiol to induce intein cleavage and ligation reaction. Successful one-pot ligation of the sDMA peptide to the C-terminus of SMN Tudor can be explained by initial binding of the sDMA ligand to the binding pocket of SMN, thereby facilitating a fast ligation reaction and preventing thiolactone formation. Interestingly, this procedure also allowed us to rapidly identify the ideal glycine linker length via quantification of ligation yields by HPLC and ESI-MS measurements. These analyses revealed that linkers with four or more glycine residues were required for the efficient ligation of SMN Tudor and sDMA peptide. To support this idea, comparative NMR analyses of SMN-sDMA proteins with different linkers and SMN Tudor saturated with a large excess of free sDMA were carried out. A short linker consisting of only one glycine residue showed the highest chemical shift perturbation while an eight-glycine linker caused no chemical shift perturbation. The results suggested that this strategy is a useful tool to stabilize weak interactions (millimolar K_D) via covalent bonds at a 1:1 stoichiometry, such as SMN Tudor and sDMA residue for structural studies.

3. Zusammenfassung

Eine Voraussetzung für die Umwandlung von PrP^C in seine pathogene PrP^{Sc}-Form ist die Membranverankerung mittels eines GPI-Ankers, deren Einfluss auf Proteinstruktur und -funktion es zu entschlüsseln gilt. Im Rahmen dieser Arbeit wurden verschiedene PrP-Varianten (PrPs) mit C-terminalem Membrananker semisynthetisch hergestellt, darunter Vollängen- (AS 23-321, „FL_PrP“) und N-terminal verkürztes PrP (AS 90-231, „T_PrP“) sowie PrP ohne seine zentrale hydrophobe Region (Δ 105-125, „ Δ CR_PrP“). Nachteil dieser Strategie war bislang die unlösliche Expression der PrP-Intein-Fusionskonstrukte in *E. coli* und die niedrige Rückfaltungseffizienz. Eine Verbesserung wurde hier erreicht, indem die PrP-Expressionskonstrukte N-terminal um die ATPase-Domäne des *E. coli* DnaK-Chaperons erweitert wurden. Dies erlaubt eine einfache und effiziente Generierung löslicher PrP-Varianten mit C-terminalen Modifikationen, bei fünffach höherer Ausbeute gegenüber den vorangegangenen Arbeiten.

Die Interaktion lipidierter PrP-Varianten mit Lipiddoppelschichten wurde analysiert. Flotationsexperimente zeigten die Bindung von PrP an zwei Arten von Phospholipidvesikel mit jeweils unterschiedlicher Lipidkomposition, vermittelt durch den C-terminalen Lipidanker. Konformationsanalysen via CD-Spektroskopie demonstrierten, dass nicht-lipidiertes PrP in Gegenwart anionischer POPG-Vesikel seine Struktur zugunsten eines höheren β -Faltblatt-Anteils verändert, lipidiertere Varianten hingegen überwiegend α -helikale Strukturelemente beibehalten oder zum Zufallsknäuel („random coil“) falten. Darüber hinaus wies nicht-lipidiertes FL_PrP eine hohe Resistenz gegenüber Proteinase K (PK) auf, während das lipidiertere Äquivalent weiterhin PK-sensitiv war. Für lipidiertere T_PrP und Δ CR_PrP wurde jedoch ebenfalls PK-Sensitivität festgestellt. Daraus kann abgeleitet werden, dass elektrostatische (geringfügig bei T_PrP) und hydrophobe (nicht bei Δ CR_PrP) Interaktionen bei der Bindung von PrP an POPG-Vesikel eine wichtige Rolle spielen. Messungen der intrinsischen Tryptophanfluoreszenz der PrP-Varianten wurden vorgenommen, um die Interaktion der N-terminalen Proteinregion mit Lipidmembranen zu untersuchen. Zwischen lipidierterem und nicht-lipidiertem PrP wurden keine Unterschiede festgestellt. Fluoreszenzquenching-Experimente hingegen wiesen darauf hin, dass der Lipidanker die Interaktion der N-terminalen Region mit der Membran sehr wohl verändert. Der C-terminale PrP-Lipidanker führte zu einer anderen Membraninteraktion als sie nicht-lipidierte Varianten

zeigten, ferner war die biochemische sowie konformationelle Charakteristik unterschiedlich. Fluoreszenz-basierte Techniken wie Calcein-Freisetzung und NBD-Emission wurden angewandt, um die PrP-Lipidvesikel-Interaktion weitergehend zu analysieren. Es zeigten sich deutliche Hinweise auf eine Porenbildung im Fall des lipidierten Δ CR_PrPs, welche aus Studien mit transgenen Mäusen als hochgradig neurotoxischer Vorgang bekannt ist und in zellbasierten Untersuchungen spontane Ionenströme induzieren konnte.

Das SMN-Protein spielt eine Rolle beim Aufbau von snRNPs, wobei seine Tudor-Domäne unter anderem Wechselwirkungen mit Sm-Proteinen eingeht, die C-terminal symmetrisch dimethyliertes Arginin (sDMA) enthalten. Um solch typischerweise schwache Interaktionen für strukturelle Studien zu stabilisieren, wurde eine semisynthetische Strategie verfolgt, im Zuge welcher die SMN-Tudor-Domäne C-terminal mit sDMA verknüpft werden sollte. Diese Untersuchungen wurde in Kooperation mit der Arbeitsgruppe von Prof. Dr. Michael Sattler (TU München) durchgeführt. sDMAs wurden in Glycin-Peptide unterschiedlicher Länge eingebaut. Über ein N-terminales Cystein wurde die Ligation mit SMN-Tudor ermöglicht, welches wiederum mit einem C-terminalen α -Thioester ausgestattet war. Die Thioester-Generierung gestaltete sich schwierig aufgrund der Bildung eines hochstabilen Thiolactons, welches eine nachfolgende Ligation mit sDMA-Peptiden verhinderte. Um dies zu umgehen, wurde eine *in situ* Ligationsstrategie entwickelt, bei welcher SMN-Intein-Fusionsprotein mit sDMA-Peptiden vorinkubiert und durch anschließende Zugabe von Ethanthiol Inteinabspaltung sowie Ligation erreicht wurde. Der Erfolg dieser Strategie kann dadurch erklärt werden, dass der sDMA-Ligand zunächst mit der Bindetasche des SMN koordiniert, folglich eine schnelle Ligation begünstigt und gleichzeitig die Thiolacton-Bildung verhindert. Überdies erlaubte die Prozedur die Identifikation der optimalen Glycin-Kettenlänge via HPLC und ESI-MS: Mindestens vier Glycine sind demzufolge für eine effiziente Ligation von SMN-Tudor und sDMA-Peptid notwendig. Um diese Feststellung zu untermauern, wurden vergleichende NMR-Analysen von SMN-sDMA mit verschiedener Glycin-Kettenlänge sowie sDMA-gesättigtem SMN-Tudor vorgenommen. Monoglycin bewirkte eine deutliche chemische Verschiebung, während ein Linker aus acht Glycinen keine Verschiebung verursachte. Die entwickelte Ligationsstrategie kann ein hilfreiches Instrument sein, schwache Interaktionen (millimolare K_D) via kovalenter 1:1-stöchiometrischer Verknüpfung für Strukturstudien zu stabilisieren.

4. Introduction

4.1 Prion diseases

Prion diseases are transmissible spongiform encephalopathies (TSEs) of an infectious, genetic or sporadic nature characterized by neurodegenerative symptoms and protein aggregation. The pathogenesis of prion diseases is mainly attributed to conformational changes of the cellular prion protein (PrP^C) (Aguzzi & Heppner, 2000; Prusiner, 1998; Weissmann, 1994). These diseases include Kuru, Creutzfeldt-Jakob disease (CJD), Gerstmann-Sträussler-Sheinker disease (GSS), and Fatal Familial Insomnia (FFI) in humans, Scrapie in sheep, Bovine Spongiform Encephalopathy (BSE) in cattle and Chronic Wasting Disease (CWD) in deer and elk.

These TSEs are always fatal and their clinical symptoms are disturbance in behavior and movement, dementia, astrogliosis, degeneration (sponge formation) in tissues of the central nervous system and absence of immunological responses. They often have an extremely long incubation time followed by a rapid progression of the diseases. Anatomical evidence is the deposition of an abnormal isoform of PrP^C, termed PrP-scrapie (PrP^{Sc}), in the central nervous system and lymphoid tissues (Kovacs *et al.*, 2002). However, not all of the mentioned clinical symptoms are observed in each TSE to the same extent.

The infectious agent and 'protein-only' hypothesis

In 1950s, studies of a disease named Kuru found among the Fore people of Papua New Guinea indicated that this spongiform encephalopathy was transmitted through cannibalism. Indeed, successful transmission of Kuru from deceased patients' brain tissue into primates induced a similar disease. The disease rapidly declined following the end of cannibalism among the Fore people. Scientists quickly linked the similarities among Kuru, CJD in humans as well as scrapie in sheep. However, the infectious agent from these diseases was found to resist UV and ionizing radiation treatments at doses that easily inactivated any nucleic acid-based pathogens (Alper *et al.*, 1967; Alper *et al.*, 1966). Based on the findings of Alper, in 1967 Griffith proposed the "protein-only" hypothesis (Griffith, 1967), which was later demonstrated and developed into the concept of 'Prion', derived from proteinaceous

and infectious, by Stanley Prusiner when he focused on purifying the scrapie infectivity by centrifugation (Prusiner *et al.*, 1977). Prusiner and colleagues identified partially proteinase K (PK)-resistant protein fragments of 27-30 kDa, termed PrP²⁷⁻³⁰, which were only present in the infected brain tissues but not in healthy tissue. Further analysis of this protein fragment by Edman sequencing (Prusiner *et al.*, 1984) proved that PrP²⁷⁻³⁰ originated from host animals (Oesch *et al.*, 1985). In addition, the mRNA level of PrP from scrapie infected animals was found to be similar to those of healthy animals (Chesebro *et al.*, 1985). Notably, PrP^C was proven to be completely sensitive to PK and soluble under physiological buffer condition, while PrP²⁷⁻³⁰ is insoluble under non-denaturing conditions and partially PK-resistant (Locht *et al.*, 1986; Meyer *et al.*, 1986; Oesch *et al.*, 1985)

4.2 The cellular prion protein, PrP^C

4.2.1 The prion protein gene, *Prnp*

The above mentioned sequencing work that was conducted by Prusiner and his colleagues led to identify the gene encoding PrP^C, termed *Prnp*. In humans, the *Prnp* gene is located on chromosome 21. It consists of three exons but the entire protein-encoding sequence is present in the second exon only (Puckett *et al.*, 1991). Today, it is known that the *Prnp* gene is highly conserved in a broad range of animals with more than 90% sequence identity (Wopfner *et al.*, 1999). The *Prnp* gene is supposed to be a housekeeping gene from a finding that it is not linked to a TATA box promoter and that it contains CpG islands (Baybutt & Manson, 1997; Prusiner, 1998; Puckett *et al.*, 1991; Saeki *et al.*, 1996).

4.2.2 Biosynthesis of PrP^C

The prion protein is highly and constitutively expressed in neurons and in the central nervous system (Kretzschmar *et al.*, 1986); and to a lesser extent in most other organs such as liver, heart, immune system, blood, bone marrow etc. ... (Linden *et al.*, 2008). Primarily translated murine PrP is composed of 254 amino acids and contains an N-terminal signal sequence (residues 1-22) for the secretory pathway, the mature protein sequence (residues 23-231) and a C-terminal signal peptide (residues 232-254) for glycosylphosphatidylinositol (GPI) attachment. The N-terminal signal sequence directs PrP to the endoplasmic reticulum (ER) where this signal sequence is cleaved off. In the

ER, PrP can be glycosylated at Asn181 and Asn197 and a disulfide bond is formed between Cys179 and Cys214. Before leaving the ER, cleavage of the C-terminal signal peptide leads the attachment of a GPI anchor at Ser231 by a still poorly understood mechanism. Mature PrP containing the posttranslational modifications (PTMs) (Figure 4.1 A) will be recruited in the membrane trafficking pathway and delivered to the cell surface (Harris *et al.*, 1993).

4.2.3 Structure of PrP^C

Most structural studies of PrP have been performed using bacterially expressed PrP. Purified recombinant PrP exists as a monomer that contains a disulfide bond and shows a CD spectrum of predominantly α -helical conformation, which is highly identical to that of PrP^C from brain tissue (Pan *et al.*, 1993). Further analyzed spectroscopic properties of recombinant PrP in far-UV and near-UV CD spectroscopies, tryptophan fluorescence and NMR measurements also resemble those of PrP^C (Hornemann & Glockshuber, 1996; Hornemann *et al.*, 1997) indicating that recombinant PrP constructs can be used as perfect substitutes of PrP^C, which needs to be purified via a time-consuming and expensive protocol, in structural studies of PrP.

To date, the solved NMR and crystal structures of murine, hamster, human, bovine, chicken, elk, turtle, cat, dog, pig, sheep, horse etc. ... recombinant prion proteins have been published (Calzolari *et al.*, 2005; Donne *et al.*, 1997; James *et al.*, 1997; Liu *et al.*, 1999; Lopez Garcia *et al.*, 2000; Lysek *et al.*, 2005; Perez *et al.*, 2010; Riek *et al.*, 1996; Riek *et al.*, 1997; Riek *et al.*, 1998; Zahn *et al.*, 2000). In agreement with the high identity in DNA sequences of about 90% of all mammalian PrP (Schatzl *et al.*, 1995), all available structures of mammalian PrP constructs are very similar. The three-dimensional structure of PrP composes an unstructured N-terminal domain (residues 23-124, numbering for mouse PrP) and a C-terminal globular segment (residues 125-228) composed three α -helices and two short, antiparallel β -strands (Figure 4.1B) (Riek *et al.*, 1997). The first half of the N-terminal domain contains a polybasic region (residues 23-27) and a series of five histidine-containing octapeptide repeats (residues 51-90), which can bind copper and other cations, as shown in various studies (Stockel *et al.*, 1998; Viles *et al.*, 1999). The central region includes a charged area (residues 105-111) followed by a highly

conserved hydrophobic fragment (HD, residues 112-130), which behaves as a membrane anchor under some circumstances (Hegde *et al.*, 1998). The two C-terminal helices 2 and 3 are linked by a disulfide bond and two sites for N-glycosylation are depicted here (section 4.2.2) (Figure 4.1).

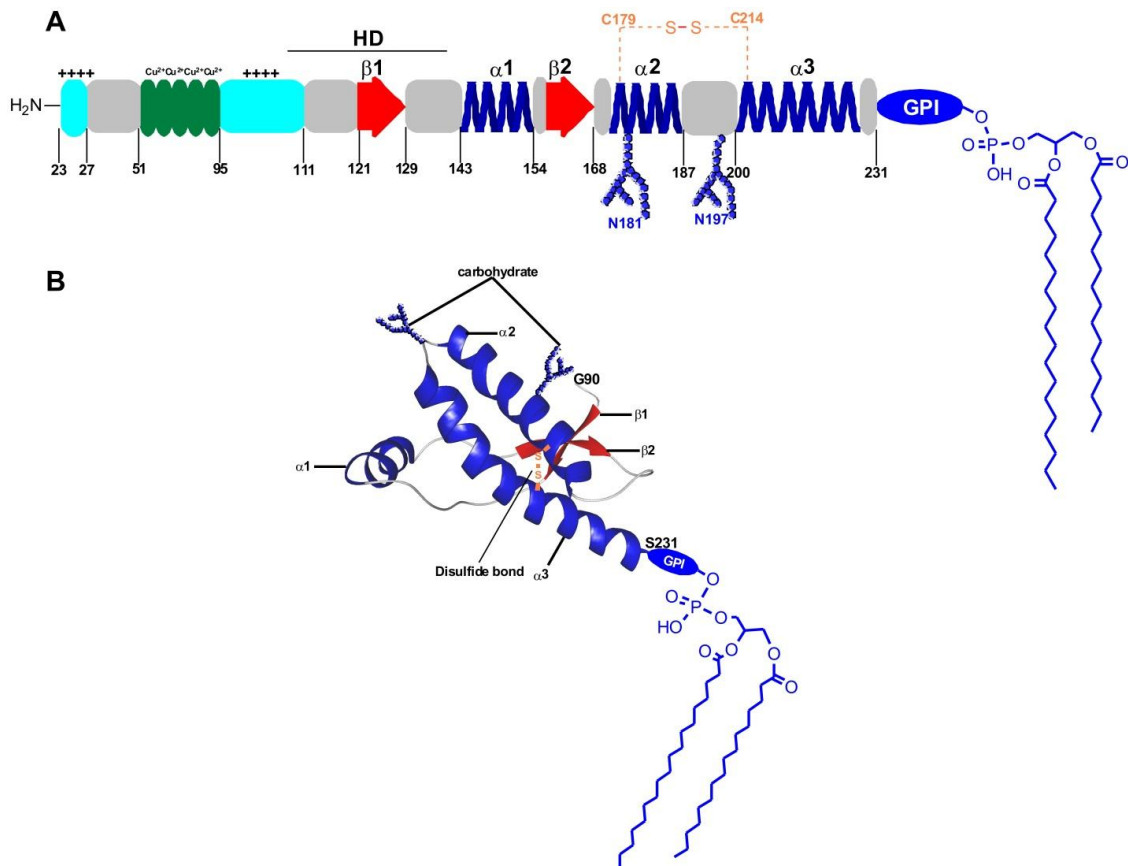


Figure 4.1 Structure of PrP^C. (A) Schematic representation of PrP^C. Residue numbers correspond to murine PrP^C. (B) Three-dimensional structure of PrP^C. The NMR structure of recombinant syrian hamster prion protein fragment (90-231), which is highly homology in amino acid sequence with murine PrP (92%) (Locht *et al.*, 1986), was taken from PDB 1B10 (James *et al.*, 1997) and modified by using the following purchased softwares: MarvinSpace 5.3.0.2 and ChemBioDraw Ultra 12.0.

The mutations of PrP^C characterized in familial prion diseases were suggested to destabilize the native structure of PrP^C, facilitate the conversion into PrP^{Sc} as well as to increase the stability of PrP^{Sc} (Cohen, 1999; Cohen *et al.*, 1994; Huang *et al.*, 1995). However, thermodynamic measurements of PrP carrying such mutations showed destabilizing effects only for a few, but not for all of these mutations (Liemann & Glockshuber, 1999; Swietnicki *et al.*, 1998). Indeed, for the disease-

related E200K mutant of PrP, the NMR structure of this mutant is similar to wild-type PrP. The only difference lies within the surface charge distribution that may lead to abnormalities in the interaction of this PrP construct with its binding partner(s) and/or cellular membrane. Consequently, these abnormalities can result in the increased conversion of E200K PrP mutant to an abnormal PrP isoform, which relates to an inherited prion disease (Zhang *et al.*, 2000).

4.2.4 PrP^C trafficking to the cell surface

Several studies provide evidence that conversion of PrP^C to a protease- and phospholipase-resistant state is a posttranslational phenomenon occurring after the protein reaches the cell surface. Methods to release PrP^C from the cell surface or to disrupt the transport of PrP^C to plasma membrane are shown to prevent or severely reduce the conversion (Borchelt *et al.*, 1992; Caughey & Raymond, 1991; Gilch *et al.*, 2001). A molecular mechanism that explains why PrP^C needs to reach the cellular membrane before its conversion is not yet fully understood. One explanation emphasizes the posttranslational modifications (N-glycosylations, GPI attachment), which are only present after complete processing and trafficking of PrP^C to the membrane, that contribute to the conversion process. Another idea relates to PrP^C functioning as a receptor anchored on the plasma membrane where it can interact and mediate the internalization of heterologous PrP^{Sc} during infection. In the third idea, lipid environment and/or a factor at the cellular surface may induce PrP^C-PrP^{Sc} interaction and favor the conversion process (Campana *et al.*, 2005). Based on these hypotheses it is clear that membrane attachment and the trafficking pathway are important not only to elucidate the unknown physiological function of PrP^C but to understand the mechanism for the conversion of PrP^C into PrP^{Sc}.

Like most cell surface anchored proteins, PrP^C moves to the ER via recognition of its N-terminal signal sequence (residues 1-23), which is subsequently cleaved in the ER lumen. In the ER, PrP^C was found to be present with three variants: a secreted form, designated ^{Sec}PrP, corresponding to the full processing of PrP^C (section 4.2.2) and two ER-transmembrane forms that span lipid bilayer of the ER membrane with a conserved hydrophobic region of PrP (residues 111-134). Depending on the orientation towards the ER lumen, the forms are designated ^{Ntm}PrP or ^{Ctm}PrP. These two topologies are estimated to account for <10% of the total PrP

during normal biosynthesis of PrP^C in the ER (Harris, 2003). SecPrP undergoes folding and maturation events shortly after or during entrance into the ER as mentioned above (section 4.2.2), include signal sequence cleavage, glycosylation, disulfide bond formation and addition of GPI anchor to become “mature” PrP^C. Passage through the Golgi apparatus is necessary for PrP^C to reach the plasma membrane (Taraboulos *et al.*, 1992). The transition of PrP^C from ER to Golgi requires association of PrP^C with ordered membrane domains (“rafts”) within the ER membrane. Results of cholesterol depletion experiments suggested that raft association is also required for correct folding of PrP^C as well as for proper glycosylation. If PrP^C does not associate with rafts in the ER, it undergoes conformational changes, which make it sensitive to proteases from the ER quality control mechanism (Sarnataro *et al.*, 2004).

4.2.5 Endocytosis of PrP^C and its implication in the conversion of PrP^C to PrP^{Sc}

Internalization of PrP^C

Early work using neuroblastoma cell line transfected with chicken PrP^C revealed a cycling of PrP between plasma membrane and endosomal compartments with a half-life of 20-30 minutes (Shyng *et al.*, 1994). In neurons, the internalization rate of PrP^C was proven to be as fast as for a typical membrane receptor, transferrin receptor with a half-life of 3-5 minutes (Sunyach *et al.*, 2003). The biological function of PrP^C internalization is not yet understood, but it seems to be inducible by copper or zinc ions. Thus, this internalization could imply a physiological function in either chelating extracellular copper ions (Lee *et al.*, 2001; Pauly & Harris, 1998; Watt & Hooper, 2003) or modulating the signal transduction behavior of PrP protein (Mouillet-Richard *et al.*, 2000). However, it is not clear whether the mechanism of copper-stimulated endocytosis of PrP^C is similar to that of constitutive endocytosis of PrP^C (Lee *et al.*, 2001; Magalhaes *et al.*, 2002; Pauly & Harris, 1998). The involvement of caveolae, caveolae-like domains (CLDs), rafts and clathrin-coated vesicles in the endocytosis of PrP^C (Harris, 2003; Prado *et al.*, 2004) have created a debate about whether the mechanism of PrP^C internalization depends on clathrin-mediated endocytosis. Evidence including that both PrP^C and PrP^{Sc} were found in lipid rafts (Baron & Caughey, 2003; Botto *et al.*, 2004; Taraboulos *et al.*, 1992; Taraboulos *et al.*, 1995) and that interference on the synthesis of cholesterol or using

chemicals which can bind to cholesterol changed PrP^C trafficking (Marella *et al.*, 2002; Naslavsky *et al.*, 1997), led to the suggestion that PrP^C is internalized independently of clathrin. However, it should be pointed out that cholesterol depletion may also impair clathrin-mediated endocytosis (Rodal *et al.*, 1999; Subtil *et al.*, 1999).

On the other hand, support for PrP^C internalization via clathrin-coated vesicles is based on the observation that chicken PrP^C concentrates in clathrin-coated vesicles in transfected neuroblastoma cells and cultured chicken neurons, as well as in chicken brain (Shyng *et al.*, 1994). Furthermore a study on mammalian PrP^C showed that many internalized PrP^C molecules are found in clathrin-coated pits. Interestingly, PrP^C seems to be present in both ordered and non-ordered areas of plasma membranes. This finding leads to the hypothesis that PrP^C can leave rafts to undergo clathrin-mediated endocytosis (Sunyach *et al.*, 2003). In addition, the N-terminal region of PrP^C was also supposed to be involved in sorting PrP^C from the cell surface towards internalization (Lee *et al.*, 2001; Nunziante *et al.*, 2003). This event was further characterized by genetically transferring the N-terminal region of PrP^C to Thy-1, a major GPI-anchored protein in neurons, which undergoes trafficking different from GPI-anchored PrP^C (Brugger *et al.*, 2004). The resulting modified Thy-1 was internalized in clathrin-coated vesicles similar to PrP^C (Sunyach *et al.*, 2003). However, the involvement of clathrin-coated vesicles in endocytosis of PrP^C is unusual since it lacks a transmembrane domain interacting with adaptor proteins and clathrin. One possible explanation is the existence of a “PrP^C receptor”, a transmembrane protein that can interact with PrP^C and mediate endocytosis of PrP^C via clathrin-coated pits (Harris, 2003). Although no “PrP^C receptor” has been identified, some candidate proteins including 37-kDa/67-kDa laminin receptor, stress-inducible protein 1 have been proposed (Gauczynski *et al.*, 2001; Zanata *et al.*, 2002).

Overall the currently available data point to clathrin-mediated endocytosis as the default pathway for internalization of PrP^C from cell surfaces. Caveolae or CLDs-related pathways offer alternatives for internalization of PrP^C in special cell types or under specific conditions (Campana *et al.*, 2005).

Role of the endocytosis pathway in PrP^C-PrP^{Sc} conversion

Besides elucidating the mechanism of conversion of PrP^C to PrP^{Sc}, determining the place where this conversion occurs is also necessary to access therapeutic strategies against prion diseases. Several studies suggest that the formation of PrP^{Sc} only takes place after PrP^C has reached the plasma membrane (Caughey & Raymond, 1991; Gilch *et al.*, 2001; Taraboulos *et al.*, 1992). However, accumulating evidences indicate that the endocytosis pathway is involved in the conversion of PrP^C to PrP^{Sc} (Borchelt *et al.*, 1992; Marijanovic *et al.*, 2009; Taraboulos *et al.*, 1992). To date there is no direct evidence for the involvement of any specific cellular compartment in this event but several compartments have been suggested: the Golgi apparatus, early/recycling endosome, lysosome, late endosome (Arnold *et al.*, 1995; Barmada & Harris, 2005; Caughey & Raymond, 1991; Godsave *et al.*, 2008). Formation of PrP^{Sc} was inhibited by lowering the temperature to block endocytosis in cell-based assays (Borchelt *et al.*, 1992). Both CLDs- and clathrin-mediated endocytosis of PrP^C were suggested to be involved in the conversion (Kaneko *et al.*, 1997; Peters *et al.*, 2003; Sunyach *et al.*, 2003; Vey *et al.*, 1996). A notable hypothesis is that the impairment of endocytosis of PrP^C can raise neurodegenerative diseases because this impairment can switch off/on neuroprotective/neuropathological signals (Biasini *et al.*, 2012).

4.2.6 Possible physiological roles of PrP^C

Although PrP^C plays a crucial role in prion diseases and has been extensively studied *in vitro* and *in vivo*, its physiological function has remained uncertain. Mice carrying *PrnP* gene knockouts showed no obvious phenotype in comparison with wild-type mice (Bueler *et al.*, 1992; Manson *et al.*, 1994). A wide range of studies suggested a role of PrP in numerous cellular processes: anti-apoptosis (Kim *et al.*, 2004; Shyu *et al.*, 2005), protection against oxidative stress (Haigh *et al.*, 2009; Milhavet & Lehmann, 2002), formation and function of synapses (Kanaani *et al.*, 2005; Moya *et al.*, 2000), cell adhesion (Malaga-Trillo *et al.*, 2009) and regulation of ion channels (Lazzari *et al.*, 2011).

4.3 Conversion of PrP^C to PrP^{Sc}

4.3.1 Comparison PrP^C and PrP^{Sc}

PrP^C and PrP^{Sc} are two isoforms of the prion protein, which is encoded by the *Prnp* gene (Basler *et al.*, 1986). They are identical in primary structure and share the same posttranslational modifications (Hope *et al.*, 1986; Stahl *et al.*, 1992; Stahl *et al.*, 1993). Only the nature of the disulfide bond in PrP^{Sc} has been discussed controversially. However, their secondary structures are quite different. According to CD and FTIR studies, PrP^C is a monomer and composed of a high content of α -helices. NMR studies of recombinant PrP^C proteins provided structural information with atomic resolution (see section 4.2.3 for more details). On the other hand, the tertiary structure of PrP^{Sc} is still not available at high resolution due to its tendency to aggregate. However, Govaerts and colleagues used electron microscopy to obtain low-resolution, two-dimensional images of prion crystals and predicted in combination with molecular modeling the basic structure of PrP^{Sc} and its existence as a trimer (Figure 4.2) (Govaerts *et al.*, 2004). Moreover, PrP^C and PrP^{Sc} can also be distinguished based on their biochemical characteristics. PrP^C is soluble in mild detergents and sensitive to proteinase K (PK). In contrast, PrP^{Sc} is highly aggregated and insoluble under nondenaturing conditions, and partially resistant to PK (Table 4.1) (Meyer *et al.*, 1986).

PrP ^C	PrP ^{Sc}
42% α -helix, 3% β -sheet	30% α -helix, 45% β -sheet
Soluble in mild buffers	Insoluble in mild buffers
PK sensitive	Partially PK resistant

Table 4.1 Comparison of biochemical characteristics of PrP^C and PrP^{Sc}

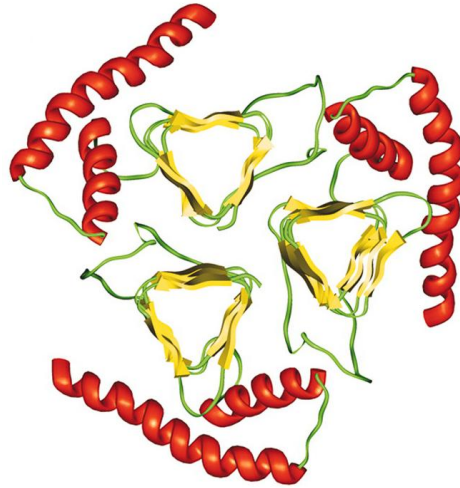


Figure 4.2 Trimeric model of prion 27-30 (Govaerts *et al.*, 2004)

4.3.2 *In vitro* conversion analysis

Prion-seeded conversion

In early efforts to elucidate molecular mechanism of the conversion, purified PrP^C (substrate), PrP^{Sc} (seed) and brain homogenate were used in *in vitro* assays to create PrP^{Sc}-like prions. However, in such cell-free system, newly formed PrP^{Sc}-like molecules were obtained with very low efficiency (Kocisko *et al.*, 1994). Later, Atarashi and colleagues reported that recombinant hamster PrP could be converted into protease resistant PrP (PrP^{Res}) and had infectious activity when seeded with diseased hamster brain homogenate via a method called Protein Misfolding Cyclic Amplification (PMCA) (Atarashi *et al.*, 2007). However, using complex brain homogenate becomes an inherent obstacle to clearly explain the association of prion infectivity with PrP^{Res} and to elucidate the mechanism behind conversion. Furthermore, subsequent PMCA experiments showed significantly higher efficiency in tests with crude brain homogenate than with purified preparations (Castilla *et al.*, 2005; Deleault *et al.*, 2005; Saborio *et al.*, 2001). These findings indicate that one or more unknown factors might be required for efficient conversion. Indeed, RNA molecules (Deleault *et al.*, 2003), glycans (Wong *et al.*, 2001), lipid membranes (Baron *et al.*, 2006) have been suggested to play an important role in the conversion of PrP^C to PrP^{Sc}. Especially, Baron and Caughey studied effects of lipid rafts on the PrP conversion (Baron *et al.*, 2002). In this report, cell-free conversion conditions were developed using ³⁵S-labeled PrP^C associated with detergent-resistant

membranes (DRMs-PrP^C) purified from neuron cells as substrate, and brain microsomes from scrapie-infected mice as a source of PrP^{Sc}. A mixing of DRMs-PrP^C and PrP^{Sc} did not result in a conversion of DRMs-PrP^C into PrP^{Sc}. However, addition of phosphatidylinositol-specific phospholipase (PI-PLC) to conversion reactions to release PrP^C from DRMs dramatically enhanced the conversion of PrP^C into PrP^{Sc}, indicating that the association of PrP^C with DRMs can sterically hinder its binding to exogenous PrP^{Sc}. On the other hand, addition of PEG to conversion reactions to induce fusion of two sets of membranes containing PrP^C and PrP^{Sc} also significantly enhanced the conversion. That means the membrane fusion may create the larger vesicles containing both PrP^C and PrP^{Sc}, and in these new vesicles, PrP^C and PrP^{Sc} might interact together and lead to the conversion. These results suggested two scenarios for initiation and propagation of PrP^{Sc} synthesis. First, if the conversion occurred on the membrane surface, it would imply an insertion of PrP^{Sc} into host cell membrane prior to induction of PrP^C conversion. Second, if the conversion takes place extracellularly, as proposed by Jeffrey and colleagues (Jeffrey *et al.*, 1997), release of PrP^C from cell membranes would be necessary. In both hypotheses, PrP-lipid interaction and the GPI anchor play important roles in the conversion. In order to further understand the role of GPI anchor in the conversion, Baron and colleagues also performed the cell-free conversion reactions using GPI anchored and GPI-free PrP^C (GPI⁺PrP and GPI⁻PrP, respectively) as substrates to examine the effect of membrane attachment on the interaction of PrP^C and PrP^{Sc} (Baron & Caughey, 2003). In case of DRMs-bound GPI⁺PrP, the conversion of GPI⁺PrP^C into PrP^{Sc} did not occur until either PI-PLC was added to the reaction or the fusion of membrane fractions was triggered by PEG addition. In contrast, DRMs-bound GPI⁻PrP was converted into PrP^{Sc} without PI-PLC or PEG treatment. Thus, these results supposed an important role of GPI anchor on the conversion.

Synthetic prions

As defined by Colby and Prusiner, synthetic prions are “infectious proteins that can be created from minimal components in the laboratory and demonstrate infectivity in living organisms” (Colby & Prusiner, 2011). In 2004, this term was first supposed by Legname and colleagues (Legname *et al.*, 2004) when they only used bacterially expressed truncated prion protein (residues 90-231) and chaotropic

chemicals to create amyloid fibrils with lethal infectivity that was demonstrated via intracerebral inoculation in mice. In contrast to the prion-seeded conversion described above, at here, neither purified PrP^C nor brain-derived materials were used in the conversion in order to exclude unclear side effects of these materials on the conversion. This *in vitro* generation of a pure PrP^{Sc}-like prion from defined starting materials was thought to explain the mechanism of conversion and addressing the question of whether PrP alone is sufficient for the conversion without any additional cellular factors. Baskakov (Baskakov *et al.*, 2002), Legname (Legname *et al.*, 2004) and Colby (Colby *et al.*, 2010) have only used *E. coli* expressed recombinant PrP (rPrP) constructs under partial denaturing conditions to form amyloid fibrils that are neurotoxic and show a low infectivity. Because rPrP is expressed in *E. coli* in inclusion bodies and purified under denaturing condition using high concentration of guanidine or urea, any detectable cellular products from *E. coli* were removed. Therefore, rPrP provides clean materials for amyloid fibril formation to study *de novo* PrP conversion. However, the low infectivity of resulting prions in animal-based assays is a significant obstacle of this strategy to mimic highly infectious characteristic of PrP^{Sc} (Supattapone, 2010).

A highly infectious prion generated from bacterially expressed prion protein mixed with anionic phospholipid POPG and RNA

In contrast to the synthetic prion idea that looks for the molecular basis of prion infectivity in PrP itself, various biochemical studies have indicated that non-proteinaceous cofactors could be required to produce infectious prions (Deleault *et al.*, 2007; Geoghegan *et al.*, 2007; Wang *et al.*, 2010a; Wong *et al.*, 2001). Notably, some *in vitro* studies proved that rPrP was able to bind to phospholipid vesicles and then changed its conformation (Morillas *et al.*, 1999; Sanghera & Pinheiro, 2002). However, these studies did not prove that after mixing with phospholipid vesicles PrP was able to resist PK, one typical characteristic of PrP^{Sc}. Recently, rPrP mixed with anionic 1-palmitoyl-2-oleoyl-phosphatidylglycerol (POPG) phospholipid was proven to convert into a PK-resistant conformation (Wang *et al.*, 2007). In a major step forward, Wang and colleagues reported that mixing rPrP with total liver RNA and POPG in serial PMCA reactions produced highly infectious recombinant prions. Interestingly, the resulting recombinant prions were stably infectious in wild-type mice, both

recombinant prion-injected mice and mice receiving second round transmissions revealed the classic neuropathology of prion disease (Wang *et al.*, 2010a). Furthermore, the highly conserved central hydrophobic region of the prion protein was identified to be crucial for lipid-induced conformational change of recombinant PrP (Wang *et al.*, 2010b). These reports show that interactions of rPrP and phospholipids play a crucial role in the conversion of rPrP to *de novo* PrP^{Sc}. However, one should be aware that rPrP lacking a C-terminal GPI membrane anchor was used in these conversion experiments. Thus, the role of the GPI anchor regarding interaction of rPrP and POPG needs to be addressed.

4.3.3 Role of ordered lipid domains (rafts) in PrP^{Sc} formation

A role of lipid rafts in the conversion process is considered since both PrP^C and PrP^{Sc} were found in rafts extracted from infected cells and from infected mouse brain (Baron & Caughey, 2003; Baron *et al.*, 2002; Botto *et al.*, 2004; Taraboulos *et al.*, 1992; Taraboulos *et al.*, 1995). PrP^{Sc} might therefore “hijack” rafts to enter the cells and possibly to initiate and/or propagate the conversion of PrP^C to PrP^{Sc}. However, the association of PrP^C and PrP^{Sc} with rafts resulted in differences between PrP^C and PrP^{Sc} in solubility and floatation rate in the density gradient (Naslavsky *et al.*, 1997). These differences indicate either that the types of rafts associated with each isoform differ or that the membrane association of each isoform has distinct characteristics. Although a clear mechanism to explain how rafts control PrP^{Sc} formation is not available yet, Campana and colleagues suggested three different models (Campana *et al.*, 2005). First, rafts are involved in targeting of PrP^C to a specific subcellular site where conversion occurs. Indeed, as mentioned above in exocytic (section 1.2.4) or endocytotic (section 1.2.5) trafficking pathways of PrP^C, rafts were already shown to effect the movement of PrP^C in cholesterol depletion assays. Second, rafts might be containing one or more factor(s) such as membrane protein(s) that are necessary for conversion. Third, rafts can promote the conversion of PrP^C to PrP^{Sc} by creating a favorable environment, in which exogenous PrP^{Sc} (seed) reaches sufficient concentrations and can closely interact with endogenous PrP^C (substrate). Indeed, Baron and colleagues proved that rafts behave as a “meeting-place” between PrP^C and PrP^{Sc}; and the conversion only occurs when the two components are inserted into contiguous membrane areas (Baron *et al.*, 2002).

Recently, by developing a new cellular system in which epitope-tagged PrP^C was expressed in PrP-knockdown neuron cell line and then exposed to RML (Rocky Mountain Laboratory) prion, Goold and colleagues found that the conversion primarily occurred on the plasma membrane and the infectious rate of cells exposed to RML prion was extremely rapid. Moreover, the role of lipid rafts in the conversion was also proven here. The epitope-tagged PrP^C expressing cells that were pretreated with either filipin, which sequesters plasma membrane cholesterol, or U18666A, which inhibits cholesterol transport to rafts, and then exposed to RML prion, revealed that the conversion of epitope-tagged PrP^C into PrP^{Sc} was severely reduced (Goold *et al.*, 2011).

4.3.4 GPI anchor in the PrP^{Sc} formation

The GPI anchor not only plays an important role in the conversion process as found by Baron and Caughey (section 4.3.2), but also contributes to PrP^{Sc} formation. Chesebro and colleagues created scrapie-infected GPI-anchorless transgenic mice, which can propagate PrP^{Sc}. However, the lack of GPI-anchored PrP^C changed the anatomic distribution of PrP^{Sc} in the brain and also eliminated typical clinical scrapie disease (Chesebro *et al.*, 2005). The PrP^{Sc} from infected mice expressing anchorless PrP is formed as extracellular amyloid plaques in contrast to those of wild-type mice predominantly seen as non-amyloid deposits (Figure 4.3). The lack of typical clinical TSE disease symptoms from anchorless PrP mice also suggest that the lesions caused by anchorless PrP^{Sc} are less problematic than those caused by wild-type PrP^{Sc} (Caughey & Baron, 2006).

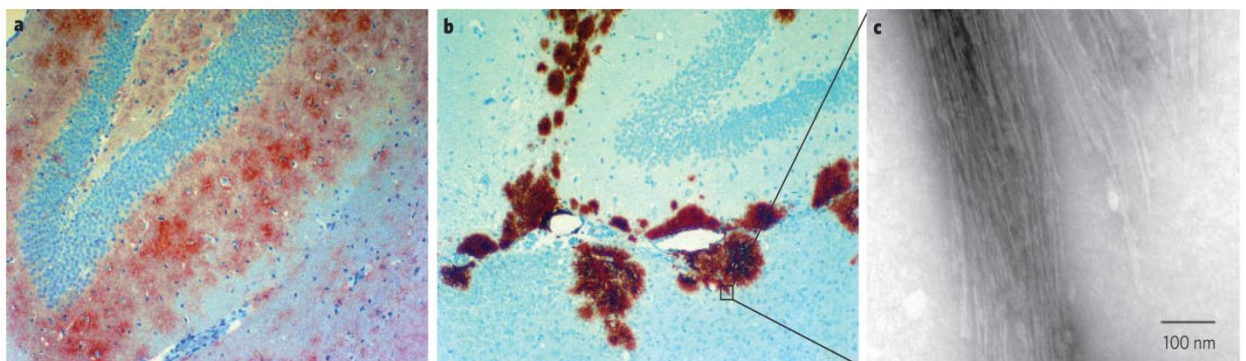


Figure 4.3 Differences in pattern and deposition in mouse brain tissue of PrP^{Sc} generated from normal PrP^C (a) and anchorless PrP^C (b). Both mouse strains

expressing wild-type PrP^C and anchorless PrP^C were infected with the 22L prion strain (Chesebro *et al.*, 2005). (c) Electron microscopy imaging for plaques in (b) to show the fibrillar nature. The figure was taken from (Caughey & Baron, 2006).

4.4 Semisynthesis of membrane-associated prion protein variants

4.4.1 Native chemical ligation

Native chemical ligation (NCL) was introduced by Kent and colleagues (Dawson *et al.*, 1994), and relies on the selective reaction between a C-terminal α -thioester group of an N-terminal peptide and an N-terminal cysteine residue of a C-terminal peptide. This NCL reaction is initiated by a transthioesterification that is followed by an S \rightarrow N-acyl transfer to form a native amide bond (Figure 4.4). The NCL reaction is typically carried out in aqueous conditions at neutral pH in the presence of thiols as ligation mediators. Internal cysteine residues inside both peptides are tolerated because typically no branched side products are observed due to the excess thiols (David *et al.*, 2004). However, recent studies described thiolactone formation within thioester peptides containing internal cysteine residues (Durek *et al.*, 2007; Holm *et al.*, 2012; Mandal *et al.*, 2012). This side reaction can be explained by a nucleophilic attack from the thiol group of internal cysteine to the thioester group. Durek and colleagues reported that incubation of a peptide thioester containing one internal cysteine residue under ligation condition can result in thiolactone formation within few seconds (Durek *et al.*, 2007). Reversibility of thiolactone by treatment with thiol reagents such as MPAA, MESNA and ethanethiol was not successful in our hands as discussed below (section 7.3.4).

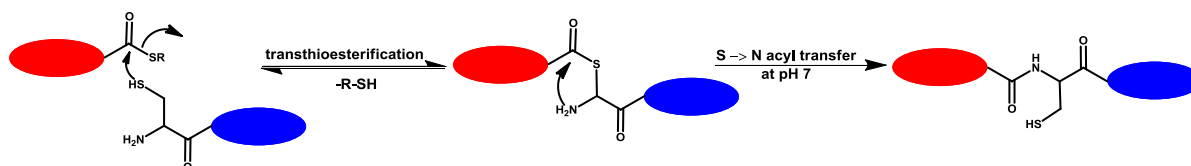


Figure 4.4 Mechanism of native chemical ligation

4.4.2 Expressed protein ligation

Expressed protein ligation (EPL) is an extension of the NCL method in which the production of protein thioesters can be achieved by using recombinant technology to generate a C-terminal fusion of inteins with the target protein (Muir *et*

al., 1998). Next, the recombinant protein thioesters are linked to a chemically synthesized peptide containing an N-terminal cysteine under similar condition for NCL to form a native peptide bond. The EPL method combines advantages from recombinant technology and peptide synthesis in order to site-specifically introduce unnatural amino acids, functional groups or posttranslational modifications into large proteins (Muir *et al.*, 1998).

In NCL method, peptide thioesters have been generated via chemical synthesis, a process that suffers size limitation of the peptide thioesters. Therefore, the NCL has been very useful for total synthesis of small proteins and protein domains but requires time-consuming and laborious works to access polypeptides greater than ~100 amino acids (Vila-Perello & Muir, 2010). The EPL method can overcome this technical challenge of NCL. Furthermore, this strategy also allows isotope-labeling of recombinant proteins for NMR studies.

Protein splicing

EPL is based on a naturally occurring enzymatic process called “protein splicing” to convert recombinant protein into protein thioesters (Muir, 2003). Protein splicing is an intramolecular posttranslational event in which the precursor protein by itself rearranges to precisely remove the internal fragment (intein) and to ligate the C-terminal and N-terminal flanking protein segments (C- or N-extein, respectively) (Paulus, 2000). In more detail, the first rearrangement process (Figure 4.5) is initialized by the first step: N → S acyl (or N → O acyl) shift in which the N-extein is transferred to the SH or OH group on the side chain of cysteine or serine. In the next step, the entire N-extein is attached to the SH group on the side chain of a conserved N-terminal cysteine of the C-extein. This attachment generates a branched intermediate which is not stable. The resulting branched intermediate is then resolved via a cyclization reaction involving a conserved asparagine residue at the C-terminus of the intein. The intein, therefore, can be excised as a C-terminal succinimide derivative. In the final step, S → N acyl shift yields an amide bond between two exteins. Although the biological function of protein splicing is still not fully understood, this process has been applied extensively in biotechnology to create selectively and homogeneously posttranslational modifications of proteins for studies

on structure and function via a strategy so-called EPL (Hackenberger & Schwarzer, 2008).

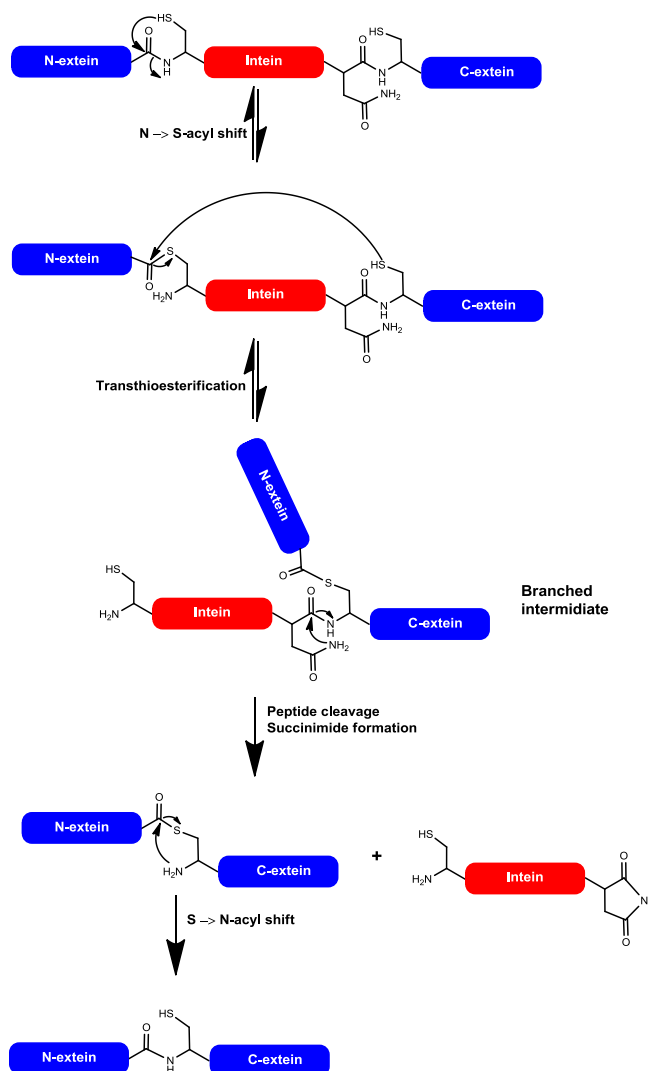


Figure 4.5 Mechanism of protein splicing

Applications of EPL

Site-selective posttranslational modifications (PTMs) of proteins: the ability to modify side chains of amino acids in chemically synthesized peptides, followed by selective introduction into proteins generates a powerful tool for structural and functional studies (Muir *et al.*, 1998). The effect of posttranslational modifications such as phosphorylation, glycosylation, acetylation and others on protein function can be elucidated when these modifications are incorporated at selective positions and if sufficient amounts of homogenous protein are available. One early example is the selective phosphorylation of a single tyrosine in the C-terminal domain of a

soluble tyrosine kinase, Src kinase (Csk) that was developed by Muir and colleagues (Muir *et al.*, 1998). A synthetic peptide containing a single phosphotyrosine residue was ligated to the C-terminus of Src homology 2 (SH2) domain from recombinantly expressed Csk. This modification resulted in an intramolecular interaction between SH2 and phosphotyrosine, and then led to increased catalytic phosphoryl transfer to a substrate when compared with non-phosphorylated Csk. Using the EPL strategy, McMillan and Bertozzi generated a multi-glycosylated protein CAM-1, a mucin-like glycoprotein that functions as a ligand for the leukocyte adhesion molecule L-selectin. In this work, three glycosylated forms of CAM-1 were produced with glycosylated residues at N-terminal, C-terminal as well as simultaneously N- and C-terminal regions (Macmillan & Bertozzi, 2004). In addition, a variety of lipid modifications including prenyl groups and GPI anchor have been introduced by EPL into proteins such as Rab GTPase proteins, PrP (Becker *et al.*, 2008; Brunsveld *et al.*, 2006; Wu *et al.*, 2010).

Segmental isotope or fluorescent labelling: the great progress of fluorescence and NMR technologies in structural studies of proteins enhance our understanding of proteins. More impressively, the EPL method can be used to selectively introduce stable isotopes or fluorescent dyes into proteins. For example, Alexandrov and colleagues introduced a dansyl probe to the C-terminus of a small GTPase Rab7, where is known to be posttranslationally prenylated by the enzyme Rab geranylgeranyl transferase (RabGGTase). Both steady-state and time-resolved fluorescence measurements were performed to study the affinity of Rab7 with RabGGTase and the escort protein REP-1 (Alexandrov *et al.*, 2002). In addition, segmental isotopic labeling using EPL has been applied to overcome the practical size limit in analysis of protein structure by NMR spectroscopy (Muir, 2003). This method allows isotopic labeling of selected segments of a protein so that unlabeled regions can later be filtered out of the NMR spectrum. Therefore, the spectral complexity can be significantly reduced for solution-based NMR measurements of large proteins. One example for this method is selective ^{15}N -labeling of a single domain among the Src- homology type 3 and 2 domains (SH3 and SH2) of Abelson protein tyrosine kinase (Xu *et al.*, 1999). One half of the protein was bacterially expressed using minimal medium containing ^{15}N isotope and then ligated with the unlabeled second protein fragment to yield the desired segmentally ^{15}N -labeled

protein. Another protein sample that also was of segmental isotope labeling via the EPL strategy is Apolipoprotein E (ApoE), an exchangeable apolipoprotein that functions as a ligand for members of the low-density lipoprotein (LDL) receptor family. Hauser and colleagues used the EPL method to generate N-terminal domain of ApoE (residues 1-183) containing ^{15}N -isotope labeled C-terminus (residues 112-183) for structure-function studies (Hauser *et al.*, 2009).

In addition, it should be considered that EPL can be used to link a recombinant protein to a nonpeptidic moiety. Examples of this strategy include the attachment of proteins to surfaces, polymers or nucleic acids (Gogolin *et al.*, 2013; Lue *et al.*, 2004; Paulick *et al.*, 2007).

4.4.1.5 Alternative approaches for protein ligation

Auxiliary mediated ligation: this method is a strategy to circumvent the cysteine residue at the ligation site. In this method, a thiol-containing auxiliary is introduced at the N-terminus of C-terminal peptide fragment, which can react with the thioester group at the C-terminus of the N-terminal peptide fragment in a similar mechanism to NCL or EPL. Next, the auxiliary group can be removed from the resulting ligation product by a treatment in acidic condition (Botti *et al.*, 2001) or UV irradiation (Kawakami & Aimoto, 2003).

Ligation-desulfurization approach: this strategy is an extension of NCL to apply for non-cysteine containing proteins/peptides. Initially, this approach was proposed by Yan and Dawson for the ligation at cysteine and subsequent desulfurization of cysteine into native alanine (Yan & Dawson, 2001). Recently, significant progress has been achieved in development of thiolated building blocks that serve as precursors to other amino acids. Ligations at phenylalanine, valine residues can be performed by using building blocks β -mercaptophenylalanine, β -mercaptovaline, respectively and subsequent desulfurization (Crich & Banerjee, 2007; Haase *et al.*, 2008).

Protein trans-splicing: this strategy is also based on the previously discussed protein splicing mechanism (Figure 4.5). However, generation of thioesters as in NCL or EPL is not required for ligation process; it relies on the natural assembly of two divided fragments of inteins (so-called split inteins) to form a fully functional intein.

Consequently the resulting functional intein can ligate the N- and C- exteins by protein splicing. Naturally occurring split inteins were first discovered in *Synechocystis sp.* strain with catalytic subunit of DNA polymerase III was expressed in two separate DnaE^N and DnaE^C fragments which could assembly to yield the full length DnaE (Wu *et al.*, 1998). To apply split inteins for generation of a semisynthetic protein, for example, a DnaE^C-C-extein peptide with a smaller C-terminal intein fragment DnaE^C can be obtained by solid phase peptide synthesis (SPPS) and then reacted with a recombinant N-extein-DnaE^N fusion protein (Ludwig *et al.*, 2009; Martin *et al.*, 2001). Interestingly, this method can also be applied for site-specific labeling of a protein in living cells as reported by Borra and colleagues. In this study, a fluorescent dye and its quencher were attached to the C-terminus and N-terminus of the DnaE^C fragment, respectively. The resulting fluorescence-quenched DnaE^C peptide was transferred into the mammalian cells, which expressed an N-terminal fusion of DnaE^N with a target protein. The C-terminal intein can assemble with its N-terminal fragment within the cells to form a fully functional intein that results in ligation of the fluorescent dye to the C-terminus of the protein. This event yields in-cell fluorescence activation and specific fluorescent labeling of the protein in living cells (Borra *et al.*, 2012).

Sortase-mediated protein ligation: one prominent example for chemoselective protein ligation catalyzed by enzymes is based on transpeptidase sortase A (Tsukiji & Nagamune, 2009). Sortase A is an enzyme that catalyzes the anchoring of membrane proteins to the cell wall of Gram-positive bacteria (Ton-That *et al.*, 1999). To utilize sortase A for protein ligation, the N-terminal protein has to be carried LPXTG sorting motif at the C-terminus and the C-terminal peptide needs to contain at least one glycine residue at the N-terminus. Sortase A can recognize the sorting motif and cleave off the C-terminal glycine and subsequently ligate the protein to the N-terminal glycine of the C-terminal peptide. The feasibility of this approach was demonstrated e.g. for the recombinant eGFP containing LPETG motif at the C-terminus, which was ligated with a short lipid-modified oligoglycine peptide comprising three glycine residues at the N-terminus (Antos *et al.*, 2008). Moreover, sortase A was used to ligate a fluorescently labeled peptide to a protein containing LPXTG motif on the surface of living cells (Tanaka *et al.*, 2008). Although sortase-mediated protein ligation was recently supposed as a versatile enzymatic protein

ligation with great potential in protein engineering (Tsukiji & Nagamune, 2009), its drawback is the remaining LPXTG motif and polyglycine in ligated proteins.

4.4.2 Semisynthesis of membrane-anchored prion proteins

Due to the key role of membrane association in the conversion of PrP^C to PrP^{Sc} (sections 4.2.4, 4.3.2, 4.3.3, 4.3.4), it is necessary to compare behavior of membrane-anchored PrP to that of non-membrane-anchored PrP within different membrane environments in *in vitro* biochemical assays analyzing folding, structure and stability. However, GPI-anchored PrP^C protein extracted from neuron cells is typically heterogeneous and contaminated. Thus, generation of lipidated PrP from recombinant technology is an alternative way. Eberl and colleagues generated lipidated PrP using recombinant murine PrP containing a six amino acid C-terminal extension (5xglycine-cysteine-OH) reacted with N-terminal cysteine of liposomes to form a disulfide bond. This lipid attachment leads to membrane association of PrP, which did not result in significant structural changes of PrP as measured by CD (Eberl *et al.*, 2004). A similar strategy using a different lipid group attached to the C-terminus of PrP via a disulfide bond was used by Hicks and colleagues (Hicks *et al.*, 2006). The reconstitution of lipidated PrP into POPC or raft membranes showed a conformational change of PrP from the β sheet-enriched structure into the α -helical structure in FTIR measurements. This result indicated a protective effect of the membrane environment on the native structure of PrP. In addition, the detergent octyl- β -D-glucopyranoside (OG) was used in this study to promote the insertion of lipidated PrP into liposomes.

The above methods can suffer potential issues such as an obstacle for using in cell-based assays and side reactions with internal cysteine residues of PrP when lipid groups were attached to PrP via a disulfide bond (Olschewski & Becker, 2008). Conversely, Olschewski and colleagues developed two strategies including EPL and protein trans-splicing to prepare lipidated PrP (Olschewski *et al.*, 2007). In these strategies, the GPI anchor mimics are composed of a peptide containing two palmitoyl groups attached to the side chains of lysine residues, a protease TEV cleavage site for optional removal of lipid anchor, a third lysine residue for coupling fluorescent dye, an N-terminal cysteine for EPL reaction, and a polyethylene glycol-like linker at the C-termini to enhance the solubility (Figure 4.6). These properties

render this lipidated peptide become the most versatile GPI anchor mimic that was already described to produce recombinant lipidated PrP (Olschewski & Becker, 2008). In EPL strategy, PrP containing a C-terminal α -thioester group (C α -thioester) was prepared by bacterially recombinant expression as a fusion with a genetically modified *Mxe* intein, followed by affinity purification with Ni-NTA resin via a C-terminal 6xhistidine tag and subsequent cleavage with MESNA (Figure 4.6 A). Two reactive moieties: lipidated peptide and PrP C α -thioester were ligated by EPL reaction and then the resulting lipidated PrP was folded. However, substantial amounts of carbamylation were observed after long handling time in urea-containing buffers for cleavage reaction and NCL (Olschewski *et al.*, 2007). To prevent this modification as well as generation and separation of PrP thioesters, protein trans-splicing was used. In this strategy, PrP was C-terminally fused with N-terminal fragment of *Synechocystis* sp. DnaE split intein (DnaE^N) and chemical synthesis of its C-terminal segment (DnaE^C) linked to the lipidated peptide. Both DnaE fragments assembly to form a fully functional intein and protein trans-splicing occurs to give lipidated PrP (Figure 4.6 B). Next, the influence of membrane association was indicated by an aggregation assay which revealed that this association delayed aggregation process of lipidated PrP when compared with non-lipidated PrP (Olschewski *et al.*, 2007). Furthermore, Becker and colleagues carried out comparative aggregation assays between this lipidated PrP and PrP ligated with a chemically synthesized GPI anchor (Becker *et al.*, 2008). The results of aggregation assays showed no significant difference between both PrP constructs. That means the biochemical property of lipidated peptide is very close similar to that of GPI anchor.

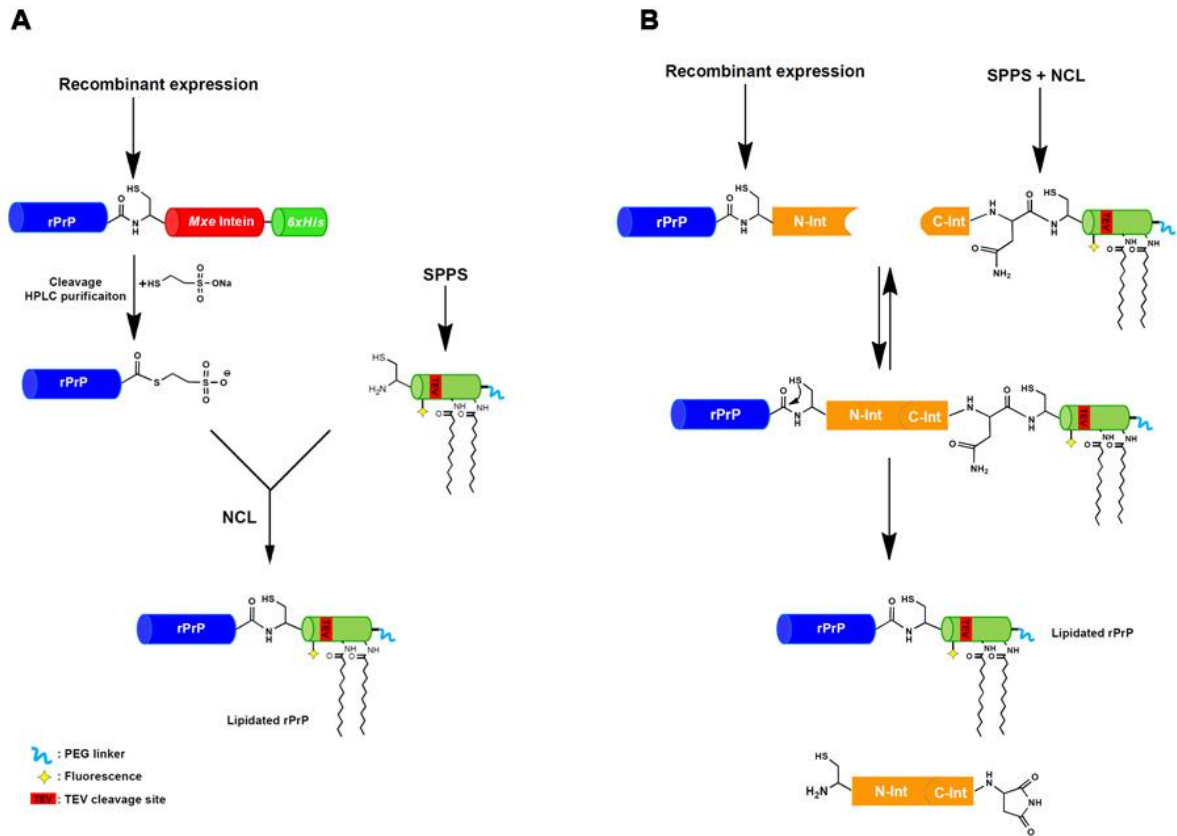


Figure 4.6 Scheme for semisynthesis of lipidated prion protein by A) EPL or B) protein trans-splicing (Olschewski et al., 2007)

5. Objectives

Posttranslational modifications (PTMs) extend the functional diversity of proteome by the covalent introduction of functional group(s) to proteins. These modifications include phosphorylation, glycosylation, ubiquitylation, methylation, acetylation, lipidation. PTMs influence many aspects of normal or pathogenic cell biology (Walsh *et al.*, 2005). Here, a semisynthesis strategy is applied to incorporate PTMs into target proteins for studying their effects on conformational and biochemical properties of these proteins.

Since C-terminal membrane attachment of PrP via a GPI anchor has been suggested to play a role in the conversion of PrP^C into PrP^{Sc} (Baron & Caughey, 2003; Goold *et al.*, 2011; Jeffrey, 2013), the first part of thesis is focusing on analyzing the effect of C-terminal membrane anchor on interaction of PrP with lipid membranes. To this end, three PrP constructs: full length PrP (residues 23-231, FL_PrP), PrP missing its central hydrophobic region (residues 23-104–126-231, Δ CR_PrP) and N-terminally truncated PrP (residues 90-231, T_PrP) will be equipped with membrane anchors. The conformational and biochemical properties of the resulting lipidated PrP variants within membrane environments as well as the influence of PrP-lipid interaction on the integrity of lipid membranes are investigated by several biophysical and biomolecular techniques such as floatation assay, CD, proteinase K digestion, fluorescence-based assays, cryo EM.

The strategy outlined above to generate lipidated PrPs requires generation of PrP with a C-terminal α -thioester group via the cleavage of PrP-*Mxe* intein fusion protein. The insoluble expression of PrP-*Mxe* intein fusion proteins in *E. coli* results in a low yield of the cleavage reaction and low folding efficiencies that subsequently limit the available amounts of lipidated PrPs. Previous studies showed that a direct N-terminal fusion of *E. coli* DnaK chaperone leads to an improved solubility of recombinantly expressed proteins in *E. coli* (Kyratsous *et al.*, 2009). Thus, a variety of N-terminal fusion constructs of *E. coli* DnaK chaperone with PrP-*Mxe* intein protein will be generated to achieve the soluble expression of PrP-*Mxe* intein fusion proteins in *E. coli*.

PTM-dependent transient interactions are relatively weak interactions that are important in many cellular processes (Perkins *et al.*, 2010). One example for such interactions is the interaction of the Tudor domain of SMN protein (SMN Tudor) and its ligand symmetrically dimethylated arginine residue (sDMA) within the unstructured C-terminal tails of Sm proteins. Due to this weak interaction, previous structural studies of SMN Tudor bound to sDMA must use highly excess of free sDMA to fully populate the complex (Tripsianes *et al.*, 2011). However, such condition is not always suitable to apply for structural studies of weak interactions in which high concentrations of protein and ligand (mM range) are required. One way to overcome this problem would be covalently linking two binding moieties. Thus, a strategy is established to ligate sDMA ligand to the C-terminus of SMN Tudor via flexible glycine linkers of different length. Next, NMR spectroscopy will be applied in collaboration with the group of Michael Sattler (TU München) to comparatively analyze the structures of resulting SMN Tudor-sDMA proteins and SMN Tudor saturated with excess of free sDMA. These NMR experiments are aimed to demonstrate the utility of our ligation approach towards structural analysis.

6. Materials and methods

6.1. Materials

6.1.1 Chemicals

All chemicals were purchased from the following companies if not noted otherwise: Merck (Darmstadt, Germany), Sigma-Aldrich (Osterode am Harz, Germany), Carl Roth (Karlsruhe, Germany), Invitrogen (Darmstadt, Germany), VWR (Darmstadt, Germany), J.T.Baker (Griesheim, Germany), NeoLab (Heidelberg, Germany), Serva (Amstetten, Austria) and Omnilab (Bremen, Germany). All buffers were made with miliQ water (dH₂O).

6.1.2 Molecular biology materials

Restriction enzymes and DNA purification kits used in cloning work were purchased from Promega (Mannheim, Germany) and Qiagen (Hilden, Germany)

Oligonucleotides for cloning work were ordered from Metabion GmbH (Martinsried, Germany).

Antibodies for Western blot assays were either received as a gift from Professor Jörg Tatzelt (Winklhofer *et al.*, 2003) or purchased from Sigma-Aldrich (Osterode am Harz, Germany) and Santa Cruz Biotechnology, Inc. (Heidelberg, Germany).

6.2 General methods

6.2.1 SDS-polyacrylamide gel electrophoresis (SDS-PAGE) and Western blot

SDS-PAGE was performed using a method of Laemmli (Laemmli, 1970). Protein samples were analyzed by electrophoretic separation in SDS-polyacrylamide gels with running gel buffer (25 mM Tris, 200 mM Glycine and 0.1% (w/v) SDS). The components to cast 4 mini gels are given in Table 6.1:

	Separating gel 15%	Stacking gel
dH ₂ O	3.6 ml	3.6 ml
Acrylamide/Bisacrylamide (30:0.78)	7.5 ml	0.9 ml
SDS-stacking gel buffer (1.5 M TrisHCl, 0.4% (w/v) SDS, pH 8.8)	--	0.7 ml
SDS-seperating gel buffer (0.5 M TrisHCl, 0.4% (w/v) SDS, pH 6.8)	3.9 ml	--
10 % (w/v) SDS	157 μ l	53 μ l
10 % (w/v) APS	157 μ l	53 μ l
TEMED	4.7 μ l	5.3 μ l

Table 6.1 Recipes for separating and stacking gels

After addition of TEMED, the separating gel mixture was briefly mixed and casted immediately. Separating gels were poured about 1 cm below the sample well comb and covered with 70% (v/v) of isopropanol in dH₂O. After complete polymerization of separating gels, the isopropanol solution was removed and the stacking gel together with a comb was added.

Sample preparation: 10 μ l of protein sample were mixed with 10 μ l of 2x SDS loading buffer (0.5 M TrisHCl, pH 6.8, 6 % (w/v) SDS, 35 % (v/v) glycerol, 3.55 % (v/v) β -mercaptoethanol and 0.05 % (w/v) bromophenol blue) and boiled for 10 minutes.

Protein detection by coomassie brilliant blue staining: SDS-gels were soaked in coomassie brilliant blue staining solution (0.1 % (w/v) coomassie brilliant blue G-250 (Serva), 10 % (v/v) acetic acid and 45 % (v/v) methanol in dH₂O) for 20 minutes at room temperature (RT) on an orbital shaker. Gels were destained in destaining solution (10 % (v/v) acetic acid and 45 % (v/v) methanol in dH₂O) at RT on an orbital shaker to visualize the protein bands.

Detection of prion protein by Western blot: the gel was soaked in transfer buffer (3.0 g Tris, 14.4 g Glycine in 200 ml of methanol and 800 ml of dH₂O). A nitrocellulose membrane (same size of the gel) was also soaked in the transfer buffer. Gel and membrane were assembled in a transferring unit (VWR) and the protein bands were electrically transferred from the gel to the membrane at a constant current of 65 mA for 1 hour. The membrane was blocked by treatment with blocking buffer (5 % (w/v) skim milk dissolved in TBST buffer (50 mM Tris-HCl, pH 8.0, 150 mM NaCl and 0.05 % (v/v) tween 20)) at 4°C, overnight (o/n). Next, the membrane was incubated with anti-prion antibody (diluted 1: 20,000 in blocking buffer) for 1 hour at RT on an orbital shaker. The membrane was rinsed for 6 x 5 minutes with TBST buffer. Then the membrane was incubated with secondary antibody, which is conjugated with HRP and can specifically recognize the anti-prion antibody, for 1 hour at RT on an orbital shaker. The membrane was rinsed for 6 x 10 minutes with TBST buffer and drained from TBST buffer. The ECL plus western blotting kit (GE healthcare) was taken from storage at 2 – 8°C and allowed to equilibrate at RT before opening. Detection solutions A and B were mixed at a volume ratio of 40:1 and pipetted on the membrane side containing protein bands. The membrane was incubated with detection reagents for 3 – 5 minutes at RT, and then either exposed to a sheet of autoradiography film (Kodak) which was later developed or imaged by a Chemidoc system (Bio-Rad) using a chemical luminescence filter to visualize protein bands.

6.2.2 CD spectroscopy

Far-UV CD spectra were recorded at 22°C on a Jasco J-715 spectropolarimeter or Applied Photophysics Chirascan Plus system. The PrP proteins were diluted in 20 mM NaOAc, pH 5.0 to final concentration of 0.1 - 0.2 mg/ml. CD spectra were acquired at a speed of 20 nm/min, 1 nm bandwidth and response time of 4 seconds. All spectra were recorded in a 0.1 cm quartz cuvette with a wavelength range between 195 nm and 260 nm, each spectrum was recorded 10 times and subsequently averaged.

6.3. Semisynthesis of lipidated PrP constructs and biochemical assays of PrP-lipid interactions

6.3.1. Cloning work

6.3.1.1 *E. coli* cell culture

The *E. coli* strain XL1 Blue was used to amplify expression plasmids. This *E. coli* strain was grown in 2YT-medium (16 g/l trypton, 10 g/l yeast extract, 5 g/l NaCl) in an incubator (37°C, 200 rpm).

6.3.1.2 Construction of expression plasmids

N-terminally truncated PrP (residues 90-231) (T_PrP): this plasmid was previously constructed in our group (Olschewski *et al.*, 2007). Briefly, mouse PrP (90–231) DNA was PCR amplified and cloned into a modified pTXB3 vector (New England Biolabs) containing the GyrA mini-intein and a chitin-binding domain (CBD) with an additional 6xHis tag between them at *NcoI* and *SapI* restriction sites; thus, the intein fragment was C terminally fused to T_PrP.

Full length PrP (residues 23-231) (FL_PrP): a similar strategy for T_PrP was applied to generate a GyrA mini-intein fusion at the C-terminus of FL_PrP. The coding sequence of mouse PrP(23-231) was PCR amplified using primers PrP23-231 F

(caccattctagaaataatattgtttaactttaagaaggagatatacatatgaaaaagcggccaaagcctggagggtggaacaccggtgg) and PrP 23-231 R (caccatgctcttccgcagctggatcttctcccgtcgaataggcctgggactcc), and the template plasmid pcDNA-MoWT PrP. The resulting PCR product was purified with Qiagen PCR purification kit, restricted and ligated into pTWIN1 plasmid (NEB) at *XbaI* and *SpeI* restriction sites, producing the recombinant plasmid pTWIN1-PrP(23-231) which expresses FL_PrP C-terminally fused to GyrA mini-intein. Next, the ligation mixtures were transformed into *E. coli* XL1 Blue and screened by colony PCR and restriction analysis to identify positive clones for sequencing.

Delta CR PrP (Δ CR_PrP): In this construct the central hydrophobic region (residues 105-125) from FL_PrP was deleted. Primers PrP23-231 F and PrP 23-231 R were also used to amplify the target gene from the template plasmid pcDNA-Mo Δ CR PrP. The gene also was cloned into pTWIN1 plasmid at *XbaI* and *SpeI* restriction sites, and screened to choose positive clones for sequencing.

Both plasmids pcDNA-MoWT PrP and pcDNA-Mo Δ CR PrP were received from Professor David Harris (Boston, USA) (Li *et al.*, 2007).

6.3.1.3 Sequencing

The obtained positive clones were sent to Geneart GmbH (Regensburg, Germany) for sequencing. The sequencing results were aligned with the theoretical sequence to check in-frame fusion of the inserted PrP genes and Mxe intein by Jellyfish software version 2.3.

6.3.2 Expression and purification of recombinant PrP containing a C-terminal thioester

6.3.2.1 Expression

E. coli strains BL21(DE3) RIL or Rosetta 2(DE3) (Invitrogen) were used for expression of T_PrP or FL_PrP and Δ CR_PrP constructs, respectively. The recombinant plasmids were transformed into BL21(DE3) RIL or Rosetta 2 chemical competent cells and plated on 2YT-agar containing 100 μ g/ml ampicillin and 30 μ g/ml chloramphenicol.

One colony for each construct was inoculated in 200 ml of 2YT-medium containing 100 μ g/ml ampicillin and 30 μ g/ml chloramphenicol at 37°C, 200 rpm shaking, o/n. The o/n-culture was transferred into 2 l of fresh 2YT-medium containing antibiotics and shaken at 37°C. Expression was induced at OD_{600nm} = 1.0 by addition of 1.0 mM IPTG to the medium and continued culturing in next 4 hours. Cells from medium were harvested by centrifugation, washed with TBS+EDTA buffer (50 mM Tris-HCl, pH 8.0, 150 mM NaCl, 0.5 mM EDTA) and stored at -80°C for subsequent steps.

6.3.2.2 Purification of PrP-Mxe intein fusion proteins

Isolation of inclusion bodies (IBs): the above harvested cells were defrosted and resuspended in TBS+EDTA buffer. Cells were lysed with a french press system (Constant Systems TS, UK) and centrifuged at 50000 x g, 30 minutes, 4°C to collect the pellet. The pellet was washed with TBS+EDTA buffer containing 0.5% (v/v) Triton X-100 and centrifuged at 50000 x g, 20 minutes, 4°C. Washing and centrifugation

steps were repeated 3 times with TBS+EDTA buffer. Next, IBs were dissolved in 8 M GndHCl, 50 mM Tris-HCl, pH 8.0 by o/n stirring at RT.

Solubilized IB solutions were centrifuged at 50000 x g, 30 minutes, 4°C. The supernatant was collected and loaded on Ni-NTA resin equilibrated with 8 M GndHCl, 50 mM Tris-HCl, pH 8.0. The resin slurry was incubated at room temperature (RT) for 30 minutes and washed with 8 M GndHCl, 50 mM Tris-HCl, pH 8.0. Finally, PrP-Mxe Intein proteins were eluted from the resin with 8 M GndHCl, 50 mM Tris-HCl, 250 mM Imidazole, pH 8.0. The PrP-Mxe Intein proteins were transferred into 8 M Urea, 50 mM Tris-HCl, pH 8.0 using a PD 10 column (GE healthcare). SDS-PAGE was used to check the affinity purification.

Purified PrP-Mxe intein proteins in 8 M Urea buffer were slowly diluted to 4 M Urea with 50 mM Tris-HCl, pH 8.0, and then Sodium 2-mercaptoethanesulfonate (MESNA) (Sigma-Aldrich) was added to reach a final concentration of 500 mM and the mixture was gently stirred at RT, o/n. Cleavage reactions were checked by SDS-PAGE. Next, 8 M GndHCl, 50 mM Tris-HCl buffer was added at the end to dissolve precipitation of PrP-C α thioester proteins. Cleavage mixtures were concentrated and immediately submitted to HPLC purification.

6.3.2.3 HPLC purification of PrP-C α thioester proteins

Buffer A: dH₂O + 0.1% (v/v) TFA

Buffer B: acetonitrile + 0.08% (v/v) TFA

The cleavage mixtures containing PrP-C α thioester proteins were loaded on a preparative C4 column (ϕ 22 mm, L 250 mm, Grace Vydac) equilibrated with 5% (v/v) of buffer B mixed with buffer A at a flow rate of 10 ml/min for 20 minutes. Next, a linear gradient of 30 to 60% (v/v) of buffer B mixed with buffer A over 60 minutes was applied to elute PrP-C α thioesters from the column. Fractions containing rPrP-C α thioester proteins were pooled and analyzed by MALDI-MS or ESI-MS and SDS-PAGE. Pure fractions were lyophilized and either stored at -80°C or directly used for EPL reactions.

6.3.3 Peptide synthesis

6.3.3.1 Synthesis of lipidated peptide

1 H-CKGENLYFQSK_{Palm}AAK_{Palm}K-(PPO)₃-A-OH 16

MW= 3168.9 Da (including 2xPalm and 3xPPO)

In order to synthesize this lipidated peptide, an Fmoc based SPPS was conducted according to the strategy created by Olschewski and colleagues (Olschewski *et al.*, 2007) using F-moc protected amino acids: Ala, Asn(Trt), Gln(Trt), Glu(OtBu), Gly, Lys(Mmt), Phe, Ser(tBu), Tyr(tBu), and Boc protected Cys(Trt) with the corresponding orthogonal protecting groups for side chain put in brackets. Briefly, 0.2 mmol of Fmoc-Ala-Wang-resin was swollen in DMF for 2 hours and Fmoc deprotection was achieved by treatment with 20 % (v/v) piperidine in DMF for 3 minutes and then 7 minutes. The resin was flow washed for 1 minute by DMF to completely remove piperidine. Next, 2.5 molar-equivalents (eq.) of Fmoc-Lys(Mmt) were activated with 2.38 eq. of 0.5 M HBTU in DMF and 5 eq. DIEA, and added to the resin for 30 minutes. After each coupling step, the resin was flow washed with DMF for 1 minute. The Fmoc deprotection and coupling steps were repeated for next amino acids. After Fmoc-Ser(tBu) was coupled to the resin, palmitoylation of Lys(11) and Lys(14) side chains was carried out.

Palmitoylation reaction: Mmt-protected Lys(11) and Lys(14) side chains were deprotected with 1 % (v/v) TFA and 1 % (v/v) TIS in DCM. The resin was flow washed for 1 minute with DCM to remove deprotection solution. Next, 20 eq. palmitoyl chloride, 20 eq. HOBt and 22 eq. triethylamine were dissolved in DCM: DMF (3:1) solution and added to the resin. The reaction was left o/n.

After the palmitoylation reaction was completed, the remaining amino acids of the peptide were coupled as described above. Finally, the resin was vigorously washed with DCM, dried in a vacuum desiccator o/n and stored in -20°C freezer.

6.3.3.2 HPLC purification of lipidated peptides

Cleavage of peptide from resin: 100 mg of the peptide resin was cleaved in 95 % (v/v) TFA, 2.5 % TIS and 2.5 % dH₂O for 3 hours at RT. Next, the crude peptide

was subsequently precipitated with cooled diethyl ether, dissolved in acetonitril/water solution (7:3, containing 0.1% TFA) and lyophilized.

The lyophilized crude peptide was dissolved in 6 M GndHCl, pH 4.7 and purified by HPLC using semi-preparative C4 column (ϕ 10 mm, L 250 mm, Grace Vydac) with elution gradient of 30 to 90% (v/v) of buffer B mixed with buffer A (section 6.3.2.3) at a flow rate of 3 ml/min for 60 minutes. Pure fractions were identified by ESI-MS and checked by analytical HPLC.

6.3.4 Expressed protein ligation (EPL) reactions

0.5 μ mole of rPrP-C α thioester proteins and 2.5 μ mole of lipidated peptides were dissolved in 500 μ l of EPL buffer: 6 M GndHCl, 300 mM Na₂HPO₄, pH 7.8, then 2 % (v/v) thiophenol were added and vigorously mixed. The EPL reactions were incubated at 37°C for 24 hours. The reactions were stopped by adding 15 % (v/v) of β -mercaptoethanol. Reaction yields were checked by SDS-PAGE and ligation products (lipidated rPrP proteins) were purified by the same HPLC procedure as used above (section 6.3.3.2) and lyophilized.

6.3.5 Screening folding condition of PrP

Lyophilized non-lipidated T_PrP was dissolved in 8 M GndHCl, 50 mM Tris-HCl, 1 mM EDTA, pH 8.5. Next, a stepwise dilution method was applied to dilute Guanidine concentration from 8 M to 2 M for 5 hours on ice with dilution buffer (50 mM Tris-HCl, 1 mM EDTA, pH 8.5) containing different concentrations of 1/0.1, 2/0.2, 3/0.3, 4/0.4 or 5/0.5 mM redox glutathione GSH/GSSG couple and then incubated o/n at 10°C. The diluted protein solutions were loaded in D-tube dialyzer 10 kDa, MWCO (Millipore) and dialyzed against storage buffer: 20 mM NaOAc, pH 5.0, the storage buffer should be exchanged at least 3 times for 8 hours at 10°C. Next, the folded protein solutions were centrifuged at 100000 x g, 1 hour, 4°C (TLA 45 rotor, Optima Beckman ultracentrifugation system) to remove misfolded PrP in pellet. The supernatants were collected and analyzed by CD spectroscopy.

6.3.6 Folding of lipidated rPrP proteins

Based on the folding conditions were found from section 6.3.5, the lyophilized lipidated rPrP proteins were dissolved in 8 M GndHCl, 50 mM Tris-HCl pH 8.5, 1 mM EDTA and 3.0/0.3 mM GSH/GSSG. A stepwise dilution strategy was also applied to dilute from 8 M to 2.5 M Gnd by dilution buffer 50 mM Tris-HCl, pH 8.5, 1 mM EDTA and 20 mM n-octyl- β -D-glucoside (OG) on ice. The folding reactions were incubated at 10°C for at least 48 hours to prevent precipitation in the following step in which lipidated PrPs were exchanged into storage buffer (20 mM Sodium acetate, pH 5.0 and 20 mM OG) using a Nap5 column (GE healthcare). Ultracentrifugation was applied and the supernatant was collected for CD spectrometry analysis.

Similar folding protocols were applied for non-lipidated PrP constructs.

6.3.7 Preparation of phospholipid small unilamellar vesicles (SUVs)

By sonication

5 mg of phospholipids were dissolved in 1 ml of chloroform in a 25 ml round bottom flask, chloroform was evaporated by nitrogen flow to form a thin lipid film. The film was dried in a vacuum desiccator for at least 2 hours or o/n. Hydration of the film was performed in 20 mM sodium phosphate, pH 7.0 for 1 hour, vortex every 10 minutes in between to have an opalescent solution (large multilamellar vesicles (MLV) were formed in this step). The MLV suspension was flushed for 15 minutes by argon and then sonicated on ice to have a clear solution. Next, an ultracentrifugation step with 100000 x g, 4°C, for 1 hour (TLA 45 rotor, Optima Beckman ultracentrifugation system) was used to remove precipitated phospholipids. The resulting vesicles were stored under argon at 4°C, o/n for the next steps.

By extrusion

To increase the efficiency of encapsulation of calcein into vesicles, an extrusion protocol was applied. After the hydration step to form MLV suspension, the MLV suspension was frozen in dry ice-methanol for 5 seconds, and vortexed rapidly to form a thin freeze layer of phospholipid on the wall of the tube. Next, the frozen phospholipid layer was thawed by warming up the tube under cool tap water and

then warm (42°C) water for 30 seconds. The freeze/thaw cycle was repeated 5 times. The lipid solution was passed 20 times through mini-extruder with a 100 nm polycarbonate membrane (Avanti Polar Lipids). The resulting SUV solution was collected and kept under argon at 4°C for next steps.

Vesicles were produced with the following phospholipids:

+ Non-charged phospholipid: DPPC, DOPC

+ Negatively charged phospholipid: POPG

+ Vesicles mimicking neuronal membrane: PC : PE : PI : SM : Chol : PG or PS = 30 : 30 : 2.5 : 5 : 22.5 : 10 (Mingeot-Leclercq *et al.*, 2002).

Quantification of phospholipid in vesicles by colorimetric method

This method is based on the formation of a colored complex between phospholipid molecules and ammonium ferrothiocyanate. The resulting red-colored complex is collected in the chloroform phase and absorbs at a wavelength of 488 nm (Stewart, 1980). Ammonium ferrothiocyanate solution was prepared by dissolving 27 g of ferric chloride ($\text{FeCl}_3 \cdot 6\text{H}_2\text{O}$) and 30 g of ammonium thiocyanate (NH_4SCN) in 1 liter of dH_2O and stored at RT in a brown bottle. A calibration curve of phospholipid was generated by measuring different amounts of DOPC. To this end, DOPC was dissolved in 2 ml chloroform and then 1 ml of ammonium ferrothiocyanate solution was added. The mixtures were vigorously vortexed and centrifuged at 1000 x g for 3 minutes. Chloroform phases were collected and absorption was measured at 488 nm. Data points of $\text{OD}_{488\text{nm}}$ and corresponding amounts of DOPC were processed to generate a linear calibration curve (Figure 6.1). The same colorimetric protocol was applied to phospholipid vesicles to determine the concentration of phospholipid in vesicles.

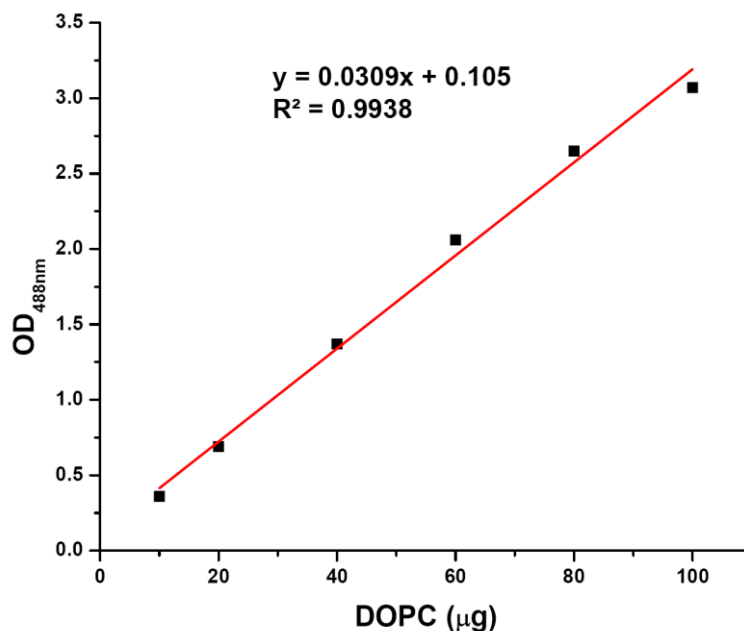


Figure 6.1 Calibration curve for phospholipid DOPC

6.3.8 Incubation of PrP with phospholipid vesicles

Only fully soluble PrP from folding step was used here. PrP was mixed with phospholipid vesicles in indicated molar ratios and incubated at RT or 37°C for 30 or 60 minutes. Mixtures were submitted to flotation assays, PK digestions or fluorescence-based assays.

6.3.9 Flootation assay

For the discontinuous flotation assays, PrP proteins and vesicles were mixed and incubated for 30 minutes at RT. The mixtures was added to Iodixanol stock solution (Optiprep, Sigma-Aldrich) to have 1 ml of 36 % (v/v) Iodixanol and transferred into centrifuge tubes. Next, 1 ml of 31 % Iodixanol solution and 0.4 ml of 5 % Iodixanol solution were added sequentially. The gradient was centrifuged at 200,000 x g, 4°C for 3 hours (MLS 50 rotor, Optima Beckman ultracentrifugation system). Next, 200- μl fractions were collected from top to bottom of the centrifuge tube and PrP in each fraction was precipitated by adding 1 volume of 40 % (w/v) TCA, incubated on ice for 20 minutes and centrifuged at 16000 x g, 4°C for 15 minutes. Pellets from TCA precipitation were washed with cold acetone and dissolved in 1x SDS loading buffer for SDS-PAGE and Western blot analysis.

6.3.10 Proteinase K (PK) digestion

20 μ l of PrP-phospholipid mixtures were subjected to PK digestions at 37°C for 30 minutes with indicated PK:PrP molar ratios of 1:4, 1:8 and 1:16. Reactions were stopped by adding 5 mM phenylmethanesulphonyl fluoride (PMSF) and kept on ice for 15 minutes. The mixtures were subjected to SDS-PAGE and Western blot analysis.

6.3.11 Preparation of calcein-containing vesicles (Cal-SUVs)

Lipid films of DOPC, POPG or phospholipid components mimicking neuronal membrane (NM-PG or NM-PS) were hydrated in 20 mM sodium phosphate, pH 7.0 containing 60 mM calcein (Sigma Aldrich). At this concentration, the calcein fluorescence is self-quenched (Sanghera & Pinheiro, 2002). The Cal-SUVs were generated using the extrusion protocol (section 6.3.7). The resulting Cal-SUVs were separated from free calcein by sucrose density gradient ultracentrifugation (Haginoya *et al.*, 2005).

A 0.5 ml portion of 9, 13.4, 17.2, 21, 25.1, 29.5, 32.5 and 37 % (w/v) sucrose solutions prepared in 20 mM sodium phosphate, pH 7.0 were loaded into centrifugation tubes to form a discontinuous gradient. 350 μ l of SUV suspension was mixed with 650 μ l of 64 % sucrose solution to generate a SUV suspension in ~40 % (w/v) sucrose aqueous and the suspension was placed at the bottom of the discontinuous sucrose gradient (Figure 6.2). After centrifugation at 200000 x g, 4°C for 3 hours (MLS 50 rotor, Optima Beckman ultracentrifugation system), the orange-colored fractions on the top of the gradient were collected for next calcein release assays.

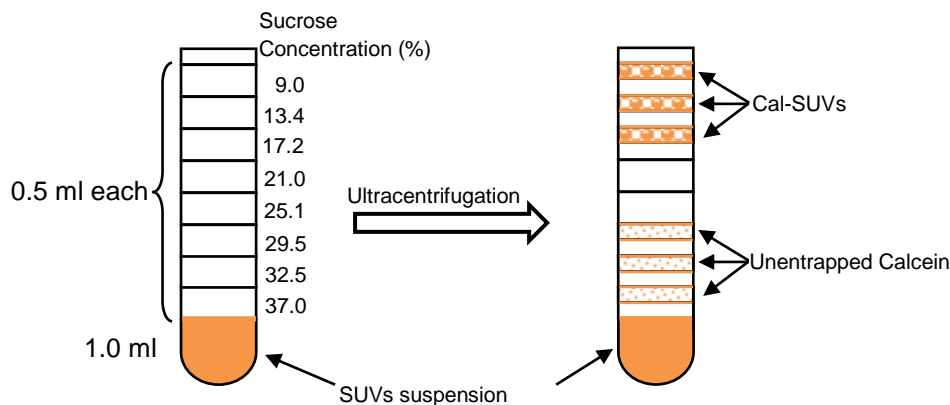


Figure 6.2 Schematic diagram for purification of Cal-SUVs by sucrose density gradient ultracentrifugation

6.3.12 Calcein release

The release of calcein from the calcein-entrapped vesicles was monitored by calcein fluorescence at 512 nm over 120 minutes after mixing five parts of Cal-SUVs and one part of protein solutions (5:1, v/v). The excitation wavelength was 490 nm. Experiments were carried out at RT. The concentration of Cal-SUVs was 50 μ M and protein concentrations varied from 10 to 500 nM. Release of calcein from vesicles leads to an increase of the fluorescence of calcein due to dilution of calcein concentration and consequent relief of self-quenching. The percentage of calcein release (R_f) was calculated based on equation 1:

$$R_f = (F_t/F_{Tot}) - (F_0/F_{Tot}) \quad (\text{eq. 1})$$

where F_t is the fluorescence intensity recorded at time t after adding PrP to vesicles, F_0 is fluorescence intensity without PrP proteins, and F_{Tot} is the total fluorescence intensity recorded after total release of calcein by disrupting the vesicles with 1 % (v/v) of Triton X-100.

Each measurement was repeated 3 times, and measured in 96-well plates with a micro plate reader (Biotek Synergy Mx).

6.3.13 NBD fluorescence quenching

The NBD-PE (N-(7-nitrobenz-2-oxa-1,3-diazol-4-yl)-1,2-dihexadecanoyl-*sn*-glycero-3-phosphoethanolamine) (Avanti Polar Lipids) was dissolved in chloroform

and added to phospholipids: DOPC, POPG alone or phospholipid mixtures mimicking neuronal membrane: NM-PG, NM-PS at 1 mole % and dried under N₂ flow to form thin films. The films were put inside a vacuum desiccator for 2 hours to remove chloroform completely. Dried films were used to produce NBD-vesicles by extrusion method (section 6.3.7).

Samples for fluorescence measurements were prepared by adding PrP at concentration of 1 μM or buffers only (blank run) and 200 μM NBD-vesicles to 20 mM sodium phosphate, 150 mM NaCl, pH 7.0. Fluorescence quenching measurements were initiated by adding 10 mM of the quencher sodium dithionite (SDT) (Merck) from a 130 mM stock solution, freshly prepared in 50 mM Tris base buffer, pH ~11. The NBD fluorescent kinetics was recorded for 900 seconds at 22°C using an excitation wavelength of 467 nm and an emission wavelength of 535 nm on a Flouromax 4 system (Horiba). The NBD fluorescence decay was calculated as a percentage of the initial NBD fluorescence measured before adding SDT (Mandal *et al.*, 2012).

6.3.14 Tryptophan fluorescence

The interaction of PrP with DOPC or POPG vesicles was monitored by a blue shift in tryptophan fluorescence wavelength. For each PrP constructs: FL_PrP, ΔCR_PrP and T_PrP, the optimal molar ratio of PrP and lipid vesicles was found by mixing 3 μM of non-lipidated PrPs with different concentrations of lipid vesicles (from 3 μM to 2 mM). Next, the optimal ratio was used to compare between lipidated and non-lipidated PrPs. Tryptophan fluorescence measurements were performed by mixing protein solution with an equal volume of lipid vesicles. After equilibration for 3 minutes four fluorescence spectra from 300 to 450 nm were recorded and averaged on a Flouromax 4 system (Horiba) with an excitation wavelength of 295 nm (2 nm bandwidth) at 22°C. Fluorescent background was also recorded and subtracted from the final spectra (Sanghera & Pinheiro, 2002).

6.3.15 Tryptophan fluorescence quenching

Tryptophan fluorescence quenching measurements were performed by adding freshly prepared aliquots of 1 M acrylamide stock solution in 20 mM sodium phosphate, pH7.0 to PrP in presence or absence of lipid vesicles: DOPC or POPG at concentrations 3 μM of PrP and 3 mM of lipid vesicles. Tryptophan fluorescence

spectra were recorded for each concentration of the quencher acrylamide. Addition of acrylamide, which can absorb at the excitation wavelength of tryptophan fluorescence, leads to the attenuation of the excitation light intensities. Thus, the measured fluorescence spectra were corrected by multiplying with the factor as given in equation 2 (Raja *et al.*, 1999):

$$\text{Factor} = \text{antilog} [(A_{\text{ex}} + A_{\text{em}})/2] \quad (\text{eq. 2})$$

A_{ex} and A_{em} are the absorbance of a given concentration of acrylamide at the excitation wavelength and the maximal emission wavelength of tryptophan fluorescence, respectively.

The fluorescence quenching data was analyzed by using the Stern-Volmer equation (Stern and Volmer, 1919) for collisional quenching as given in equation 3:

$$F_0/F = 1 + K_{\text{SV}}[Q] \quad (\text{eq. 3})$$

F_0 is the initial fluorescence, F is the fluorescence at the acrylamide concentration $[Q]$, and K_{SV} is the Stern-Volmer's constant. A plot of F_0/F versus $[Q]$ gives a linear plot which yields the K_{SV} value.

6.3.16 Cryo electron microscopy (EM) measurements

This work is collaboration with Guenter Resch (Electron Microscopy, Campus Science Support Facilities GmbH, Vienna, Austria). Two samples including POPG vesicles alone and POPG vesicles mixed with lipidated $\Delta\text{CR_PrP}$ were prepared and visualized under a TEM system (FEI Tecnai F30 Helium "Polara"). The resulting images were processed and added a scale bar by using Image J software.

6.4 Construction of plasmids for soluble expression of PrP-Mxe intein in *E. coli*

6.4.1 Plasmid construction

The *E. coli* K12 DnaK-encoding gene was PCR-amplified and cloned into plasmid pET30b (Novagen) at *Nde*I and *Bam*HI sites to yield plasmid pET30-DnaK with additions of an N-terminal 6xHis-tag for affinity purification and a C-terminal *Xho*I site for subcloning. Subsequently, the gene encoding for T_PrP was PCR-amplified and cloned into pET30-DnaK at *Xho*I and *Bam*HI with additional insertion of a TEV-

cleavage site between PrP and DnaK to give plasmid pET30-HDP which encodes the following fusion construct: 6xHis-DnaK-TEV-PrP (HDP).

To remove the substrate binding domain (SBD) from a DnaK-PrP fusion construct and also replace the TEV-cleavage site by a Sortase A-site, the T_PrP encoding gene was cloned into pET30-DnaK at *NcoI* and *BamHI* to obtain the pET30-ASP plasmid, which can express the 6xHis-ATPase-SrtA-PrP (ASP) construct. To generate soluble PrP containing a C-terminal α -thioester group for EPL reactions, the ASP construct was C-terminally fused with the *Mxe* GyrA mini-intein and a chitin-binding domain (CBD) by simple subcloning an *NcoI-BamHI* fragment from a pTXB3-PrP plasmid into pET30-ASP plasmid to form the construct: 6xHis-ATPase-SrtA-PrP-MxeIntein-6xHis-CBD (ASPM).

6.4.2 Protein expression and purification

Small-scale expression tests:

A single colony was picked and inoculated in 5 ml of 2xYT medium at 37°C, o/n. Next, a 25 ml fresh 2xYT medium was inoculated with 1 ml of pre-culture at 37°C until $OD_{600nm} = 0.5$. At that point 0.2 mM of IPTG was added to induce expression of PrP constructs at 25°C o/n. Cells were harvested, re-suspended in PBS buffer and lysed by ultrasonication (Bandelin sonopuls HD2070 system) on ice, followed by centrifugation at 16000 x g for 20 minutes at 4°C. Pellet, supernatant as well as total protein from lysate were loaded on SDS-PAGE to analyze the expression and solubility of PrP constructs.

Expression and purification of PrP fusion constructs:

Similar expression conditions as described above were applied for 1 liter-culture expression for each of PrP fusion constructs: HDP, ASP and ASPM. The cells were harvested and resuspended in lysis buffer (20 mM NaPi, pH 7.5, 300 mM NaCl, 10 mM Imidazole, 2 mM DNaseI (Roche), 2 mM PMSF). The suspension solution was passed 2 times through french press (18000 psi, Basic Z, Constant Cell Disruption System) and the lysate was centrifuged at 50000 x g for 30 minutes at 4°C to collect the soluble fraction which was subsequently loaded on NiNTA column equilibrated with lysis buffer. The column was washed by 5 column volumes of lysis

buffer and eluted with elution buffer (20 mM NaPi, pH 7.5, 100 mM NaCl, 250 mM Imidazole). The fractions of NiNTA purification were loaded on SDS-PAGE to analyze solubility and purity of proteins.

6.4.3 Protease cleavage reactions

Purified HDP protein was cleaved by TEV protease as previously described (Phan *et al.*, 2002). Briefly, a ratio of HDP and TEV is 30:1 (w:w) was mixed in 50 mM Tris-HCl, pH 8.0, 0.5 mM EDTA, 2 mM PMSF and 3 mM/0.3 mM GSH/GSSG, and incubated at 10°C o/n.

Finding optimal condition for Sortase A cleavage reaction of ASP protein: the cleavage of purified ASP protein by SrtA in several different molar ratios of ASP to SrtA: 1:1, 1:2, 1:5, 1:10 was carried out in 50 mM Tris-HCl, pH8 buffer containing CaCl₂ and Gly-Gly-Gly (3xGly) to facilitate the performance of SrtA (Ton-That *et al.*, 1999). The yield of cleavage reactions was analyzed by SDS-PAGE. Next, the cleavage reactions were centrifugally separated into two fractions: supernatant (S) and pellet (P), and were subjected to SDS-PAGE analysis together with one sample of each cleavage reaction before centrifugation, total (T). The optimal condition was applied for cleavages of purified ASP and ASPM proteins.

6.4.4 Preparation of ASP fusion protein containing a C-terminal α -thioester

Purified ASPM protein was immobilized on chitin beads and cleaved by addition of 250 mM sodium 2-mercaptoethanesulfonate (MESNA) in 50 mM Tris-HCl, pH 8.0 at 4°C o/n. The resulting ASP containing C-terminal α -thioester (ASP-SR) found in the flow through of the cleavage reaction was submitted to a Superdex 75 (16/60) column equilibrated with 50 mM Tris-HCl buffer at a flow rate of 0.5 ml/min. Pure fractions of ASP-SR were pooled and concentrated by using centrifugal amicon 30 kDa MWCO (Milipore).

6.4.5 Synthesis of NBD-labeled peptide

The NBD peptide with amino acid sequence: H-Cys-Gly-Lys_{NBD}-Gly-(His)₆-OH was synthesized by Boc-based SPPS as previously described (Becker *et al.*, 2003). Next, the peptide was cleaved from the resin by HF solution. Crude peptide were

subsequently precipitated with cooled diethyl ether, dissolved in acetonitril/water mixtures (1:1, containing 0.1% TFA) and lyophilized. The peptide was purified by HPLC using a semi-preparative C8 column (ϕ 10 mm, L 250 mm, Grace Vydac) with a flow rate of 3 ml/min and a linear gradient from 5 to 45% (v/v) of buffer B mixed with buffer A (section 3.3.2.3) for 60 minutes. The purity of NBD peptide was analyzed by analytical HPLC with C18 column and the mass of peptide was confirmed by ESI-MS.

6.4.6 Expressed protein ligation

Expressed protein ligation (EPL) was carried out in 50 mM Tris-HCl, pH 8.0, 2% (v/v) ethanethiol by using concentrations of 50 μ M ASP-SR and 500 μ M NBD peptide at room temperature for 24 hrs. Reactions were analyzed by SDS-PAGE followed by fluorescence scanning and coomassie staining. Reaction mixtures were dialyzed against 50 mM Tris-HCl buffer and Sortase A was added.

6.4.7 Aggregation assays

A semi-automated aggregation assay using a 96-well plate was carried out as previously described (Breydo *et al.*, 2008). Briefly, the reaction mixtures were prepared in 20 mM NaOAc, pH 5.0 buffer containing 0.2 mg/ml of PrP variants and 10 μ M ThT as well as 2 M Guanidine-HCl were added. After thoroughly mixing the solution was divided in three wells of the 96-well plate (160 μ l/well) together with one glass bead (2 mm diameter, Merck) and the plate was covered with a plate sealer. Next, the plate was continuously shaken at 37°C in a microplate-reader system (Biotek Synergy Mx) and ThT fluorescence was recorded every 10 min at the excitation wavelength of 444 nm and an emission wavelength of 485 nm.

6.5 Semisynthesis of SMN-sDMA proteins

6.5.1 Plasmid construction

DNA encoding for the Tudor domain of human SMN protein (residues 81-149) was PCR amplified and cloned into a modified pTXB3 vector (New England Biolabs) containing the GyrA mini-intein and a chitin-binding domain (CBD) with an additional 6xHis tag between them at *Nco*I and *Spe*I restriction sites. A similar screening

procedure as described in section 6.3.1.2 was applied to choose positive clones which were later sequenced to confirm in-frame fusion of the inserted SMN gene and *Mxe* intein.

6.5.2 Expression and purification of ^{15}N - ^{13}C labeled SMN Tudor-*Mxe* intein fusion protein

For expression of isotope-labeled SMN, the pTXB3-SMN harboring BL21(DE3)RIL cells were inoculated o/n at 37°C in 10 ml of M9 minimum medium containing ^{13}C -glucose and ^{15}N -ammonium chloride and 100 µg/ml of ampicillin and 30 µg/ml of chloramphenicol. The entire cultured medium was transferred into 1 liter of warm (37°C) M9 minimum medium and grown at 37°C until the absorption at 600 nm reached 0.6. Expression was induced by addition of 1mM of IPTG and cultures were grown at 20°C, o/n. Cells were harvested by centrifugation, resuspended in lysis buffer (50 mM Tris-HCl, pH 7.5, 300 mM NaCl, 10 mM imidazole) and lysed with a french press (Basic Z, Constant Cell Disruption System). The lysate was centrifuged at 50000 g for 30 minutes at 4°C and the supernatant was loaded on a Ni-NTA column previously equilibrated with lysis buffer. The column was washed by 5 column volumes of lysis buffer and SMN Tudor-Intein-6xHis was eluted with a buffer containing 50 mM Tris-HCl, pH 7.5, 300 mM NaCl and 330 mM imidazole. The eluate fractions were loaded on a Superdex 75 (16/60) column equilibrated with 50 mM Tris-HCl, pH 7.5, 500 mM NaCl. The pure fractions were identified by SDS-PAGE and pooled for next steps.

6.5.3 Synthesis of sDMA peptides

F-moc-based SPPS was used to synthesize sDMA peptides. Briefly, 0.2 mmol of Fmoc-glycine-Wang resin (Novabiochem) was swollen in DMF for 2 hrs. F-moc deprotection was achieved by treatment with 20% (v/v) piperidine in DMF for 3 minutes and 7 minutes, 2.5 eq. of Fmoc-symmetric dimethylarginine (sDMA) were activated with 2.38 eq. of 0.5 M HBTU in DMF and 5 eq. DIEA, and added to the resin for 30 minutes. Peptides containing 4, 2 and 1 glycine residue between the N-terminal cysteine and sDMA were prepared. Each step was followed by 1 minute flow-washes with DMF to remove excess reagents. Before cleavage the peptide-resins were vigorously washed with DCM and cleaved with a mixture of 2.5% dH_2O ,

2.5% triisopropylsilane (TIS) in TFA for 3 hrs. Crude products were subsequently precipitated with cooled diethyl ether, dissolved in acetonitril/water mixtures (1:1, containing 0.1% TFA) and lyophilized. All peptides were purified by HPLC using a semi-preparative C8 column (ϕ 10 mm, L 250 mm, Grace Vydac) and linear gradient from 2 to 40% of buffer B mixed with buffer A (section 6.3.2.3) for 60 minutes. Pure fractions of the peptides were identified by ESI-MS.

6.5.4 Expressed protein ligation and purification of SMN-SDMA proteins

100 μ M of purified SMN-Intein-6xHis protein was mixed with 500 μ M of sDMA peptides in 500 μ l of 50 mM Tris-HCl at pH 8.0 and 2% (v/v) ethanethiol were added. The EPL reactions were incubated at room temperature for up to 24 hours and 12 mM of TCEP was subsequently added to keep the cysteine residues reduced. Crude ligation products were purified by Ni-NTA column. The flow-through containing the ligation product without a Histag (SMN-sDMA proteins) were loaded on a Superdex 75 (16/60) column and separated from excess sDMA peptides using a buffer consisting of 20 mM NaPi, pH 6.8, 100 mM NaCl and 0.02 % NaN_3 .

6.5.5 NMR spectroscopy

NMR measurements were carried out at 298^oK on a Bruker Avance III 750-MHz spectrometer equipped with a TXI probe head. For each ligated protein, the concentration was 200 μ M in a buffer containing 20 mM NaPi, pH 6.8, 100 mM NaCl, 2mM deuterated DTT, and 7% (v/v) $^2\text{H}_2\text{O}$ for the lock.

7. Results and discussions

7.1. Semisynthesis of C-terminally lipidated prion protein variants (PrPs) and the effect of a C-terminal membrane anchor on the interactions of PrP with membranes

7.1.1 PrP constructs

Previous studies suggest that binding of prion protein to lipid membranes includes electrostatic and hydrophobic interactions (Sanghera & Pinheiro, 2002; Wang *et al.*, 2010b). Concerning the electrostatic interaction, the PrP 23-120 N-terminus contains two clusters of basic amino acid residues: one at the very N-terminus (residues 23-27) and the other in the middle region (residues 95-110, cyan panels in Figure 7.1). The hydrophobic interaction has been shown to be mainly mediated by the central hydrophobic region (residues 110-125) (Wang *et al.*, 2010b). In order to study the effect of the C-terminal GPI anchor on the interaction of prion protein and lipid membranes, PrP variants including full length PrP (residues 23-231) (FL_PrP); Δ CR_PrP with central hydrophobic region (residues 105-125) removed; and N-terminally truncated PrP(residues 90-231) (T_PrP) were prepared in both lipidated and non-lipidated forms as shown in Figure 7.1.

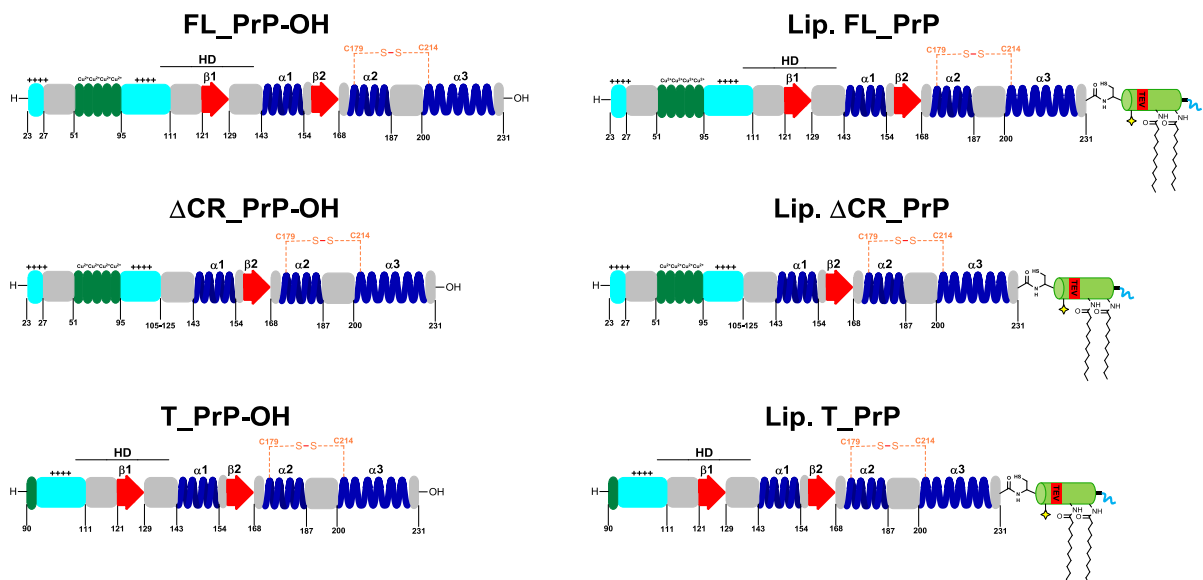


Figure 7.1 Schematic representation of PrP constructs

7.1.2 Preparation of PrP- α thioesters

7.1.2.1 Construction of plasmids

Genes encoding for FL_PrP and Δ CR_PrP were cloned into plasmid pTWIN1 at XbaI and SpeI restriction sites to generate FL_PrP and Δ CR_PrP in fusion with *Mycobacterium xenopii* GyrA mini-intein (*Mxe* intein) at the C-termini. These constructs were generated in accordance to the method previously described by Olschewski and colleagues (Olschewski *et al.*, 2007) (Figure 7.2 A, bottom). The resulting plasmids (Figure 7.2 A) were sequenced (GeneArt GmbH, Regensburg) and aligned with the expected sequence.

7.1.2.2 Intein cleavage and HPLC purification

The resulting PrP-intein fusion proteins were expressed in *E. coli*, and purified from inclusion bodies under denaturing conditions by affinity chromatography using Ni-NTA resin (section 6.3.2.2).

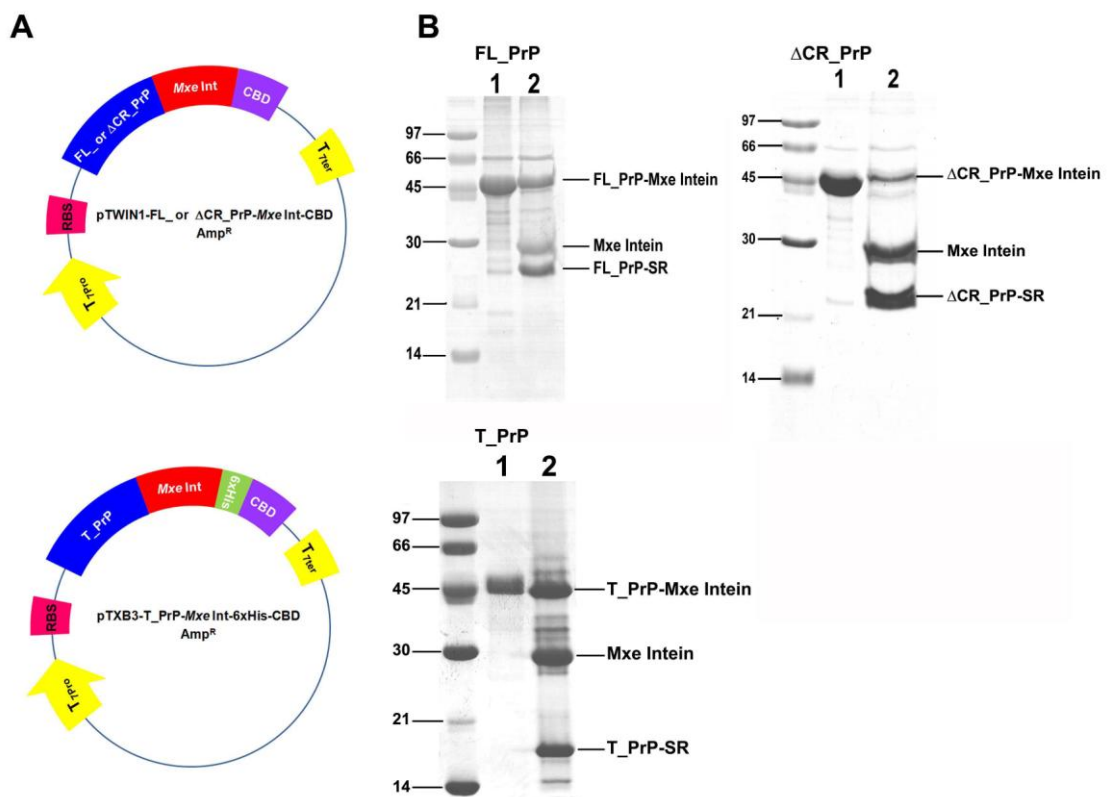


Figure 7.2 A) Plasmid maps of FL_PrP or Δ CR_PrP (top) and T_PrP (bottom) C-terminally fused to *Mxe* intein. B) Cleavage reactions of PrP-intein fusion proteins.

To achieve partial folding of the *Mxe* intein for cleavage reactions, PrP-intein fusion proteins were transferred from guanidine-containing buffer into 4 M urea buffer. Addition of MESNA induced the cleavage reactions and resulted in PrP proteins with C-terminal α -thioesters. SDS-PAGE analysis of the cleavage reactions in lane 2 of Figure 7.2 B shows two new bands, one corresponding to PrP-C α -thioesters and the other to *Mxe*-intein-6xHis-CBD. Next, the resulting PrP-C α -thioesters were separated from *Mxe* intein and remaining PrP-*Mxe* intein by reversed phase HPLC (section 6.3.2.3). SDS-PAGE analysis shows a single band of PrP-C α -thioesters for FL_PrP and T_PrP (Figure 7.3 A). In case of Δ CR_PrP construct, besides a predominant band corresponding to Δ CR_PrP-C α -thioester, the second band was supposed to be a formation of dimer of Δ CR_PrP (Figure 7.3 A) as previously described (Knaus *et al.*, 2001; Pavlicek *et al.*, 2007). The molecular mass of the resulting PrP-C α -thioesters was also determined by MALDI-MS with high agreement with calculated mass (Figure 7.3 B).

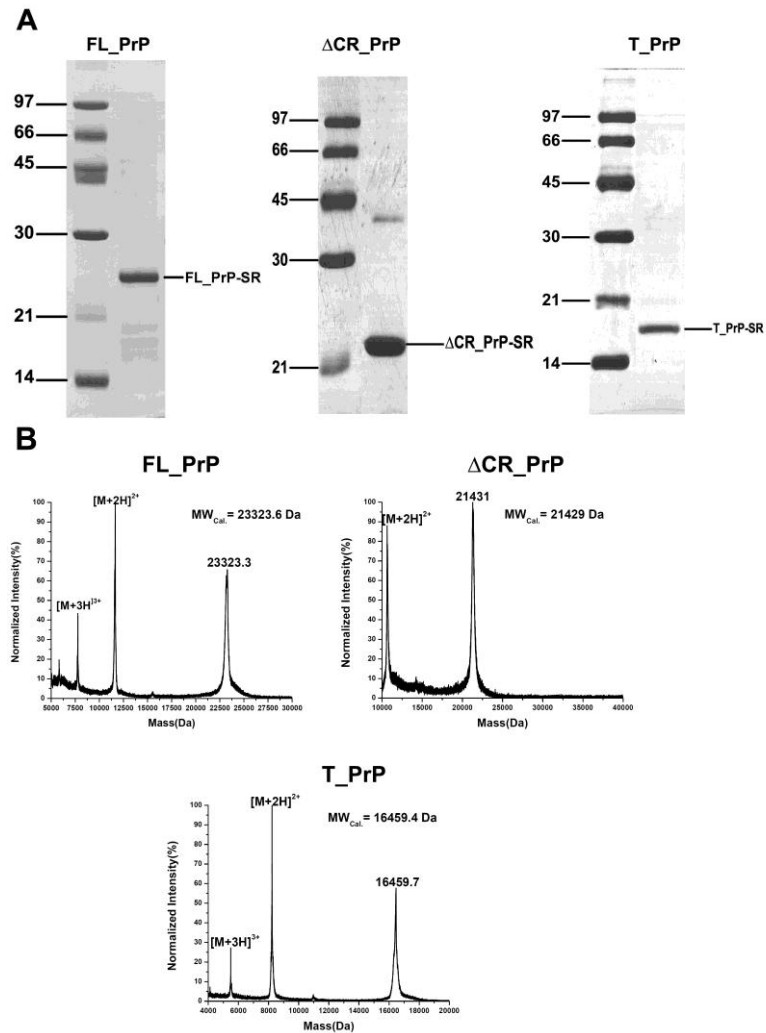


Figure 7.3 Purified PrP-C α -thioesters A) SDS-PAGE and B) MALDI-MS analyses.

7.1.3 Synthesis and purification of membrane anchor peptide

The attachment of a GPI anchor at the C-terminus of eukaryotic proteins is a posttranslational event that locates the modified proteins on the outer leaflet of cellular membranes (Paulick *et al.*, 2007). A native GPI anchor consists of a phosphoethanolamine linker, a conserved glycan core and a phospholipid tail (Figure 7.4 A). Even though the chemical synthesis of a GPI anchor has been already achieved, the supply of sufficient amounts remains a challenge. On the other hand, a peptide synthesis approach was developed to produce a GPI-mimicking lipidated peptide (Figure 7.4 C) in multimilligram amounts. Subsequently, the lipidated peptide was ligated to PrP. The biochemical characteristics of the resulting lipidated PrP were very similar to that of PrP containing a synthetic GPI anchor (Figure 7.4 B) in

aggregation assays (Becker *et al.*, 2008). This lipidated peptide contains an N-terminal cysteine for EPL reactions and two palmitoyl groups at the side chains of two lysine residues for interactions with phospholipid membranes. However, the double-palmitoylated peptide gave problems in purification and in its subsequent use in ligation reactions due to its low solubility. In order to solve this problem, a short polyethyleneglycol (PEG)-like solubilization tag was introduced at the C-terminal alanine residue (Becker *et al.*, 2004). In addition, a TEV cleavage site (red residues ENLYFQ in Figure 7.4 C) was inserted for optional detachment of PrP from the membrane anchor.

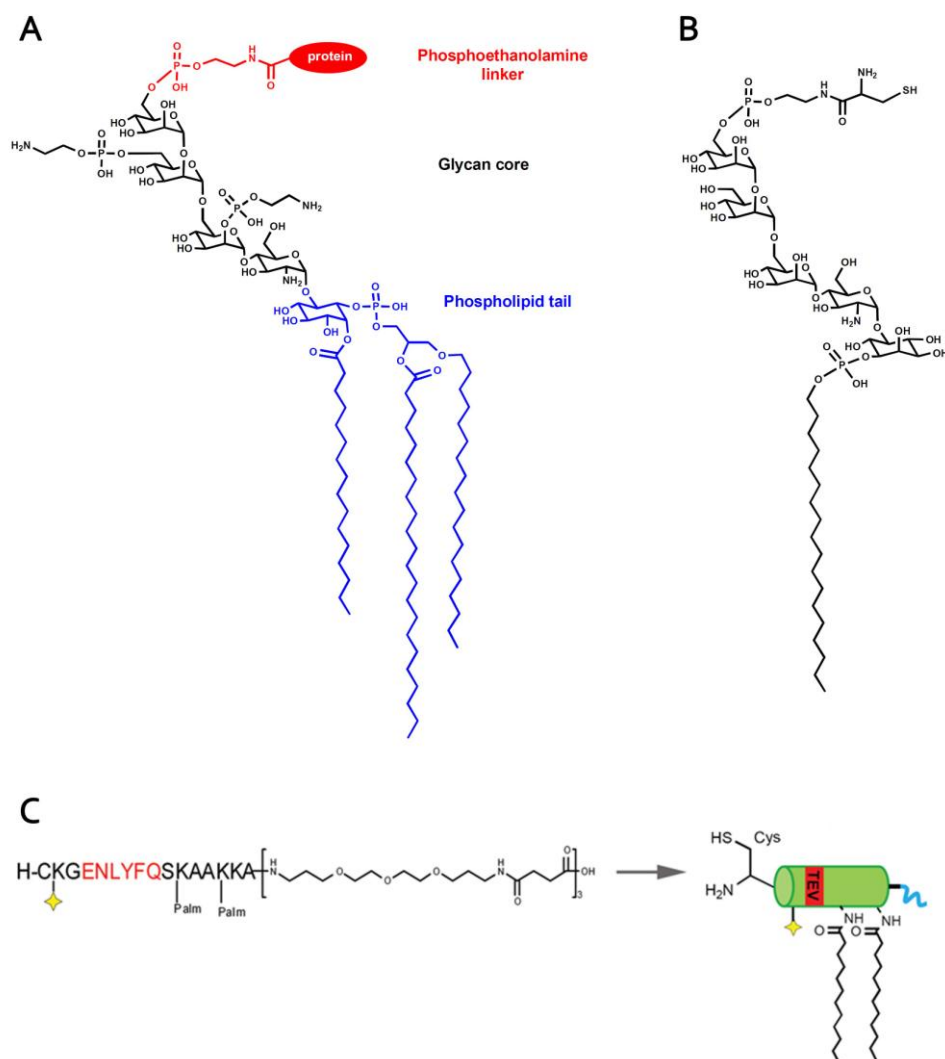


Figure 7.4 A) Structure of native GPI anchor from human erythrocyte acetylcholinesterase (Paulick *et al.*, 2007). B) Synthetic GPI anchor containing C18 alkyl chain and a cysteine residue for NCL (Olschewski & Becker, 2008). C) Lipidated

peptide that was used in this thesis from the strategy previously developed in our group (Olschewski et al., 2007).

Fmoc-based SPPS strategy was applied for synthesis of the lipidated peptide. Subsequently, the crude peptide was purified by HPLC. Pure fractions of the peptide were collected and analyzed by ESI-MS and analytical HPLC.

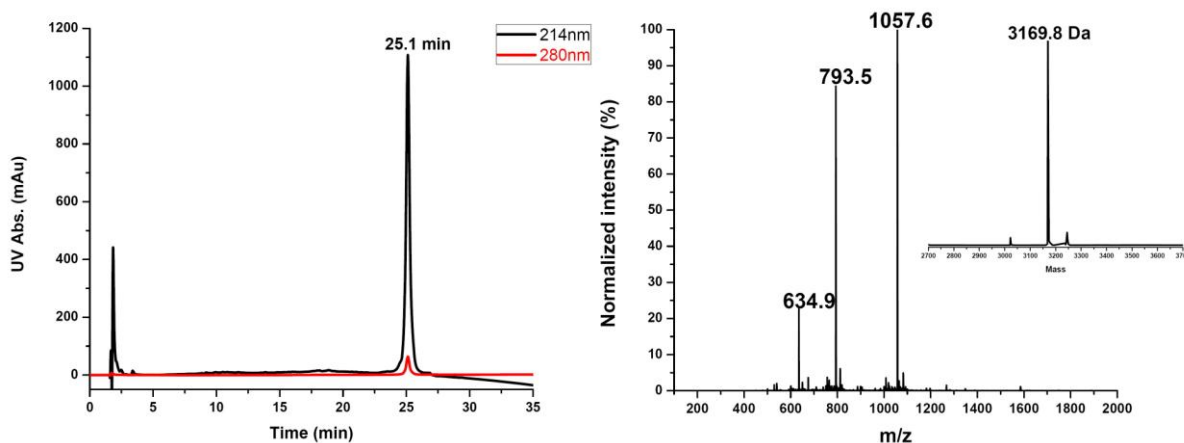


Figure 7.5 Analytical HPLC chromatogram (left) and ESI-MS spectrum (right) with deconvoluted mass spectrum of membrane anchor.

The main peak seen in the analytical HPLC chromatogram (Figure 7.5, left) at a retention time of 25.1 min can be assigned to the expected product. In ESI-MS measurement (Figure 7.5, right), the charge states of the peptide at three (1057.6), four (793.5) and five (634.9) positive charges resulted in a deconvoluted mass of 3169.8 Da, which is in good agreement with the calculated mass of 3168.1 Da. Typically, 30 mg of pure lipidated peptide from a 0.2 mmol synthesis scale can be produced.

7.1.4 Expressed protein ligation (EPL) and HPLC purification of lipidated PrP proteins

7.1.4.1 EPL reactions

PrP-C α thioester proteins were mixed with the lipidated peptide within guanidine-containing buffer and reactions were initiated by addition of 2% (v/v) thiophenol. SDS-PAGE analyses of EPL reactions show new bands with molecular

masses corresponding to the expected ligation products of lipidated peptide and PrP proteins. The yield of each EPL reaction is approximately 50 % (Figure 7.6).

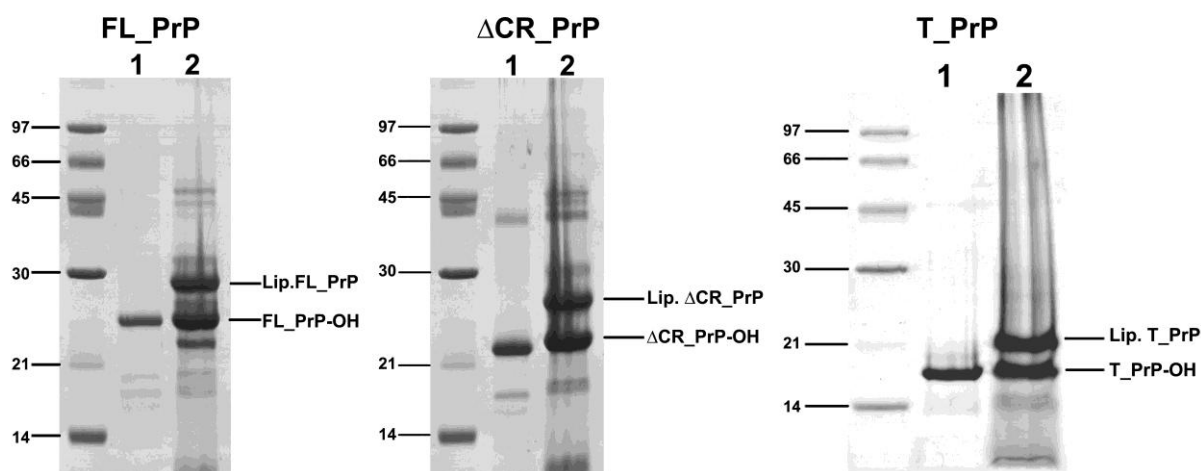


Figure 7.6 SDS-PAGE analysis of EPL reactions between the lipidated peptide and PrP-C α thioester proteins

7.1.4.2 HPLC purification of lipidated PrP proteins

Lipidated PrPs were purified via RP-HPLC and pure fractions of lipidated PrPs were pooled and lyophilized to give a total yield of 20% based on the amount of PrP-C α thioesters were used in EPL. All SDS-PAGE analyses show a unique band representing the pure lipidated PrP proteins (Figure 7.7 A) with masses determined by MALDI-MS (T_PrP) or ESI-MS (Δ CR_PrP and FL_PrP) (Figure 7.7 B) in good agreement with calculated masses.

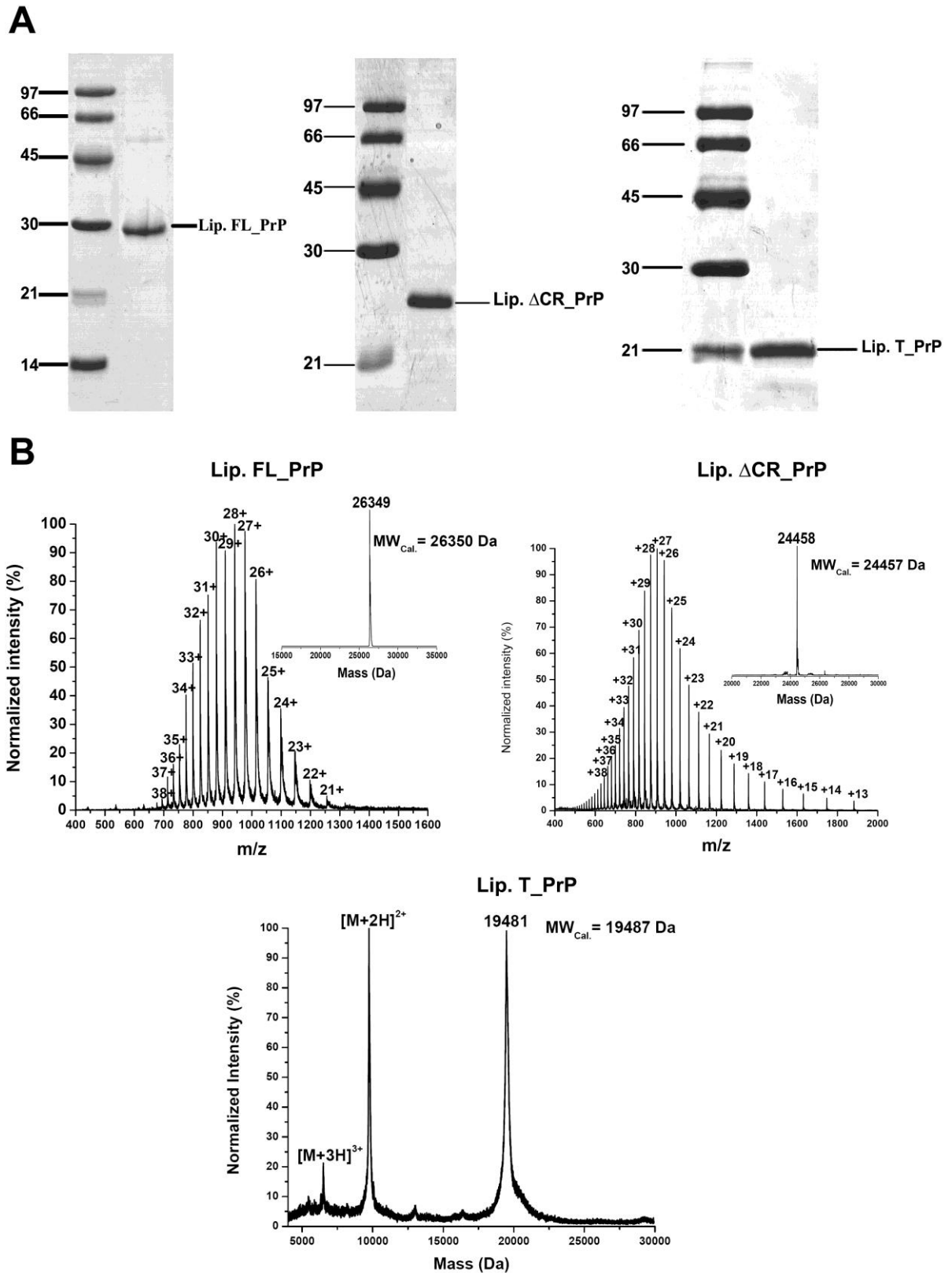


Figure 7.7 A) SDS-PAGE and B) Mass spectrometry analyses of purified lipidated PrP proteins. The difference of -6 Da between the calculated and found molecular mass for lipidated T_PrP was contributed from mass error of MALDI-MS system.

7.1.5 Folding of PrP variants

Most likely due to the key role of the disulfide bond in folding and stability of prion proteins (Maiti & Surewicz, 2001), recombinant expression of prion protein constructs typically results in inclusion bodies in *E. coli*. Therefore, the optimal folding condition to facilitate native disulfide bond formation between Cys179 and Cys214 needs to be identified. Non-lipidated T_PrP was folded via step-wise dilution of guanidine chloride from 8 to 2 M with dilution buffer containing different concentrations of the glutathione redox couple GSH/GSSG: 1/0.1, 2/0.2, 3/0.3, 4/0.4, 5/0.5 mM (Patil *et al.*, 2008). Folded T_PrP was dialyzed against storage buffer (20 mM sodium acetate, pH 5.0) and then ultra-centrifuged to remove aggregated T_PrP. The supernatant was collected and PrP was quantified. The yields of each folding reactions are presented in Table 7.1. Next, the secondary structure of folded T_PrP was analyzed by CD spectroscopy and CDNN software version 2.1 (Applied Photophysics Chirascan Plus) to evaluate secondary structure content.

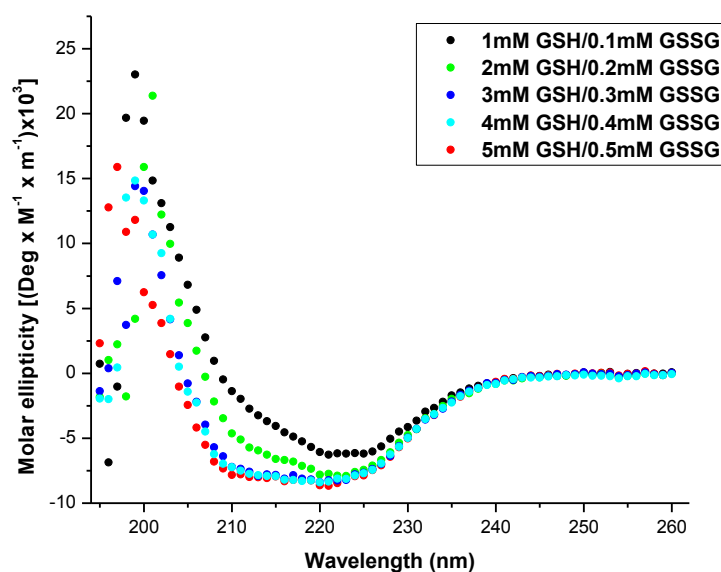


Figure 7.8 CD spectra of T_PrP folded in the presence of different concentrations of the glutathione redox couple

GSH/GSSG (mM)	α -helices (%)	Folding yield (%)
3/0.3	35.5	75
4/0.4	34.6	72
5/0.5	34.4	68
2/0.2	30.7	42
1/0.1	25.6	38
From literature (Han & Hill, 2008)	36	N/A

Table 7.1 Folding yield and percent of α -helix contributing to secondary structure of folded T_PrP with varying concentrations of the glutathione redox couple.

Based on the CD spectra (Figure 7.8) and folding yield (Table 7.1), the optimal concentration of glutathione redox couple is 3/0.3 mM GSH/GSSG that resulted in folded T_PrP with a 35.5% α -helical content, which is in consistent with reported typical secondary structure of PrP^C (36% α -helix) (Han & Hill, 2008). This condition also gave the highest refolding yield (75%) and was applied to fold all lipidated PrPs with a small modification: instead of a dialysis step, a Nap-5 column (GE healthcare) was used for buffer exchange from guanidine into storage buffer. All CD measurements showed predominantly α -helical structures for both lipidated and non-lipidated PrPs (Figure 7.9).

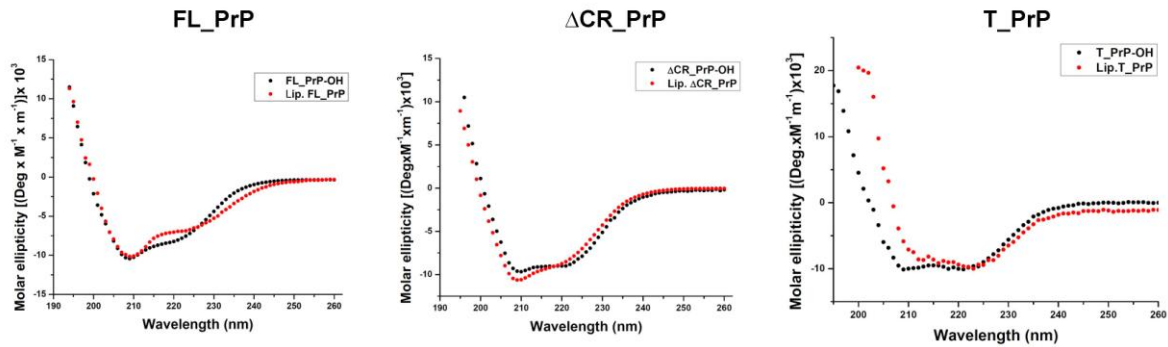


Figure 7.9 CD spectra of lipidated (red) and non-lipidated (black) PrP variants.

7.1.6 Flootation assays

To assess the binding of prion proteins to vesicles, a floatation assay in a discontinuous iodixanol gradient (36, 31 and 5 % (v/v) iodixanol) was used. This approach has been previously described to be useful in analyzing the interaction of prion protein and vesicles (Wang *et al.*, 2007; Wang *et al.*, 2010b). Since vesicles do not contain iodixanol inside and are loaded in the highest density iodixanol solution (36 % (v/v) iodixanol), a buoyant force exceeds the centrifugal force and leads to vesicles floating on top of the gradient under ultracentrifugation step (Bigay & Antony, 2005) as depicted in Figure 7.10.

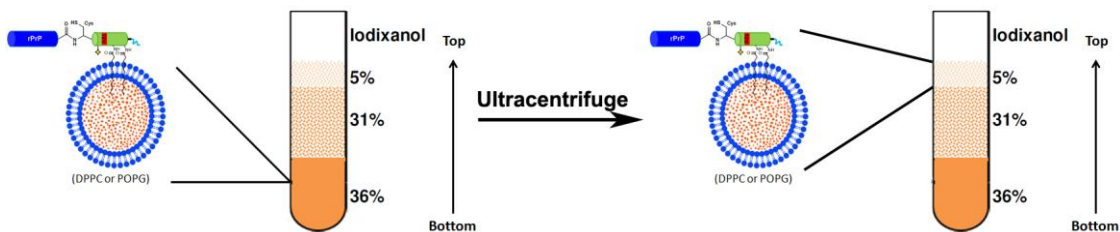


Figure 7.10 Scheme for floatation assay that was used to analyze the binding of prion proteins to phospholipid vesicles.

In order to evaluate this assay and to prove that vesicles float, two kinds of phospholipid small unilamellar vesicles (SUVs): DPPC (a temperature-dependent gel-phase and non-charged phospholipid) and POPG (anionic phospholipid) were loaded underneath the iodixanol gradient. After ultracentrifugation, 12 fractions were collected from the top to bottom of the centrifuge tube. In order to detect phospholipid, each fraction was mixed with ammonium ferrothiocyanate which forms a colored complex with phospholipids. This complex can be dissolved in chloroform and extracted from water phase. It absorbs strongly at 488 nm (section 6.3.7). As

shown in Figure 7.11, in comparison with total amount of phospholipid before loading (fraction 0), almost all DPPC (left) and POPG (right) vesicles are present in fractions 1, 2, 3 at the top of the gradient, indicating successful floatation of the vesicles.

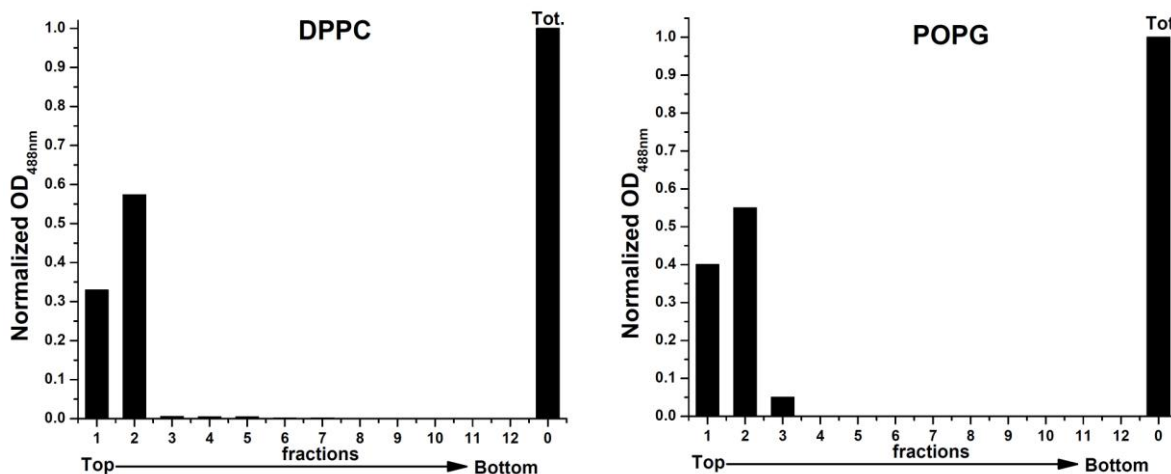


Figure 7.11 Colorimetric measurements were used to determine which fractions collected from flotation assay containing DPPC (left) or POPG (right) vesicles. Fraction 0: total amount of phospholipid before loading, fractions 1-12 were collected from the top to bottom of ultracentrifuged iodixanol gradient.

Next, the binding of PrPs to phospholipid vesicles was analyzed by mixing PrPs with phospholipid vesicles and loading underneath the discontinuous iodixanol gradient. After ultracentrifugation, twelve fractions of the gradient were collected and analyzed by Western-blot (WB) using M20 anti-prion antibody (Santa Cruz Biotechnology) (section 6.2.1). To confirm that prion protein could not be floated in the iodixanol gradient alone, a negative control with non-lipidated FL_PrP was loaded to the iodixanol gradient and fractions from the gradient were collected and analyzed by WB. FL_PrP was completely deposited at the 36% iodixanol layer where it was initially loaded to the gradient (Figure 7.12 A). In case of floatation assays using non-charged phospholipid DPPC, the non-lipidated PrPs were deposited at the bottom of centrifuge tube (Figure 7.12 B, D, F). This result revealed that these PrP variants did not bind to DPPC vesicles. On the opposite, the lipidated PrPs revealed strong binding to DPPC vesicles with their deposition in the fractions 1, 2, 3 at the top of centrifuge tube (Figure 7.12 C, E, G). Thus, lipidated PrPs show a specific binding to vesicles via their C-terminal lipid anchor as demonstrated previously (Olschewski *et al.*, 2007).

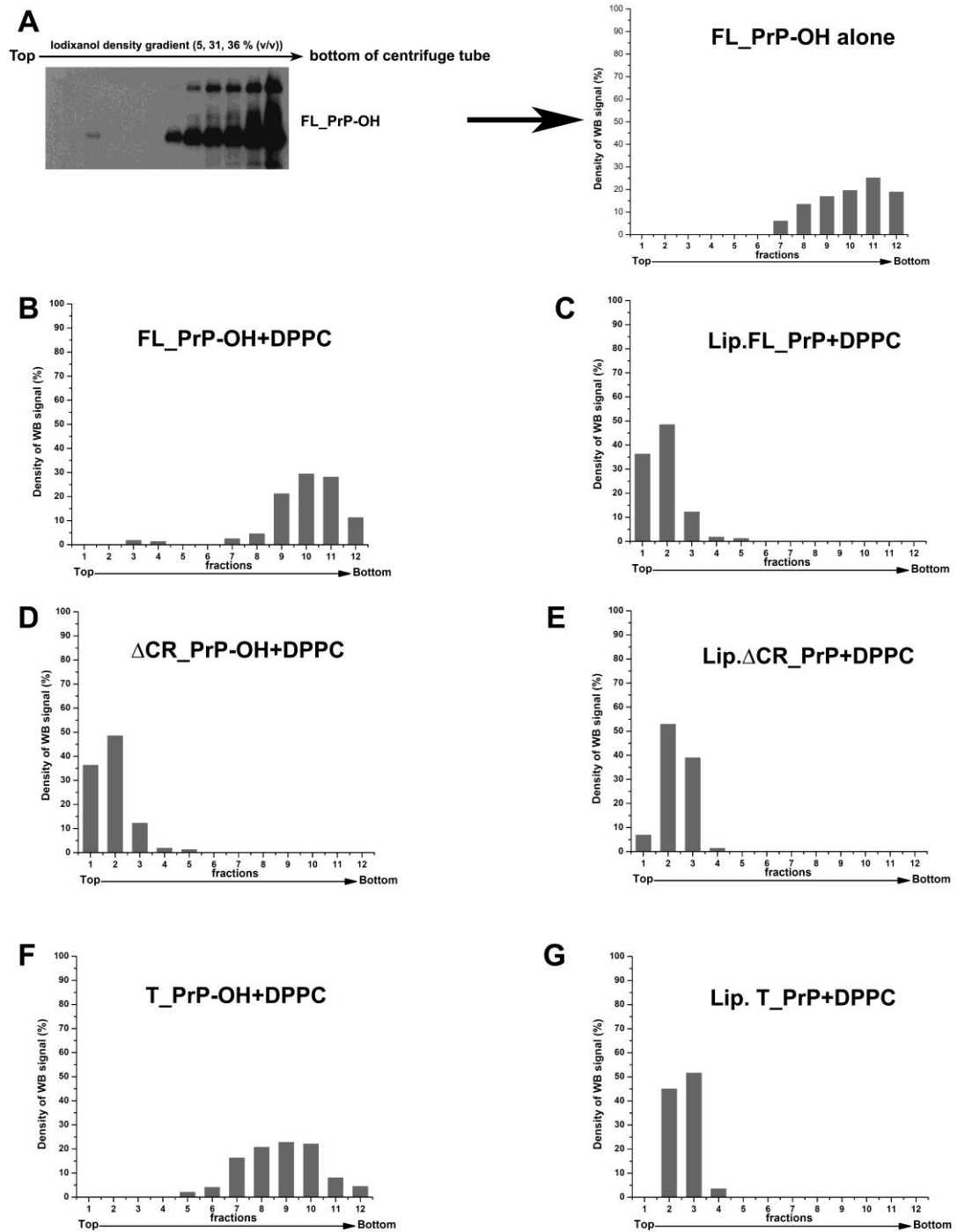


Figure 7.12 Interactions of PrPs with non-charged DPPC vesicles were analyzed by floatation assays and WB. Quantification of all blots was performed by using Image J software. A) Only non-lipidated FL_PrP was loaded under the discontinuous iodixanol gradient. Non-lipidated (B, D, F) and lipidated (C, E, G) forms of FL_PrP, Δ CR_PrP and T_PrP were mixed with DPPC vesicles and loaded under the iodixanol gradient, respectively. All Western blots can be found in appendix 1.

On the other hand, the high affinity binding of prion protein with anionic phospholipid POPG was shown to induce structural changes from α -helical into β -sheet-rich structures (Sanghera *et al.*, 2011; Sanghera & Pinheiro, 2002; Wang *et al.*, 2007). Therefore, the interaction of PrPs with POPG vesicles was analyzed. In contrast to the behavior with DPPC vesicles described above, all of the lipidated and non-lipidated PrPs showed a strong interaction with POPG (Figure 7.13 A, D, G). However, treatment of prion protein-POPG mixtures with 10 mM NaOH, which can partially extract prion protein from POPG vesicles (Wang *et al.*, 2007), showed a difference between lipidated and non-lipidated prion proteins. In case of non-lipidated prion proteins, their interactions with POPG vesicles were disrupted by NaOH and large amount of the proteins were deposited at the bottom of the iodixanol gradient (Figure 7.13 B, E, H). In contrast, the interactions of lipidated PrPs and POPG vesicles showed stability to NaOH extraction, with lipidated PrPs mainly present in the top fractions of the iodixanol gradient (Figure 7.13 C, F, I). These results indicate that the C-terminally lipidated peptide stabilizes a strong interaction of PrP with phospholipid vesicles.

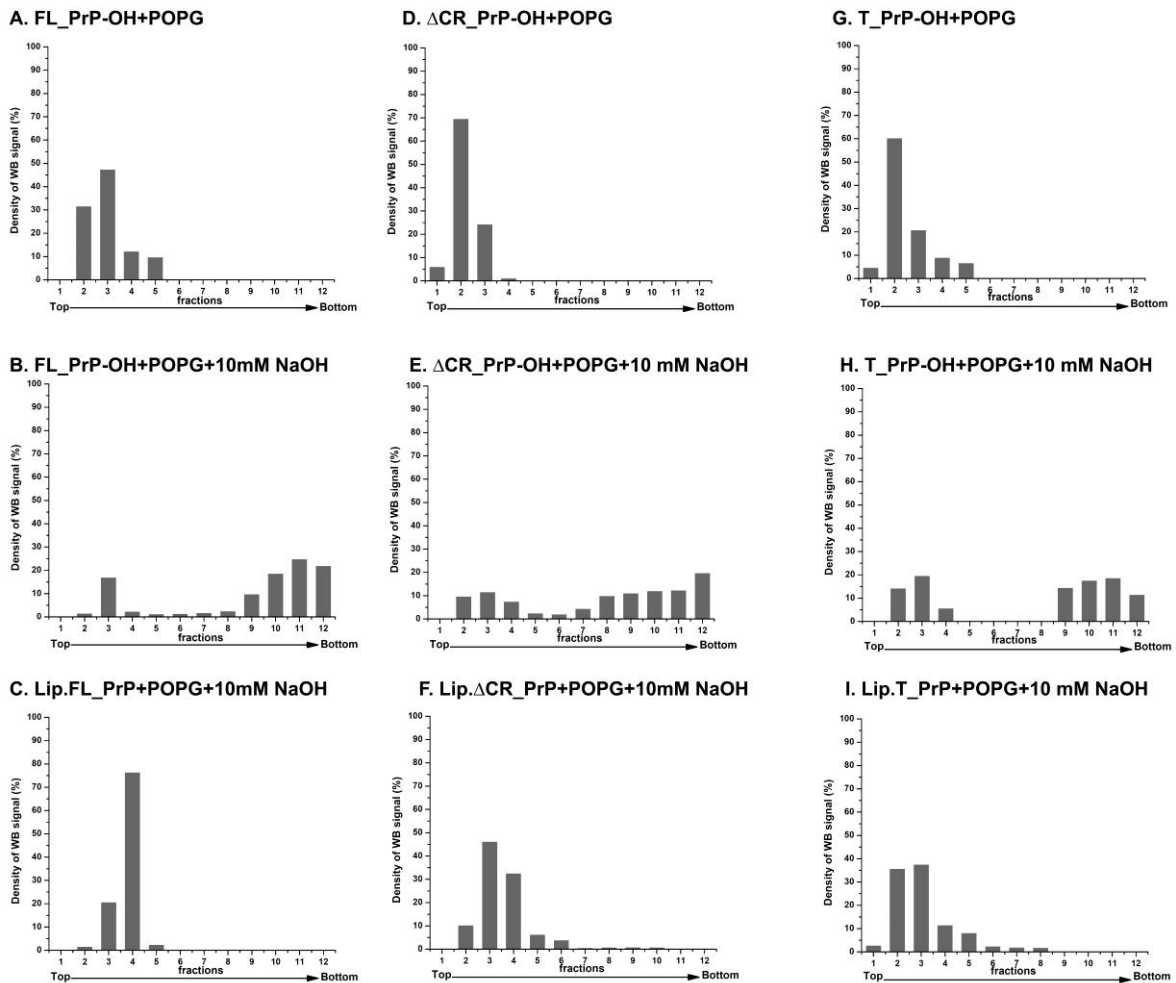


Figure 7.13 Interactions of anionic POPG vesicles with PrPs and NaOH extraction to evaluate the strength of PrPs' binding to POPG vesicles were analyzed by floatation assays and WB with quantification of all blots was performed as described in Figure 7.12. A, D and G) The mixtures of non-lipidated PrP variants with POPG vesicles were loaded under the iodixanol gradient. The mixtures of non-lipidated (B, E, H) and lipidated (C, F, I) forms of PrP variants with POPG vesicles were treated with 10 mM NaOH and then loaded under the iodixanol gradient. All Western blots can be found in appendix 2.

7.1.7 Proteinase K resistance

Proteinase K (PK) resistance is one of the typical characteristics of PrP^{Sc} and distinguishes it from PrP^C which can be digested completely (section 4.3.1). Here, PK digestion was used to evaluate whether the binding of PrPs to anionic POPG vesicles, as demonstrated above, can produce PK-resistant PrP variants. PK

digestion was carried out with PK:PrP molar ratios of 1:16, 1:8 and 1:4 and analyzed by WB, one sample without PK treatment was always included as negative control. The PK resistant bands of non-lipidated FL_PrP mixed with POPG vesicles were detected while FL_PrP incubated in the absence of POPG vesicles remained PK-sensitive (Figure 7.14 A, left). This result is in good agreement with a previous study by (Wang *et al.*, 2007). In contrast, lipidated FL_PrP incubated with POPG vesicles still remained PK-sensitive under similar conditions (Figure 7.14 A, right). This information indicates that binding of lipidated FL_PrP to POPG vesicles differs from that of non-lipidated FL_PrP. This different binding prevents formation of PK-resistant PrP and allows PK to access and digest the protein completely.

In case of T_PrP and Δ CR_PrP, no PK resistance was observed and both lipidated and non-lipidated variants remained PK-sensitive (Figure 7.14, B and C). This finding is consistent with the idea that both electrostatic (weak in T_PrP) and hydrophobic (lacking in Δ CR_PrP) interactions play important roles in the interaction of PrP with anionic POPG vesicles (Sanghera & Pinheiro, 2002; Wang *et al.*, 2010b). Therefore, the PK resistance observed for non-lipidated FL_PrP bound to POPG vesicles could be from the protection of vesicles to prevent the access of PK rather than POPG-induced formation of large aggregates of PrP as reported by Wang and colleagues (Wang *et al.*, 2007). To clarify this conclusion, treatment of non-lipidated FL_PrP bound to POPG vesicles with 1 % (v/v) Triton X-100 (that dissolves the vesicles) before addition of PK was performed. Indeed, the samples treated with Triton X-100 showed a significantly reduced PK-resistance for FL_PrP (Figure 7.14 D and E). Based on these PK digestion results, it can be surmised that the interactions of lipidated PrPs with POPG vesicles are different from those of non-lipidated PrPs. Lipidation may allow PK to easily access PrP and to digest the protein completely.

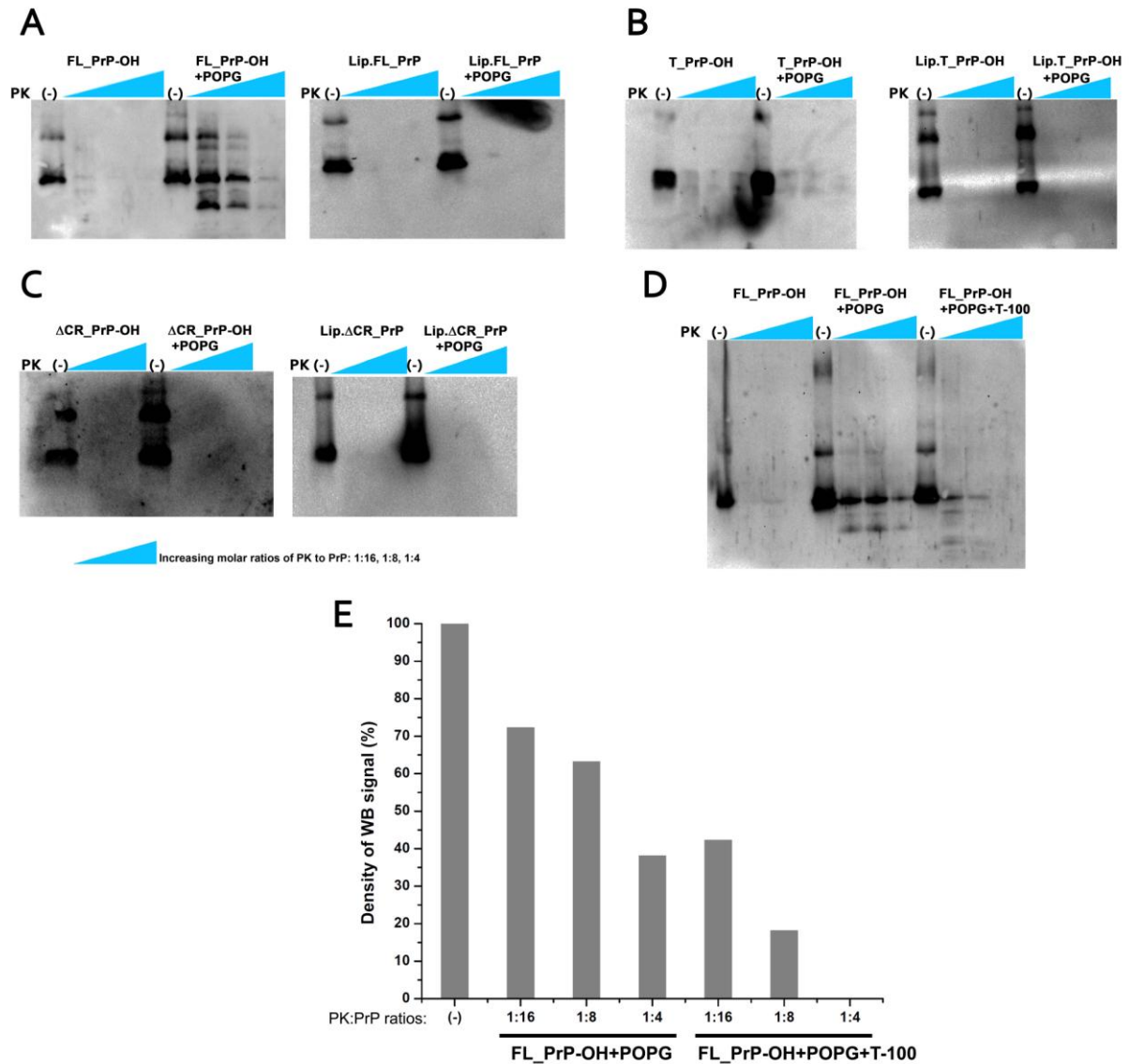


Figure 7.14 PK digestions of PrPs: FL_PrP (A), T_PrP (B) and ΔCR_PrP (C) after incubation at 37°C for 1 hour with buffer alone (left) or POPG phospholipid vesicles (right) in each panel, the results of non-lipidated and lipidated PrPs were present in left and right side of figure, respectively. (D) PK digestions of non-lipidated FL_PrP alone or the mixtures of non-lipidated FL_PrP and POPG vesicles with and without adding 1 % of Triton X-100 (T-100). (E) The quantitative graph for density of WB samples in (D) was conducted as described in Figure 7.12. The PK:PrP molar ratios were 1:16, 1:8 and 1:4.

7.1.8 Fluorescence-based analysis of PrP interactions with vesicles

7.1.8.1 Calcein release from vesicles

In order to investigate whether binding of prion proteins can affect the stability of lipid membranes, an established method based on the release of calcein from lipid vesicles was used. This method has been widely applied to study the extent of vesicles destabilization induced by binding of proteins (Garg *et al.*, 2012; Savva *et al.*, 2013) and peptides (Yoneyama *et al.*, 2009). Calcein was loaded into vesicles at high concentrations, at which the fluorescence is self-quenched. If binding of prion proteins to vesicles induces the release of calcein, this will result in an increase of fluorescence caused by calcein dilution (Sanghera & Pinheiro, 2002) as depicted in Figure 7.15. The amount of calcein release can be calculated by using the equation 1 (see in section 6.3.12).

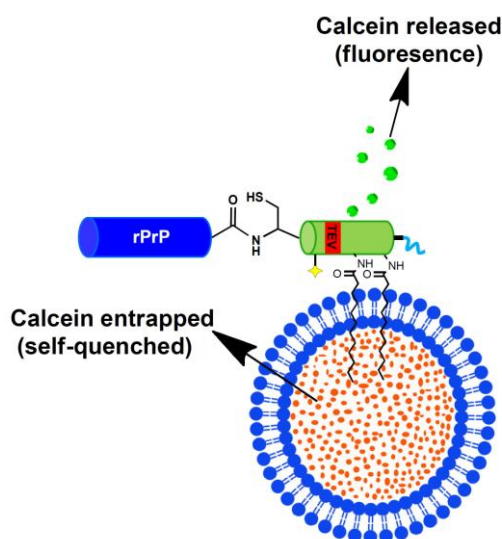


Figure 7.15 Calcein release assay. Binding of prion proteins to the calcein-loaded vesicles could induce the release of calcein, which increases fluorescence.

A linear correlation range between concentration and fluorescence intensity of calcein needs to be determined to allow precise calculation of F_{Tot} in equation 1. In Figure 7.16, a concentration range of calcein from 0.5 to 5.5 μM shows a linear correlation with fluorescent intensity. This range was used as an indicator to adjust the volume of calcein-loaded vesicles for all assays so that the fluorescent intensity corresponding to F_{Tot} would be less than the fluorescence intensity of 5.5 μM of calcein.

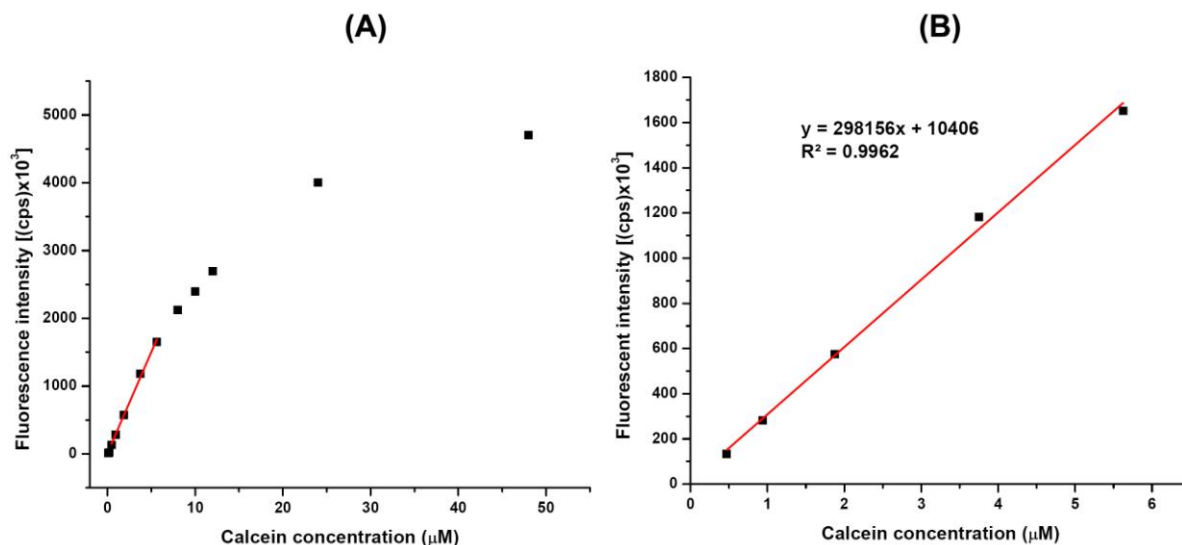


Figure 7.16 Titration curve for correlation between concentrations and fluorescence intensities of calcein (A) and (B) shows the linear range

Based on the fluorescent parameters found above, calcein release assays were used to analyze the interactions of non-lipidated PrPs with POPG vesicles. Titration curves relating concentrations of non-lipidated PrPs and fluorescent intensity of calcein release were plotted (Figure 7.17). Addition of non-lipidated PrPs to anionic POPG vesicles leads to a concentration dependent release of calcein. The maximum release of calcein was achieved at a protein-to-lipid molar ratio of 1:100. Based on these titration curves a concentration of 100 nM PrP was selected for all future experiments to compare amounts of calcein released from POPG vesicles which were mixed with lipidated or non-lipidated PrPs. This concentration is the minimum concentration of PrPs that was required to obtain sufficient fluorescence intensity.

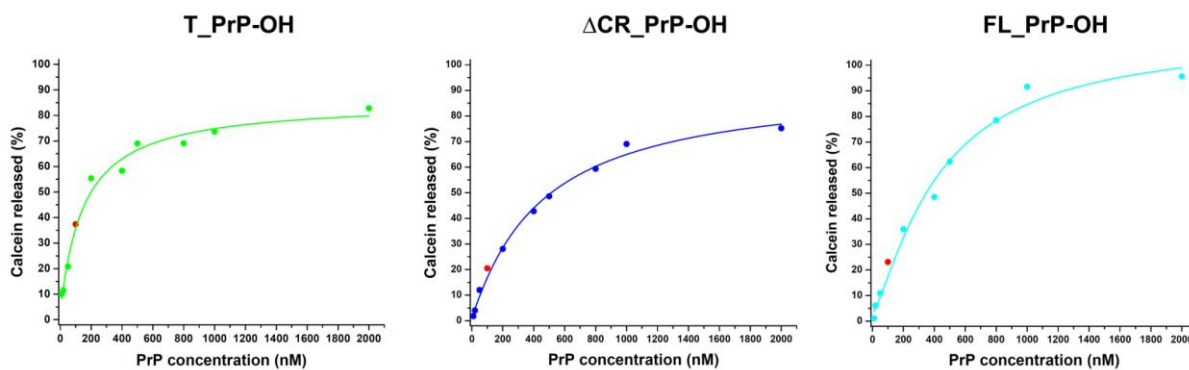


Figure 7.17 Titration curves relating amounts of calcein released from calcein-loaded POPG vesicles and concentrations of non-lipidated PrPs: T_PrP, Δ CR_PrP and FL_PrP. A concentration of 100 nM PrP (red dots) was selected for next assays with lipidated PrPs.

The amounts of calcein released from interactions of DOPC vesicles with lipidated and non-lipidated PrPs showed no significant difference when compared to background control (BG) with absence of any PrP (Figure 7.18, right). This result suggested that no binding of non-lipidated PrPs to DOPC vesicles occurs as found from floatation assays above. Interestingly, the already established interactions of lipidated PrPs with DOPC vesicles also had no influence on the release of calcein. That means the insertion of C-terminal membrane anchor into the vesicles did not permeabilize lipid bilayers.

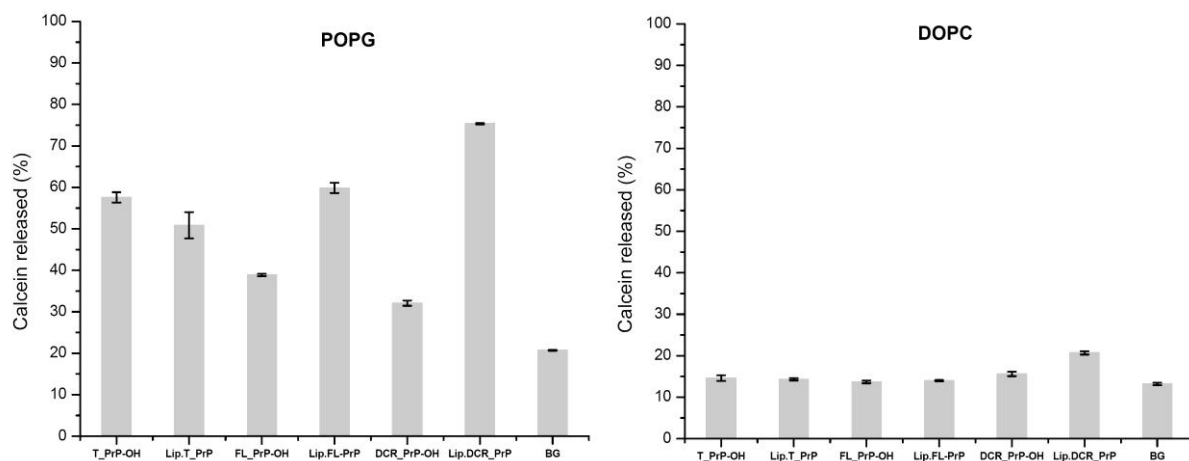


Figure 7.18 Comparison of the interactions of PrPs with two types of calcein loaded vesicles: anionic phospholipid POPG (left) using 100 nM PrP proteins and 200 μ M vesicles, and non-charged (zwitterionic) phospholipid DOPC (right) using 1 μ M PrP

proteins and 200 μ M vesicles. One sample, containing only calcein loaded vesicles, was included as background control (BG).

In contrast to interaction of PrPs with non-charged DOPC vesicles, the interaction of PrPs with anionic POPG vesicles leads to a distinct release of calcein when compared to BG sample (Figure 7.18, left). The binding of PrPs to POPG vesicles has a destabilizing effect on the membrane. This observation proves that electrostatic interaction is prerequisite for the binding of PrP to lipid membranes.

In extension of the established calcein release assay, vesicles consisting of a phospholipid mixture that mimics neuronal membranes were produced using different kinds of phospholipids including PC : PE : PI : SM : Chol : PG or PS with molar ratios 30 : 30 : 2.5 : 5 : 22.5 : 10, respectively (section 6.3.7). Two kinds of anionic phospholipids (POPG and POPS) were used to learn whether the difference in anionic phospholipid component can affect the interaction of PrPs with neuronal membrane. As shown in Figure 7.19, no significant difference of calcein release was observed for the binding of PrPs to NM-PG and NM-PS vesicles. One interesting observation is that the amounts of calcein released from lipidated PrPs are always higher than those from non-lipidated ones, only the T_PrP construct showed almost no difference (Figure 7.18, left and Figure 7.19). These results indicated that the anchoring of PrP constructs via their C-terminal lipid anchor may lead the N-terminal polybasic region of PrP (residues 23-27), which was lacking in the T_PrP construct, to enhance the electrostatic interaction of PrP with anionic phospholipid membranes. Indeed, Wang and colleagues already determined that this region initiates the electrostatic interaction between PrP and anionic phospholipid (Wang *et al.*, 2010b). Moreover, Turnbaugh and colleagues recently found that this polybasic region dictates the efficiency of prion propagation by binding to PrP^{Sc}. A deletion of this region can dramatically reduce susceptibility of prion protein to prion infection and significantly elongate the survival of transgenic (Δ 23-31 PrP) mice after scrapie inoculation (Turnbaugh *et al.*, 2012).

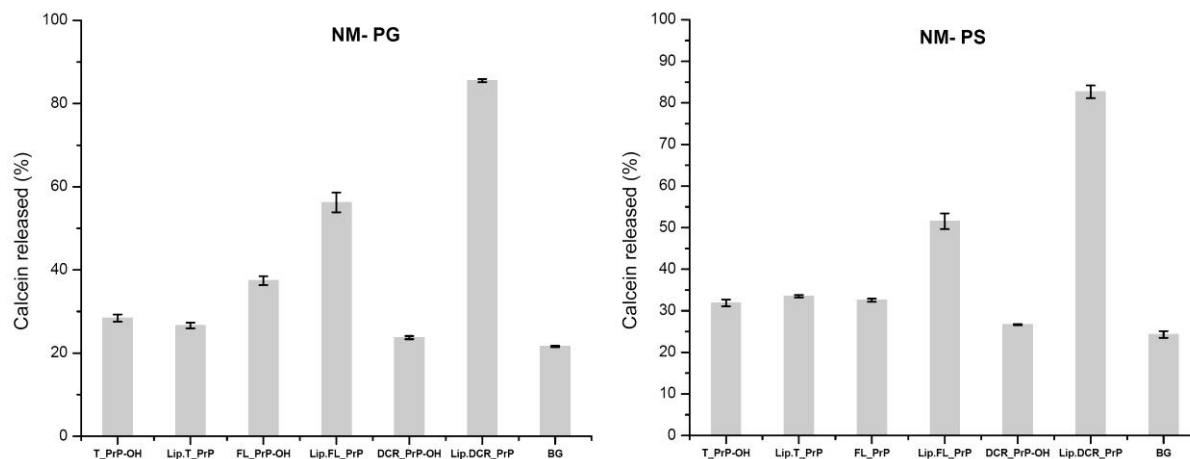


Figure 7.19 Comparison of interactions of PrPs with two different calcein loaded neuronal membrane mimic vesicles: using POPG (left) or POPS (right) as anionic phospholipid component; a protein-to-lipid ratio of 1:350 was used.

Interestingly, the interactions of lipidated Δ CR_PrP with POPG, NM-PG and NM-PS vesicles revealed the highest extent of calcein release (Figure 7.18, left and Figure 7.19). This finding can be explained by a potential pore formation of this construct within phospholipid membranes consisting of anionic phospholipids. Based on electrophysiological measurements with neuronal cells expressing Δ CR_PrP, Solomon and colleagues illustrated how Δ CR_PrP construct might form ion channels or pores (Solomon *et al.*, 2010; Solomon *et al.*, 2011).

7.1.8.2 NBD-PE fluorescence quenching

In order to further understand the effects of PrP binding on the integrity of lipid bilayers, NBD-fluorescence quenching was used to detect how much and how fast the quencher sodium dithionite can influx through a PrP-loaded vesicle and quench NBD fluorescence. Fluorescently labeled PE (NBD-PE) with an NBD fluorophore attached to the head-group of phosphatidylethanolamine (PE) was incorporated within the vesicles at a ratio of labeled to unlabeled lipids of 1 mole %. NBD is localized close to the head group of the lipids and thus is a sensitive probe to detect the interaction of proteins/peptides with the lipid bilayer. In addition, the accessibility of the dithionite quencher to NBD moieties was also correlated to bilayer disruption by proteins/peptides (Halevy *et al.*, 2003; McIntyre & Sleight, 1991) as illustrated in Figure 7.20. In presence of the dithionite quencher, intact vesicles retain NBD fluorescence from the labeled head-group of inner layer leaflet (Figure 7.20, A, top).

If the vesicles contain pores, dithionite can penetrate into the vesicles and quench this remaining NBD fluorescence at the inner leaflet of vesicles as well (Figure 7.20, A, bottom). This process is illustrated in Figure 7.20, B where 1% (v/v) Triton X-100 was used to destabilize the vesicles. For these measurements, the fluorescence recordings were initiated after manual addition of the quencher dithionite to the vesicles. Due to Triton X-100 treatment vesicles broke down completely and NBD fluorescence quenching (Figure 7.20, B, red line) was so fast that only the final 30% of fluorescence decay was observed.

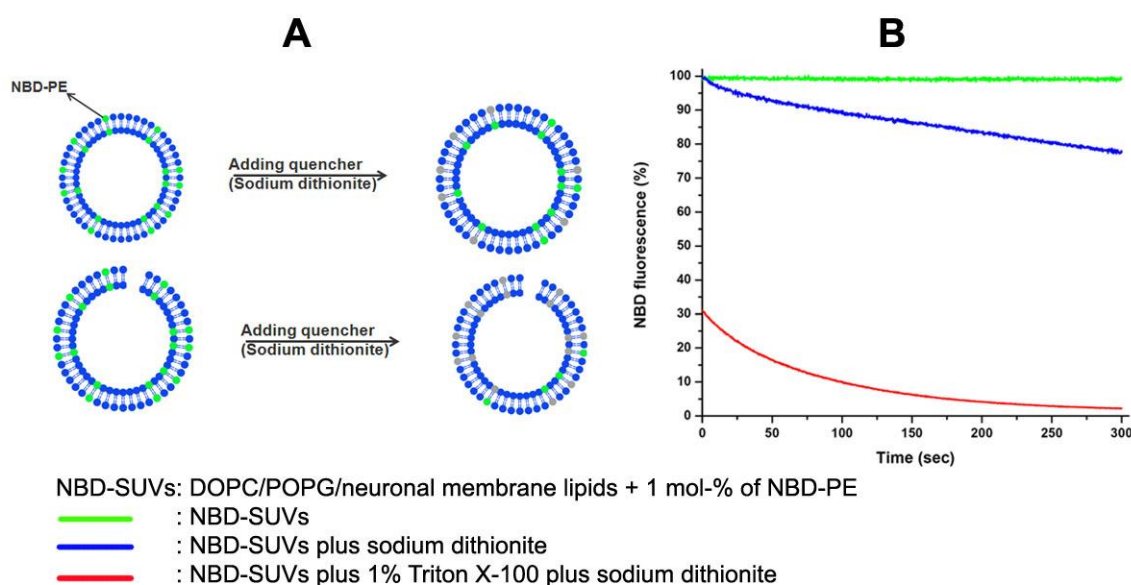


Figure 7.20 A) Principle of NBD fluorescence quenching assay with NBD-PE (green) incorporated into the vesicles. Addition of the quencher sodium dithionite leads to a loss in NBD fluorescence (gray). B) NBD fluorescence quenching measurements of (A). The quencher dithionite was manually mixed with the NBD-labeled vesicles and NBD fluorescence decay was recorded with a delay of 10 seconds.

Figure 7.21 depicts dithionite-induced fluorescence quenching of NBD-PE incorporated into DOPC (top) and POPG (bottom) vesicles, after these vesicles were mixed with different PrP constructs. The control (SUVs only) is based on incubation of the vesicles with dithionite in absence of any PrP. In both kinds of vesicles, addition of any PrP variants induced faster fluorescence quenching. In case of PrPs mixed with NBD-DOPC vesicles, no distinguishable difference of NBD fluorescence quenching was recorded between different PrP variants (Figure 7.21, top). This observation indicates that no effect on the intact of NBD-DOPC vesicles from both

non-lipidated and lipidated forms of PrP variants as found in calcein release assays above. Interestingly, the interactions of T_PrP and FL_PrP with NBD-POPG vesicles also did not show any significant difference between non-lipidated and lipidated variants (Figure 7.21, bottom), most likely implying that their interactions with NBD-POPG vesicles did not permeabilize this kind of vesicles. This finding and the previous results of calcein release assays revealed that the binding modes of T_PrP and FL_PrP to POPG vesicles did not either induce pore formation or destabilize POPG vesicles. In contrast, the interaction of lipidated Δ CR_PrP and NBD-POPG vesicles led to the highest quenching effect (Figure 7.21, bottom, cyan). This result provides further proof that lipidated Δ CR_PrP induces pores in POPG vesicles. Moreover, when compared with non-lipidated Δ CR_PrP, which did not permeabilize NBD-POPG vesicles (Figure 7.21, bottom, blue), the C-terminal lipid anchor of lipidated Δ CR_PrP seems to be a crucial factor contributing to pore formation.

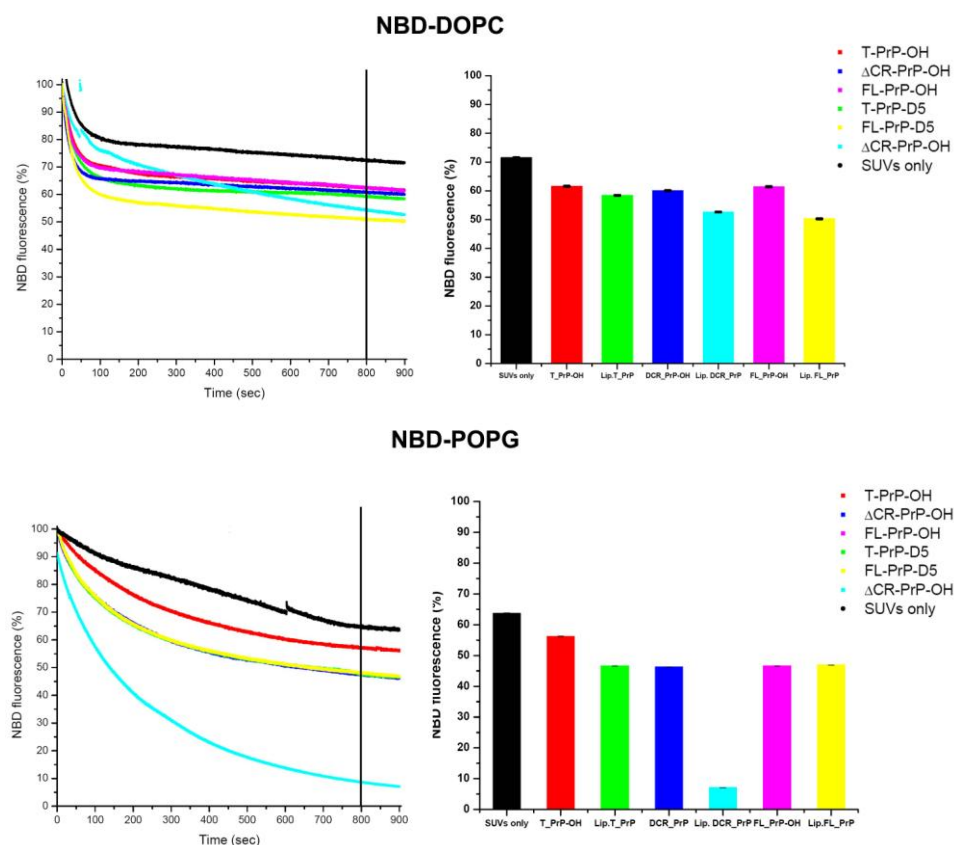


Figure 7.21 Fluorescence quenching assay for PrP variants mixed with NBD-DOPC vesicles (top) and NBD-POPG vesicles (bottom). The left side shows NBD fluorescence decay recorded in 900 seconds. After 800 seconds, the remaining NBD fluorescence was measured, averaged and summarized in a bar graph (right side).

Furthermore, similar fluorescence quenching assays were performed with different concentrations (from 0 to 1 μM) of lipidated $\Delta\text{CR}_\text{PrP}$. The quenching rate has a fast and a slow component, the fast one corresponds to the quenching of fluorophores immediately accessible to the quencher on the outer surface of vesicles. The slower component represents the averaged rate of penetration of the quencher through the bilayer, to quench the fluorophores on the inner leaflet. Langner and Hui suggested a single exponential function to express both the components of the quenching rate (Langner & Hui, 1993). Here, the generated data points were perfectly fitted by exponential function to create a titration curve of concentration of lipidated $\Delta\text{CR}_\text{PrP}$ versus NBD fluorescence. The data depicted in Figure 7. 22 demonstrate that the extent of NBD fluorescence quenching increased with the concentration of lipidated $\Delta\text{CR}_\text{PrP}$.

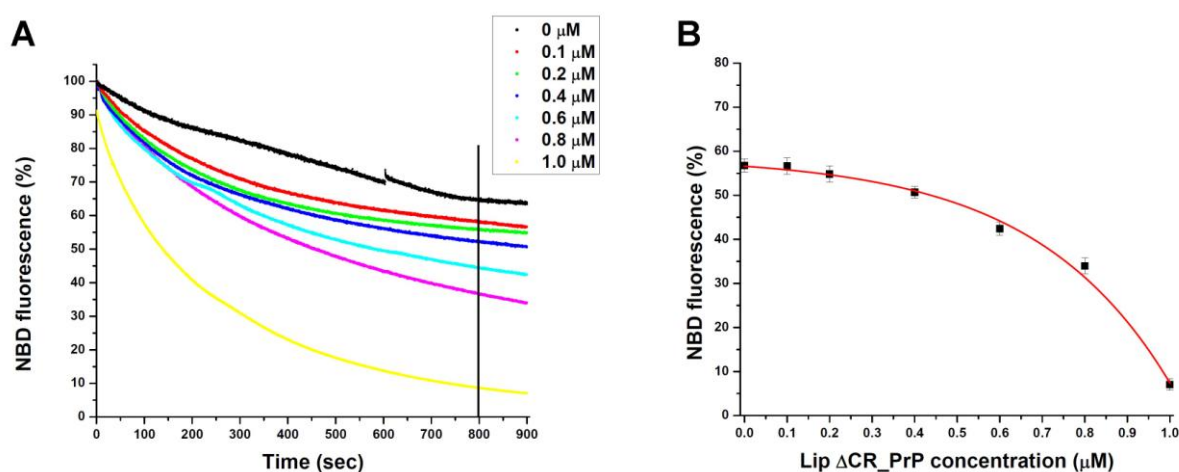


Figure 7. 22 Lipidated $\Delta\text{CR}_\text{PrP}$ causes the influx of the quencher dithionite into NBD-POPG vesicles in a concentration-dependent manner. A) Different concentrations of lipidated $\Delta\text{CR}_\text{PrP}$ from 0 to 1.0 μM were mixed with NBD-POPG vesicles (200 μM of lipids) and 10 mM dithionite was added. After 800 seconds (vertical line) the remaining fluorescence was measured. B) Averages of two independent measurements were plotted.

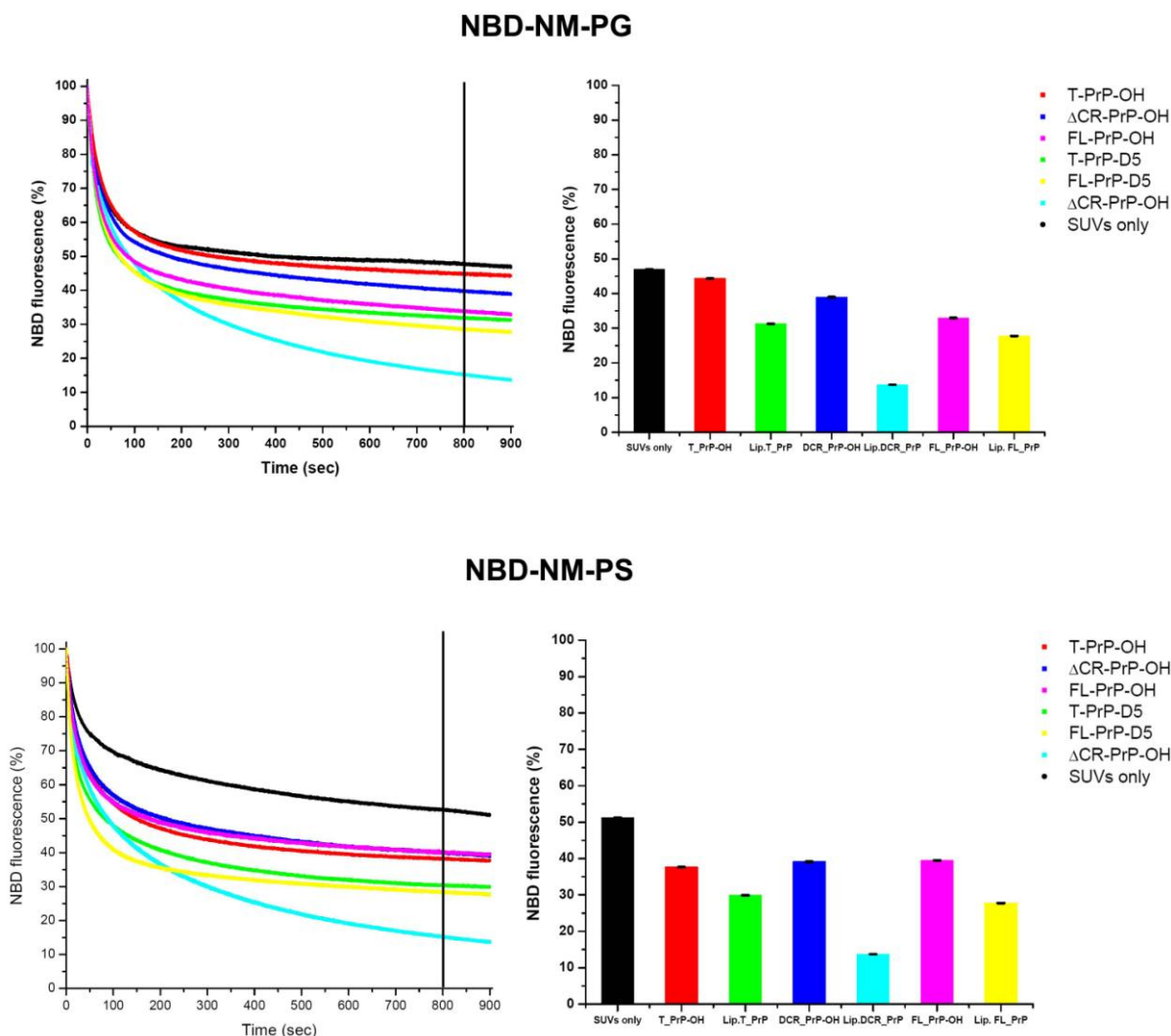


Figure 7. 23 NBD fluorescence quenching assay for PrP proteins mixed with neuronal membrane mimicking vesicles containing anionic phospholipid POPG (top) or POPS (bottom). The left side is NBD fluorescence decay recorded in 900 seconds. After 800 seconds (left side, vertical lines), the remaining NBD fluorescence was measured, averaged and summarized in a bar graph (right side).

In extension of this assay, vesicles mimicking neuronal membranes (NM-PG and NM-PS with the phospholipid components as described above (section 7.1.8.1)) including 1 mole % NBD-PE were prepared and mixed with lipidated and non-lipidated PrPs. Although NM-PG and NM-PS vesicles were made of different anionic phospholipid components (POPG and POPS, respectively), NBD fluorescence quenching data depicted in Figure 7. 23 for the interactions of both vesicles with PrPs reveal a close similarity and are in a very good agreement with previous results obtained from calcein release assays (Figure 7.19). However, NM-PG and NM-PS

vesicles were less stable than POPG vesicles (seen during preparation of calcein-loaded vesicles in section 6.3.11), thus the fluorescence quenching processes of NM-PG and NM-PS for all samples including controls (Figure 7. 23, SUVs only, black) are much higher and faster than that of NBD-POPG. In addition, the fluorescence quenching results in Figure 7. 23 showed that the C-terminal lipid anchor increased the extent of NBD fluorescence quenching in vesicles mimicking neuronal membranes. This observation most likely reflects a preferred localization of lipidated PrPs at the lipid-water interface where the NBD probe attached to the hydrophilic head group of PE also localizes. Interestingly, similarly to the observation from NBD-POPG vesicles, the interactions of lipidated Δ CR_PrP with NM-PS or NM-PG vesicles also resulted in the highest extents of NBD fluorescence quenching (Figure 7. 23, cyan). Therefore, the results from NBD fluorescence quenching strongly support the potential pore formation of lipidated Δ CR_PrP on membranes containing anionic phospholipids as found in calcein release assays (section 7.1.8.1).

7.1.9 Cryo electron microscopy (EM)

Cryo electron microscopy on SUVs was performed to learn whether the binding of lipidated Δ CR_PrP to POPG vesicles leads to either destabilization of vesicles or pore formation in lipid bilayers. Two cryo samples including POPG vesicles only and POPG vesicles mixed with lipidated Δ CR_PrP were prepared and visualized with a TEM system (FEI Tecnai F30 Helium "Polara"). The images in Figure 7. 24 show that the binding of lipidated Δ CR_PrP to POPG vesicles does not influence the integrity of the vesicles when compared with POPG vesicles alone. This result further supports the theory of pore formation by lipidated Δ CR_PrP.

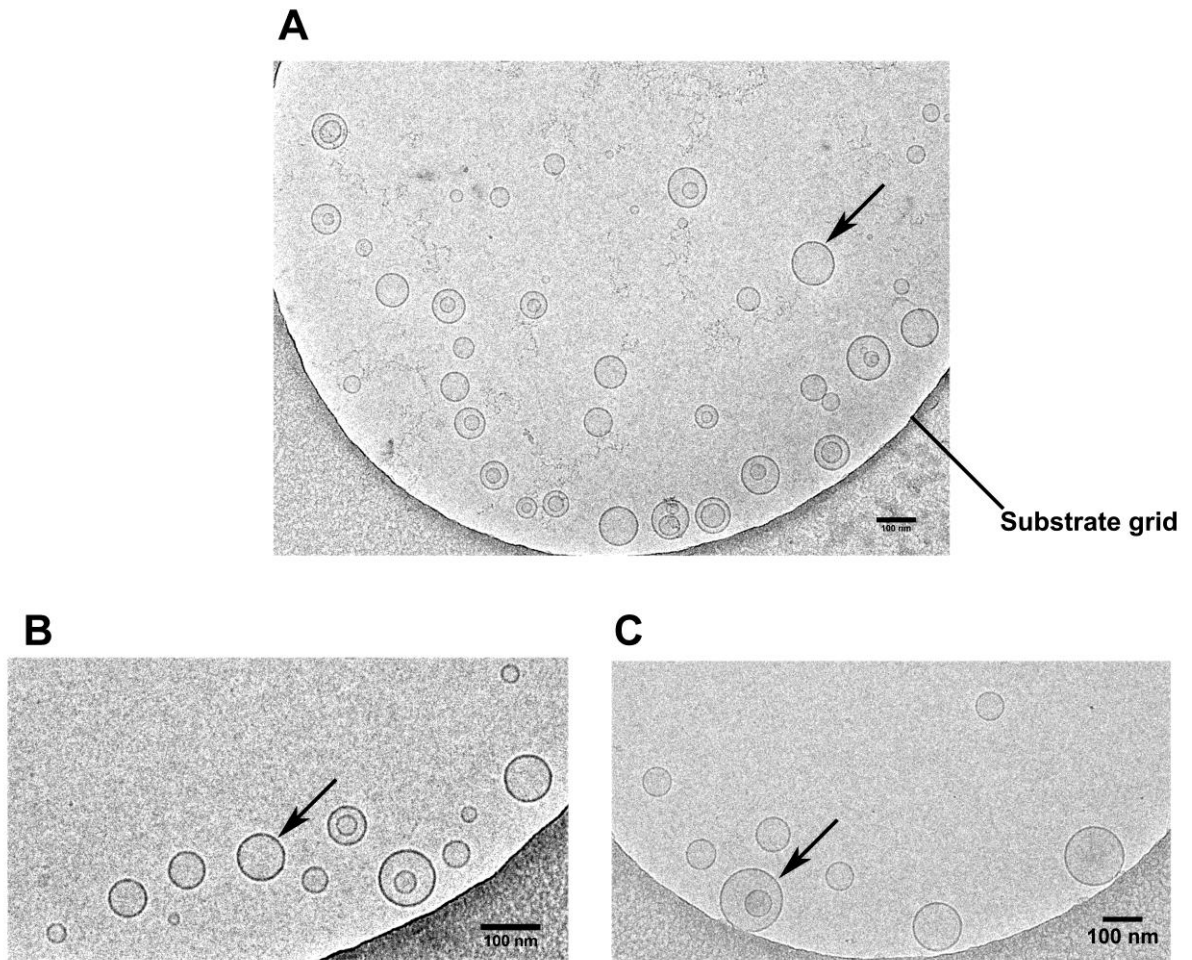


Figure 7. 24 Cryo EM images of POPG vesicles (arrows) mixed with lipidated Δ CR_PrP (A, B) and POPG vesicles alone (C). The scale bar is 100 nm

7.1.10 PrP conformation and membrane interaction

Far UV circular dichroism (CD) spectroscopy was used to investigate whether lipidated and non-lipidated PrPs undergo conformational changes during interaction with phospholipid vesicles. PrP variants were incubated with phospholipid vesicles at 25°C and CD spectra were recorded.

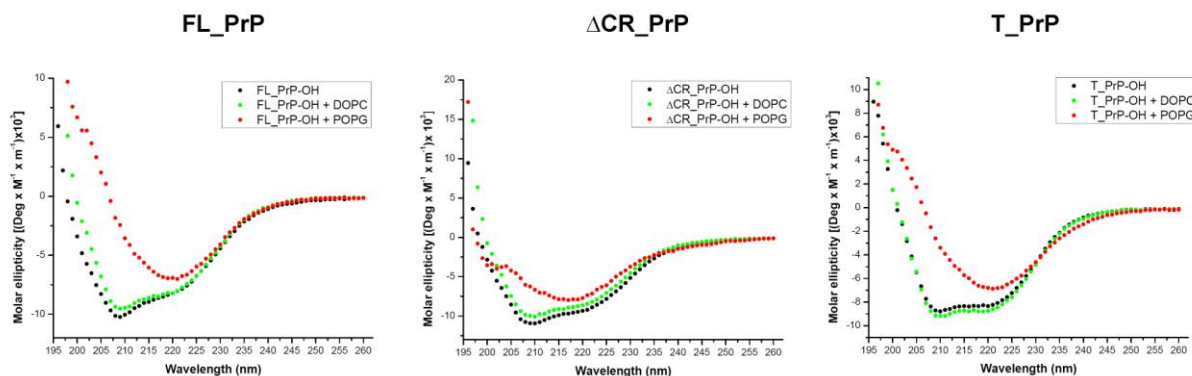


Figure 7. 25 CD spectra for non-lipidated PrPs alone (black) or mixed with DOPC (green) and POPG (red) vesicles.

The CD data depicted in Figure 7. 25 and Table 7.2 for non-lipidated PrPs demonstrated that PrP mixed with non-charged DOPC vesicles (green) did not change their predominantly α -helical conformation and remain almost indistinguishable from PrPs in the absence of lipids (black line). In contrast, the incubation with anionic POPG vesicles leads to a significant change in secondary structure of PrP from a typically α -helical to a β -sheet-rich structure (Figure 7. 25, red) with a huge increase of β -sheet and random coil contents (Table 7.2). The conformational changes of non-lipidated FL_PrP and T_PrP upon interaction with POPG vesicles found here are consistent with previous reports (Sanghera & Pinheiro, 2002; Wang *et al.*, 2007). In addition, the same effect for non-lipidated Δ CR_PrP was also found here.

	α -helices (%)	β -sheets (%)	Turns (%)	Random coils (%)
FL_PrP-OH	43.68	13.97	16.28	26.10
FL_PrP-OH+DOPC	32.74	17.42	17.02	32.84
FL_PrP-OH +POPG	11.78	28.30	17.48	42.48
Lip.FL_PrP	37.63	16.03	16.85	29.52
Lip.FL_PrP+DOPC	39.97	15.28	16.65	28.14
Lip.FL_PrP+POPG	33.75	18.20	17.48	30.55
Δ CR_PrP-OH	34.77	16.66	16.90	31.67
Δ CR_PrP-OH+DOPC	32.07	17.66	17.07	33.13
Δ CR_PrP-OH +POPG	24.03	21.14	17.55	37.25
Lip. Δ CR_PrP	32.13	17.70	17.10	33.20
Lip. Δ CR_PrP+DOPC	34.25	17.22	16.82	31.68
Lip. Δ CR_PrP+POPG	34.36	18.01	17.40	30.26
T_PrP-OH	36.00	15.94	16.44	31.60
T_PrP-OH+DOPC	35.28	16.31	16.62	31.79
T_PrP-OH +POPG	17.59	24.60	17.17	40.62
Lip.T_PrP	33.75	15.87	15.34	35.00
Lip.T_PrP+DOPC	35.58	15.04	16.96	32.42
Lip.T_PrP+POPG	36.27	15.63	16.07	32.23

Table 7.2 Secondary structure parameters of PrPs alone or upon interaction with DOPC or POPG vesicles. The CD spectra measured above (Figure 7. 25 and Figure 7. 26) were analyzed and deconvoluted by CDNN software.

Furthermore, the conformation of lipidated PrPs upon interaction with anionic POPG vesicles were also analyzed by CD spectroscopy and depicted in Figure 7. 26.

Surprisingly, lipidated PrP variants conformations mostly did not convert into β -sheet rich structures during interaction with POPG vesicles as observed for non-lipidated PrPs. In case of the lipidated T_PrP and Δ CR_PrP constructs, their secondary structures mostly maintained typical α -helical conformations (Figure 7. 26) without significant changes in secondary structure parameters (Table 7.2). Although there is a change in conformation, the interaction of lipidated FL_PrP with POPG vesicles only did lead to a random coil enriched structure instead of β -sheet structure as for non-lipidated FL_PrP (Figure 7. 26 and Table 7.2). This finding suggests that the secondary structure of PrP attached to the lipid membrane via lipid anchor is different from that of non-lipidated PrP (Table 7.2) and that this possibly accounts for the differences in biochemical characteristics such as PK resistance as described above.

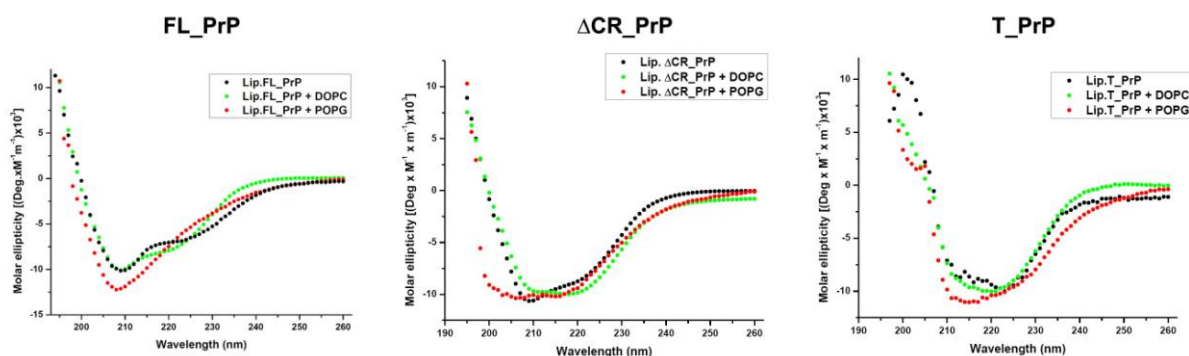


Figure 7. 26 CD spectra for lipidated PrPs alone (black) or upon interaction with DOPC (green) and POPG (red) vesicles

7.1.11 Characterizing the interactions of PrP variants with membranes via tryptophan fluorescence

Intrinsic tryptophan fluorescence provides a useful spectroscopic technique to study binding of proteins or peptides to lipid membranes (Srikumar *et al.*, 1999). The indole side chain of tryptophan appears ideally suited for interaction with the polar-apolar interface, thus tryptophan residues are recognized from structure studies of membrane-bound proteins to be prominent at the interface of water and phospholipid, and preferably insert into this interface (Chan *et al.*, 2006; Yau *et al.*, 1998). Tryptophan fluorescence reveals a decrease in quantum yield and a blue shift of the maximal emission wavelength when tryptophan residue transfers from an aqueous solution (hydrophilic) into a lipid phase (hydrophobic) (Christiaens *et al.*,

2002). On the other hand, tryptophan fluorescence quenching by water-soluble quenchers like acrylamide and iodide can provide information about the gross location of tryptophan residues in the complex three-dimensional structure of membrane-bound proteins (Eftink, 1991). In case of prion protein, seven tryptophan residues are present in the unstructured N-terminal region (residues 23-99) (Figure 7. 27) and this region is also supposed to play a key role in interaction of prion proteins and phospholipid membranes (Sanghera & Pinheiro, 2002; Wang *et al.*, 2007).

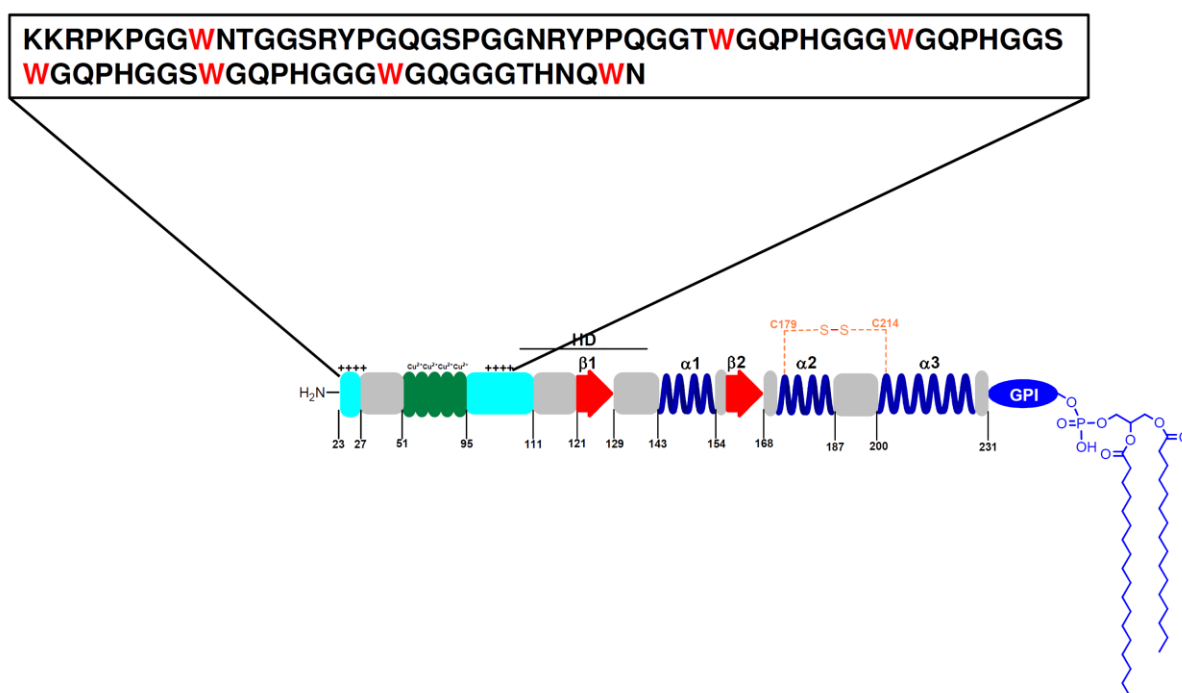


Figure 7. 27 Schematic representation for FL_PrP construct with tryptophan residues (red letters in box) which are present in the unstructured N-terminal region (residues 23-99)

Tryptophan fluorescence based assays were carried out to further study the effect of C-terminal lipid anchor attachment on the interaction of the N-terminal region with lipid membranes.

7.1.11.1 Tryptophan fluorescence measurements

The fluorescence emission spectra of PrPs in an aqueous solution have a maximum at 348 nm (λ_{max}) and are consistent with a relatively polar environment of tryptophan residues as known from previous studies (Morillas *et al.*, 1999; Sanghera

& Pinheiro, 2002). Moreover, these studies demonstrated that strong interaction of non-lipidated PrP and anionic POPG vesicles lead to a significant blue shift of the tryptophan fluorescence λ_{\max} . The molar ratios of non-lipidated PrPs and POPG vesicles, at which the maximum blue shift ($\Delta\lambda$) of tryptophan fluorescence occurs, were found and depicted as red dots (7, 8 and 10 nm for T_PrP, Δ CR_PrP and FL_PrP, respectively) in Figure 7. 28. These molar ratios were selected for subsequent experiments.

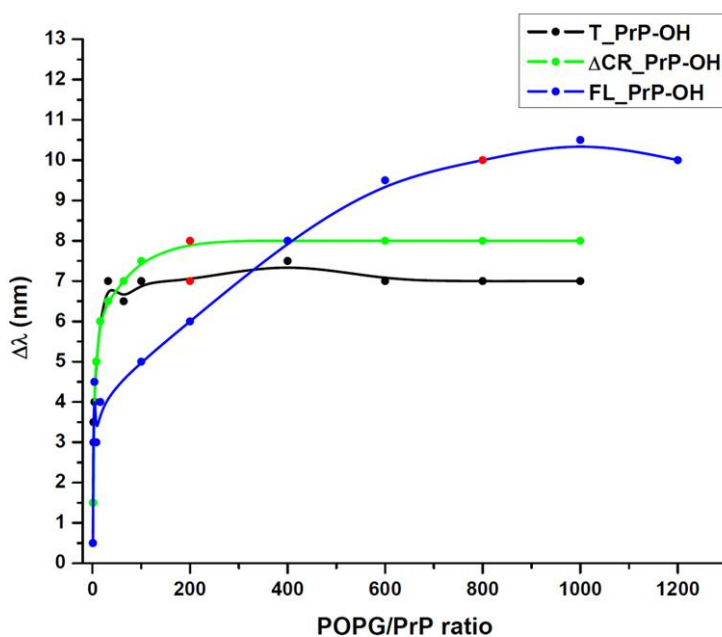


Figure 7. 28 The blue shift ($\Delta\lambda$) of the tryptophan fluorescence emission maximum of non-lipidated PrPs: T_PrP (black), Δ CR_PrP (green) and FL_PrP (blue) with POPG vesicles. The red dots correspond to the beginning of saturation and were chosen to compare with lipidated PrPs later. All the tryptophan fluorescence emission wavelengths can be found in appendix 3.

A comparison between the extent of blue shifts of lipidated and non-lipidated PrPs was performed and depicted in Table 7.3. Incubation of proteins with membrane vesicles consisting of non-charged DOPC phospholipid did not result in any measurable changes, suggesting the lack of protein-membrane interaction, which is in high agreement with the results described above. In case of PrPs mixed with anionic POPG vesicles, there was no difference between PrPs with or without C-terminal lipid anchor. The presence of a C-terminal lipid anchor did not affect the

fluorescence properties of tryptophan residues, which mostly located at the N-terminal region (23-99) of PrPs. This result proves that the C-terminal anchoring of PrP to the membrane did not alter the interaction of the N-terminal region of PrP with phospholipid membrane as found in previous studies (Morillas *et al.*, 1999; Sanghera & Pinheiro, 2002; Wang *et al.*, 2010b).

	Blue shift with POPG (nm)	Blue shift with DOPC (nm)
T_PrP-OH	7	-0.5
Lip. T_PrP	7	0.5
Δ CR_PrP-OH	8	0.5
Lip. Δ CR_PrP	8	0.5
FL_PrP-OH	10	-0.5
Lip. FL_PrP	11	-0.5

Table 7.3 Blue shift of the tryptophan fluorescence emission maximum of lipidated and non-lipidated PrPs with POPG and DOPC vesicles at the lipid/PrP ratios selected from Figure 7. 28 (red dots): 800 for FL_PrP and 200 for T_PrP and Δ CR_PrP. The blue shift was calculated by subtracting the peak wavelength of tryptophan fluorescence recorded in aqueous solution to peak wavelength after mixed PrPs with phospholipid vesicles: POPG or DOPC.

7.1.11.2 Tryptophan fluorescence quenching

Quenching of tryptophan fluorescence is a useful method to learn about the extent of solvent exposure of tryptophan residues in proteins and can be applied to elucidate protection of tryptophan residues upon binding and insertion into lipid membranes (Liu & Deber, 1997). In order to obtain insight on the interaction of PrPs with anionic POPG vesicles, tryptophan fluorescence quenching assays were carried out here using the polar quencher acrylamide.

The tryptophan fluorescence quenching experiments were performed as described in Material and Method (section 6.3.15). Linear Stern-Volmer plots were

created for the quenching of tryptophan fluorescence of non-lipidated FL_PrP in phosphate buffer and the buffer containing 8 M urea (Figure 7.29 A). The resulting Stern-Volmer constants (K_{SV} , equation 3, section 6.3.15) were found to be 5.96 (± 0.18) M^{-1} and 6.16 (± 0.26) M^{-1} for non-lipidated FL_PrP in phosphate buffer and denaturing conditions, respectively (Table 7.4). The minor difference between both conditions suggests that tryptophan residues of folded FL_PrP are equally accessible to the quencher acrylamide in solution. Next, linear Stern-Volmer plots corresponding to the quenching of tryptophan fluorescence of each PrP constructs in solution and mixed with lipid vesicles were created and depicted in Figure 7.29 B, C and D. The resulting K_{SV} values were summarized in Table 7.4.

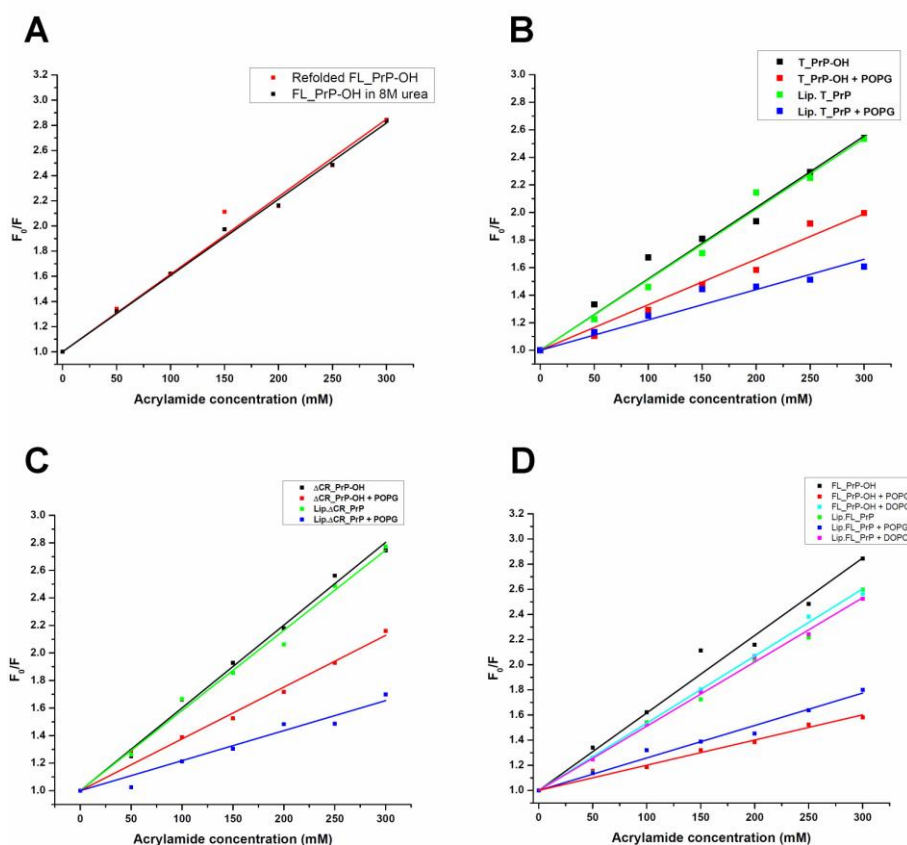


Figure 7.29 Stern-Volmer plots for tryptophan fluorescence quenching measurements of A) non-lipidated FL_PrP in phosphate buffer (red) or in presence of 8 M Urea (black); B, C and D) non-lipidated and lipidated PrPs in solution (black and green) or bound to POPG vesicles (red and blue), DOPC vesicles (cyan and magenta) for T_PrP, ΔCR_PrP and FL_PrP, respectively.

The K_{SV} values for PrPs in the presence of POPG vesicles were found to be significantly lower than those of PrPs in solution. This finding indicates that the tryptophan residues in PrP have become less accessible to the quencher acrylamide due to their binding to POPG vesicles, and this most likely indicates insertion of tryptophan residues into the lipid membrane (Sanghera & Pinheiro, 2002). To further explain this insertion, the same experimental procedure was applied for non-lipidated and lipidated FL_PrP mixed with DOPC vesicles. The resulting K_{SV} values were found to be $5.83 (\pm 0.11) M^{-1}$ and $5.20 (\pm 0.11) M^{-1}$ for lipidated and non-lipidated FL_PrP in interaction with DOPC vesicles, which is close for these PrPs in solution: $5.96 (\pm 0.18) M^{-1}$ and $5.31 (\pm 0.12) M^{-1}$, respectively (Table 7.4). The minor difference in K_{SV} data with and without DOPC vesicles indicates no protection of tryptophan residues because no strong binding of PrP to DOPC vesicles occurred as demonstrated above (sections 7.1.8.1, 7.1.8.2), thus the C-terminal lipid anchor attachment did not change this trend in interaction of PrP N-termini with lipid membranes either as previously observed (section 7.1.11.1).

	Solution	POPG	DOPC
T_PrP-OH	$5.63 (\pm 0.85) M^{-1}$	$3.08 (\pm 0.20) M^{-1}$	--
Lip. T_PrP	$5.41 (\pm 0.45) M^{-1}$	$2.42 (\pm 0.36) M^{-1}$	--
Δ CR_PrP-OH	$5.96 (\pm 0.55) M^{-1}$	$3.71 (\pm 0.84) M^{-1}$	--
Lip. Δ CR_PrP-OH	$5.78 (\pm 0.51) M^{-1}$	$2.17 (\pm 0.2) M^{-1}$	--
FL_PrP-OH	$5.96 (\pm 0.18) M^{-1}$	$1.98 (\pm 0.13) M^{-1}$	$5.83 (\pm 0.11) M^{-1}$
	$6.16 (\pm 0.26) M^{-1}$ in 8 M urea		
Lip. FL_PrP	$5.31 (\pm 0.12) M^{-1}$	$2.71 (\pm 0.46) M^{-1}$	$5.20 (\pm 0.11) M^{-1}$

Table 7.4 Stern-Volmer constant (K_{SV}) values of PrPs in solution or mixed with POPG and DOPC vesicles

On the other hand for the interactions of PrP variants with anionic POPG vesicles, the lipid anchor strongly influences the K_{SV} values. For T_PrP and Δ CR_PrP constructs, the interaction of lipidated versions with POPG vesicles

resulted in far lower K_{SV} values than those found for non-lipidated versions (Table 7.4). In this case, the C-terminal lipid anchor enhanced the insertion of tryptophan residues of T_PrP and Δ CR_PrP into lipid bilayers of POPG vesicles. In contrast, the lipid anchor limited the interaction of tryptophan residues from FL_PrP with anionic POPG vesicles. Indeed, their K_{SV} values indicated that the tryptophan residues from lipidated FL_PrP have become more accessible to the polar quencher acrylamide than those from non-lipidated FL_PrP. That means the insertion of tryptophan residues of non-lipidated FL_PrP into lipid bilayers is stronger than those of lipidated FL_PrP. This finding reveals that the C-terminal lipid anchor reduced the strong insertion of tryptophan residues of FL_PrP into lipid bilayers of POPG vesicles.

Overall the C-terminal lipid anchor likely modulates the binding of N-terminal region of PrP variants to anionic POPG vesicles in two modes that either enhances this binding in case of T_PrP and Δ CR_PrP (weak binding), or limits this binding for FL_PrP (strong binding).

7.1.12 Discussion

7.1.12.1 The C-terminal lipid anchor influences the biochemical and conformational characteristics of PrP in membrane environments

PrP is a GPI-anchored protein that is localized at the outer leaflet of the plasma membrane (Caughey & Raymond, 1991). This close association with the lipid membranes points toward the fact that the conversion of PrP^C into PrP^{Sc} is occurring in this membrane environment as suggested in previous studies (Baron & Caughey, 2003; Goold *et al.*, 2011). Therefore, several studies on the interactions of PrP with phospholipid membranes by using recombinant PrPs were previously carried out (Critchley *et al.*, 2004; Morillas *et al.*, 1999; Sanghera *et al.*, 2011; Sanghera & Pinheiro, 2002; Wang *et al.*, 2010a; Wang *et al.*, 2007). However, most of these studies only used recombinant PrPs without GPI anchor. Due to the presence of a GPI anchor at C-terminus of PrP, the behavior of “tethered” PrP on membranes might be different from that of “free” PrP.

In floatation assays, high affinity binding of PrPs to anionic POPG vesicles was observed as mentioned in previous studies (Robinson & Pinheiro, 2010;

Sanghera & Pinheiro, 2002; Wang *et al.*, 2007; Wang *et al.*, 2010b). The results from our floatation assays also revealed that lipidated PrPs specifically and strongly bind to phospholipid vesicles via their C-terminal lipid anchor. Additionally, the interactions with anionic POPG vesicles also induced a conversion of typical α -helical structure into β -sheet enriched structures of non-lipidated PrPs. This finding is in good agreement with previous studies (Morillas *et al.*, 1999; Sanghera *et al.*, 2011; Sanghera & Pinheiro, 2002; Wang *et al.*, 2007; Wang *et al.*, 2010b). However, lipidated PrPs did not undergo this conformational change into β -sheet rich structures. Lipidated T_PrP and Δ CR_PrP constructs still retained a predominantly α -helical structure and lipidated FL_PrP partially converted into random coil. This result suggests that the interaction of lipidated PrP with lipid membrane is different from that of non-lipidated PrP. The lipid anchor most likely modulates this interaction so that PrP can prevent a conformational change into a β -sheet enriched structure.

In addition to inducing a conformational conversion of non-lipidated PrPs, the interaction of such PrPs with anionic POPG vesicles was also found to lead to increased PK resistance (Wang *et al.*, 2007), one of the typical biochemical characteristics of PrP^{Sc} (section 1.3.1). In case of non-lipidated PrPs mixed with POPG vesicles, the PK assays showed that non-lipidated FL_PrP construct becomes resistant to PK as described by Wang and colleagues (Wang *et al.*, 2007; Wang *et al.*, 2010b). But two constructs, T_PrP (weak in electrostatic interaction with POPG) and Δ CR_PrP (lacking core hydrophobic region for hydrophobic interaction with POPG), still remained sensitive to PK. This finding could mean that the extent of interaction of both latter constructs with anionic POPG are lower than that of FL_PrP, which can be protected from PK by insertion into POPG vesicles, as demonstrated by Triton X-100 treatment in PK digestions, as well as tryptophan fluorescence quenching measurements. Interestingly, the interaction of lipidated FL_PrP with POPG was sensitive to PK. One possible event is that the interaction of lipidated FL_PrP with POPG vesicles leads this protein fully exposed to PK, thus it can be digested completely by PK.

7.1.12.2 The binding mode of lipidated PrPs to membranes is very distinct from that of non-lipidated PrPs

A convenient method to study the binding of PrP to membranes is intrinsic tryptophan fluorescence. The current tryptophan fluorescence results show that the N-terminal region of PrP (residues 23-99) binds to anionic POPG vesicles, but not to non-charged DOPC vesicles. This observation is highly consistent with previous studies (Sanghera & Pinheiro, 2002). Interestingly, a similar effect was recorded for lipidated and non-lipidated PrPs in interactions with POPG vesicles. That means the lipid anchor did not alter the binding ability of N-terminal region of PrP. This observation supports the opinion is that beside the C-terminal attachment to cell surface via GPI anchor, a direct interaction of PrP with phospholipid membranes should be considered as observed for other lipid-anchored proteins: Src proteins, HIV-1 gag protein, myristoylated alanine-rich C kinase substrate (Gerlach *et al.*, 2010; Sanghera & Pinheiro, 2002).

Although the lipid anchor did not influence the binding ability of N-terminal region of PrP to lipid membranes as discussed above, the tryptophan fluorescence quenching results showed a different extent for the insertion of tryptophan residues within this region of lipidated PrPs into lipid membranes when compared with non-lipidated PrPs. In case of T_PrP and Δ CR_PrP constructs, comparison of K_{SV} values between lipidated and non-lipidated PrPs reveals that the lipid anchor enhanced the insertion of tryptophan residues into the bilayer. Thus it enhanced the binding of this region of lipidated T_PrP and Δ CR_PrP proteins to the vesicles. In contrast, the lipid anchor limits the extent of this binding of lipidated FL_PrP. Not only effects on the binding of N-terminal region of PrP, the lipid anchor also influences the interaction of the structured C-terminal domain of PrP with lipid membranes. The results from CD measurements and PK digestions as discussed above reveal this influence (section 7.1.12.1). The lipid anchor likely controls the interaction of the C-terminal domain of PrP with anionic phospholipid vesicles so that biochemical and conformational characteristics of lipidated PrPs are very distinct from those of non-lipidated PrPs. Therefore, the membrane attachment via the C-terminal membrane anchor plays an important role in structural properties of PrP. Supporting for this idea is the difference in sensitivity of PrP^C to treatment with the enzyme GPI-specific phospholipase

(PIPLC) when compared with PrP^{Sc}. Whereas PrP^C was easily cleaved by PIPLC and removed from the membrane surface, PrP^{Sc} was retained on the membrane under similar treatment (Stahl *et al.*, 1990). The results revealed that an altered association of PrP with lipid membranes via the GPI anchor may be a crucial factor in mechanism of prion conversion.

7.1.12.3 Potential pore formation by lipidated Δ CR_PrP

In order to identify regions of PrP^C involved in the formation of PrP^{Sc}, some studies with genetic deletions in the central hydrophobic region (CR) (HD in Figure 7.1) of PrP^C produced a neurotoxic PrP construct (Baumann *et al.*, 2007; Li *et al.*, 2007; Shmerling *et al.*, 1998). In particular, the deletion of 20 amino acids of the CR (residues 105-125) generates a neurotoxic mutant named Δ CR_PrP (Li *et al.*, 2007). Transgenic mice expressing Δ CR_PrP mutant developed a spontaneous neurodegenerative disease that resulted in neonatal lethality. Interestingly, Δ CR_PrP was found to contain the full set of the posttranslational modifications (N-glycosylations, GPI attachment) of wild-type PrP^C (Winklhofer *et al.*, 2003). Expression of Δ CR_PrP in some of transfected cell lines was found to induce spontaneous ionic currents, similar to those from different point mutations in the central hydrophobic region that are linked to familial prion diseases in humans; and these ionic currents can be silenced by co-expression of PrP^C (Solomon *et al.*, 2010; Solomon *et al.*, 2011). Relying on biophysical results from the cell-based assays, Biasini and colleagues suggested two possible explanations for these ionic currents that either Δ CR_PrP and the familial mutants in the CR influence endogenous ion channel(s) or these PrP constructs themselves form an ion channel or a pore in the cellular membrane (Biasini *et al.*, 2012; Biasini *et al.*, 2013).

From the calcein release assays, the highest extent of calcein release from the binding of lipidated Δ CR_PrP to POPG vesicles was observed when compared with the remaining PrPs. A possible explanation for this event is that the binding of lipidated Δ CR_PrP disrupts the structure of vesicles and consequently induces the membrane permeabilization, similar to other transmembrane proteins or peptides described previously (Butko *et al.*, 1996; Garg *et al.*, 2012; Vogt & Bechinger, 1999). In order to prove this, NBD fluorescence quenching assays were performed. The

polar quencher sodium dithionite cannot penetrate intact vesicles easily, thus only NBD fluorophores on the exposed outer leaflet of lipid bilayers can be quenched effectively. However, binding of PrP to the membrane, which leads to membrane permeabilization or pore formation on lipid membranes, can create an influx of dithionite into vesicles and lead to severe fluorescence quenching. Interestingly, binding of lipidated Δ CR_PrP to lipid membranes led to an impressive quenching of NBD fluorescence significantly higher than observed for the remaining PrPs. These results strongly support the theory of pore formation by lipidated Δ CR_PrP.

In addition, the characteristics of pore formation from Δ CR_PrP construct were also found in these assays. First, this event only occurred when Δ CR_PrP carried a C-terminal lipid anchor. The extent of calcein release and NBD fluorescence quenching from the interaction of lipidated Δ CR_PrP with lipid membranes was always higher than those from the interaction of non-lipidated Δ CR_PrP construct under otherwise similar conditions. That means a specific binding to the vesicles via the C-terminal lipid anchor is required for pore formation of lipidated Δ CR_PrP. To support this idea, Solomon and colleagues found that the immobilization on the cellular membrane is necessary step for the potential pore formation of Δ CR_PrP in cell-based experiments (Solomon *et al.*, 2011). Second, the electrostatic interaction between Δ CR_PrP and anionic phospholipids is also required for efficient pore formation. In presence of anionic phospholipids (POPG or POPS), lipidated Δ CR_PrP induces the highest amounts of calcein released from calcein-loaded vesicles as well as the highest intensity of NBD fluorescence quenched by influx of the quencher dithionite into the vesicles. In case of DOPC (a non-charged phospholipid) vesicles these effects were abrogated. This finding strongly supports the fact that Δ CR_PrP construct with additional deletion of the N-terminal polybasic region (residues 23-31), that was expressed in neuron cells, did not influence ion channels on the cellular membrane (Solomon *et al.*, 2011). Finally, pore formation of lipidated Δ CR_PrP on lipid membranes did not affect the integrity of vesicles. Comparative cryo EM measurements for POPG vesicles alone or mixed with lipidated Δ CR_PrP did not show any difference. The POPG vesicles still retain their integrity and pore formation by lipidated Δ CR_PrP is a reasonable explanation for all effects described here.

7.1.13 Future works

The current data show that lipidated PrPs have quite distinct lipid membrane-binding properties when compared to non-lipidated PrPs. Especially, this lipid anchor prevents the conformational conversion of PrP from α -helical into β -sheet enriched structures during interaction with anionic POPG vesicles. This conversion is one of key factors found to produce highly infectious prion from recombinant PrP (Wang *et al.*, 2007). Previous studies using cell-based assays also suggest that the GPI anchor plays a key role on the conversion of PrP^C to PrP^{Sc} (Baron *et al.*, 2002; Goold *et al.*, 2011). Therefore, it is necessary to obtain more *in vitro* evidence in deciphering the role of GPI anchor in this conversion. To this end, comparative infectivity studies that rely on production of infectious prion from recombinant non-lipidated and lipidated FL_PrP constructs can be performed. Based on the semisynthesis strategy described above, sufficient amount of lipidated FL_PrP can be produced to use in these studies.

On the other hand, the interaction of lipidated Δ CR_PrP with lipid membranes showed a potential pore formation of this PrP construct in the membranes. However, further studies to prove the pore formation of lipidated Δ CR_PrP are required. Utilizing electrophysiological measurements, one can learn how lipidated Δ CR_PrP construct forms pores in membranes and also possibly characterize conductivity properties of the resulting pores. In addition, *in vitro* viability/toxicity assays by mixing lipidated Δ CR_PrP with cultured neuronal cell lines, which originate from different parts of the mouse brain, should be aimed to answer the question of whether there is a specific part of the brain that promotes the pore formation of lipidated Δ CR_PrP.

7.2 Recombinant expression of soluble prion protein for C-terminal modification

This section was published in FEBS Letter (2013) 587, 430-435 with title: "Recombinant expression of soluble murine prion protein for C-terminal modification"

7.2.1 Introduction

The EPL strategy used above to produce lipidated PrPs is based on expression of PrP in fusion with an *Mxe* intein in *E. coli* in order to generate PrP with a C-terminal α -thioester group. However, these constructs were typically deposited in

inclusion bodies in *E. coli*. Generation of PrP α -thioesters required solubilization of these inclusion bodies under denaturing conditions, which severely limited the yield of the intein cleavage and subsequent EPL reactions (sections 7.1.2 and 7.1.4).

In order to improve semisynthetic access to posttranslationally modified PrP, one strategy for soluble expression of PrP-*Mxe* intein constructs in *E. coli* was developed. Access to larger amounts of soluble, folded PrP will allow more straightforward access to homogeneously modified PrP variants, e.g. carrying a C-terminal membrane anchor and/or N-glycosylations. Efforts to achieve this goal by co-expression of PrP with bacterial chaperones in the cytoplasm of *E. coli* in order to assist the folding of prion protein failed (Kyratsous *et al.*, 2009).

However, previous experiments by others have shown that a direct N-terminal fusion of *E. coli* DnaK chaperone leads to an improved solubility of recombinantly expressed proteins in *E. coli* (Kyratsous *et al.*, 2009). Therefore, a variety of N-terminal fusion constructs of DnaK with PrP-*Mxe* intein protein were cloned, expressed and tested as described in Figure 7. 30.

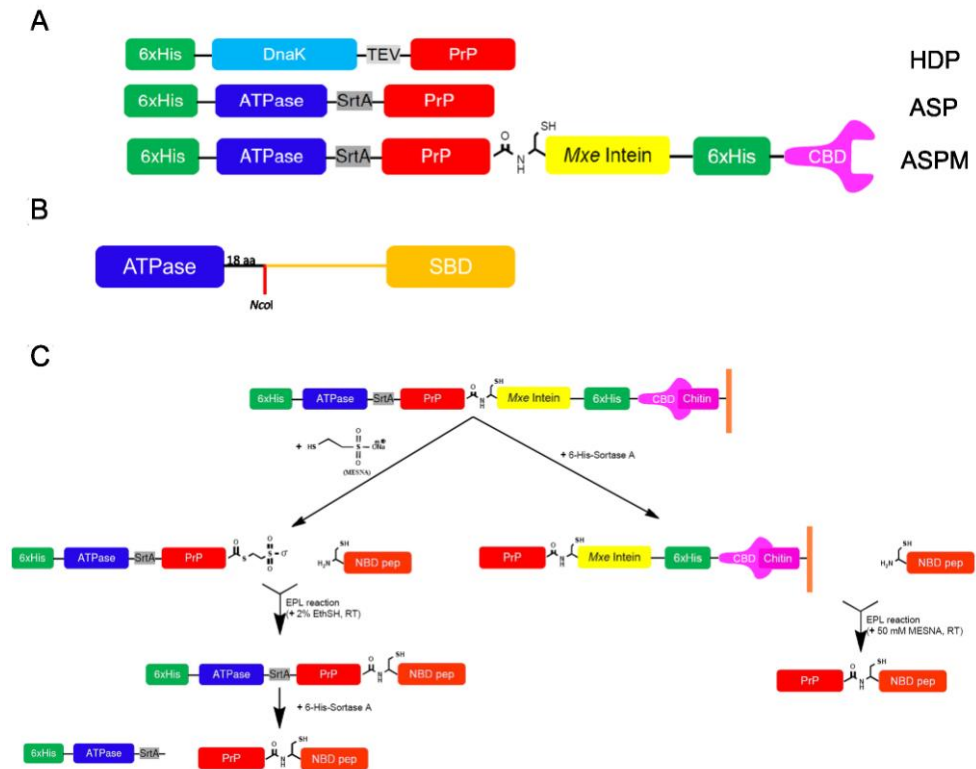


Figure 7. 30 A) Scheme of all generated fusion proteins. B) *NcoI* site in DnaK. C) Semisynthesis strategy to create soluble PrP with C-terminal modifications.

7.2.2 Construction, expression, and purification of DnaK-PrP fusion protein

The plasmid expressing *E. coli* DnaK with an N-terminal 6xHis tag (Figure 7.30) was constructed. The resulting plasmid (pET30-DnaK) is transcribed under control of an IPTG-inducible T7 promoter. Expression and purification of this His-DnaK construct provided 14 mg of His-DnaK from 1 liter medium in 3 hrs after induction (Figure 7.31 A). Subsequently, the mouse PrP(90-231) encoding gene was cloned into pET30-DnaK to form plasmid pET30-HDP. Expression of the resulting His-DnaK-PrP (HDP) construct was evaluated by SDS-PAGE. IPTG-induced overexpression of HDP provides the target protein mainly in the soluble fraction (Figure 7.31 B), which is in good agreement with a similar strategy previously applied for soluble expression of full-length PrP (Kyratsous *et al.*, 2009). HDP protein was purified by Ni-NTA affinity chromatography followed by size exclusion chromatography (SEC) using a Superdex 200 (16/60) column to achieve high purity in combination with an excellent overall yield of 42 mg HDP from 1 liter of *E. coli* culture (overnight expression, Figure 7.31 C).

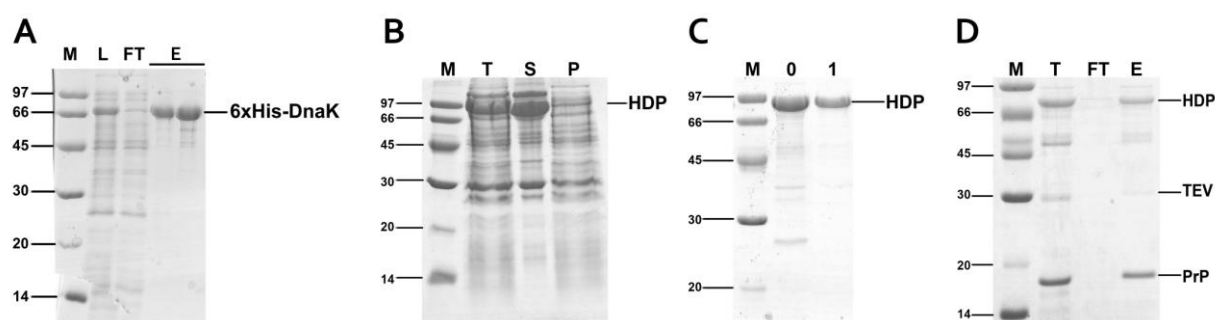


Figure 7.31 SDS-PAGE analysis of 6xHis-DnaK and soluble DnaK-PrP fusion protein (HDP). A) Expression and affinity purification of 6xHis-DnaK, M: Molecular weight marker, L: lysate, FT: flow through, E: elution after incubation with Ni-NTA resin. B) Expression of HDP, T: total cell extract, S: soluble fraction, P: pellet fraction. C) Purification of HDP, 0: Ni-NTA eluate, 1: pure fraction from SEC. D) TEV cleavage, T: total reaction mix, FT: flow through, E: elution after incubation with Ni-NTA resin

7.2.3 Cleavage of DnaK from DnaK-PrP

Purified HDP protein was cleaved by addition of recombinantly expressed TEV protease (see section 6.4.3). Favorable redox conditions for this cleavage reaction as well as for maintaining the crucial internal disulfide bridge in PrP were achieved by

addition of the redox couple GSH/GSSG. Protease cleavage was monitored by SDS-PAGE and was complete after o/n incubation at 10°C. Even though control of the redox conditions helped to stabilize PrP, a subsequent centrifugation step was required to remove precipitated PrP. Approximately 10% of PrP precipitated under these conditions. Separation of the remaining soluble PrP from the DnaK-tag and from TEV protease was expected to work via Ni-NTA affinity purification. PrP should be collected in the flow-through while DnaK and TEV should bind to the Ni-NTA matrix via their respective His-tags. However, this strategy for separating PrP from DnaK was unsuccessful in our hands. Only minor amounts of soluble PrP were found in the flow-through and the majority of PrP eluted together with DnaK at concentration of 250 mM imidazole (Figure 7.31 D). This behavior can be explained by a rather strong interaction between the substrate binding domain (SBD) of DnaK with PrP as observed in other cases (Mayer *et al.*, 2000; Rial & Ceccarelli, 2002). Based on this assumption we removed the DnaK-SBD and speculated that the ATPase domain by itself would impart similar solubilizing properties as the complete DnaK protein.

7.2.4 Removal of SBD from DnaK-PrP

To this end, advantage of a natural *NcoI* site ideally positioned just at the beginning of the SDB within the DnaK gene was taken (Figure 7. 30 B). Moreover, the TEV protease cleavage site was replaced with a Sortase A (SrtA) site to circumvent the use of reducing agents during TEV cleavage reactions, which causes partial precipitation of PrP. These changes led to the ATPase-SrtA-PrP (ASP) construct, which was tested for soluble expression in two *E. coli* strains: BL21(DE3)RIL and Origami 2 (DE3) RIL. The latter one has been supposed as an *E. coli* strain that greatly enhances disulfide bridge formation in the cytoplasm (Bessette *et al.*, 1999). Here, no significant differences in solubility and expression levels between both strains were observed (Figure 7.32 A). This comparison reveals that the ATPase domain of DnaK in the ASP construct is sufficient to ensure soluble overexpression in the cytoplasm of *E. coli*.

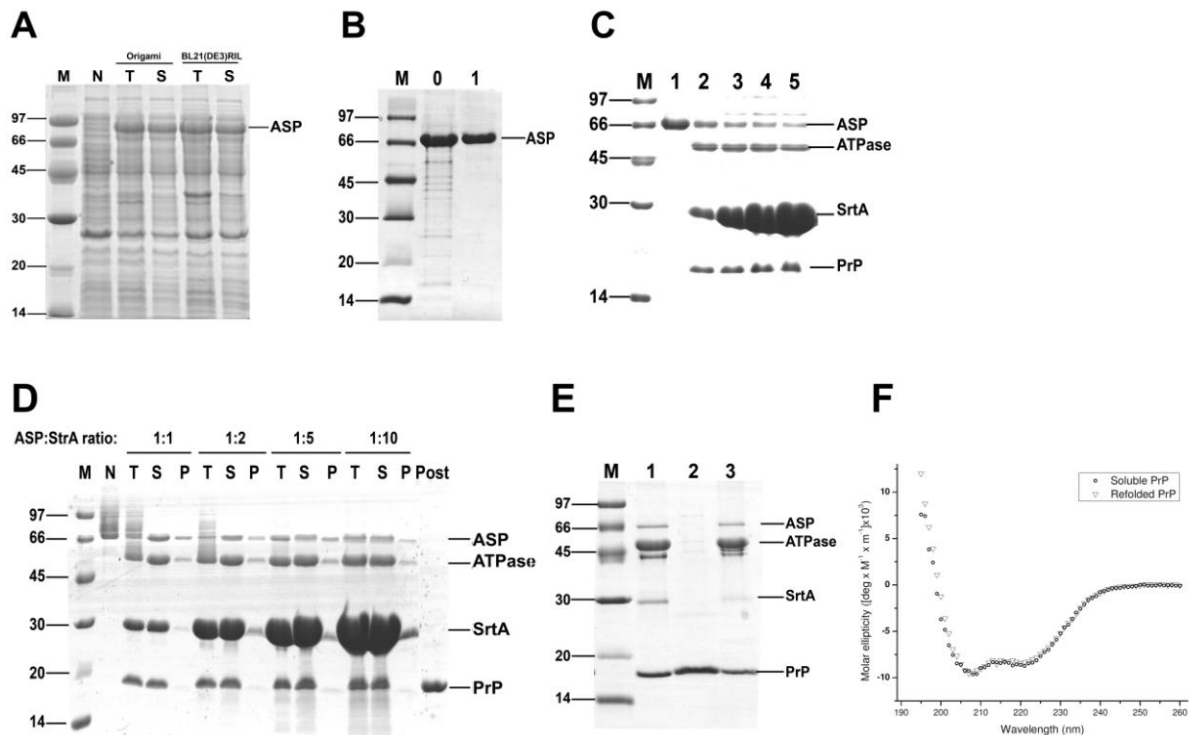


Figure 7.32 SDS-PAGE analysis of ATPase-PrP fusion protein (ASP). **A)** Soluble expression in two *E. coli* strains: BL21(DE3)RIL and Origami2(DE3)RIL, N: control without IPTG, T: total cell extract, S: soluble fraction of lysed cells. **B)** Purification of ASP, 0: Ni-NTA eluate, 1: pure fraction from SEC. **C)** Screening to identify optimal conditions for SrtA cleavage. Cleavage reactions of ASP by SrtA with different ASP:SrtA molar ratios of 1:1, 1:2, 1:5 and 1:10 in lanes 2 to 5, respectively, and lane 1 is ASP only. **D)** The cleavage reactions were centrifugally separated into two fractions: supernatant (S) and pellet (P), and were subjected to SDS-PAGE analysis together with one sample of each cleavage reaction before centrifugation, total (T). **E)** SrtA cleavage, 1: total reaction mix, 2: flow through, and 3: elution from Ni-NTA resin. **F)** CD spectra of soluble PrP from ASP construct (circles) and refolded PrP protein (triangles) from inclusion bodies.

Purification was achieved by Ni-NTA affinity chromatography and provided highly pure ASP protein with an average yield of 85 mg per liter culture (Figure 7.32 B). This finding confirms our initial assumption that the SBD of DnaK mediates tight binding to PrP but plays only a minor role in solubilizing it. Cleavage of purified ASP protein by SrtA was optimized by screening several conditions (Figure 7.32 C). Optimized conditions resulted in quantitative release of soluble PrP from the ASP

construct (Figure 7.32 C and D). The identity of PrP was confirmed by western blot analysis (Figure 7.33, lane 2).

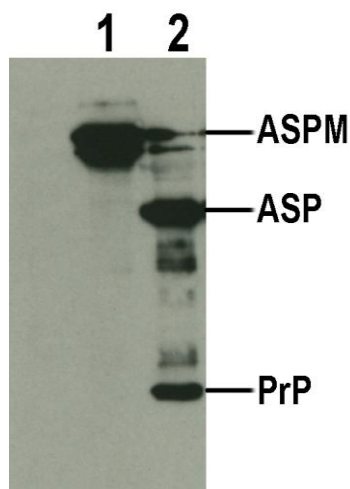


Figure 7.33 Western blot analysis of ASPM (lane 1) and SrtA cleavage of ASP (lane 2)

7.2.5 High yield production of soluble PrP(90-231) from ASP construct

Optimal conditions for expression, cleavage and purification of soluble PrP as identified above were applied for processing 85 mg of pure ASP obtained from 1 liter of *E. coli* culture to produce soluble PrP. Only minor amounts of PrP are retained on the Ni-NTA matrix via unspecific interaction (Figure 7.32 E). Removal of the SBD almost completely alleviates the problem of PrP not eluting from to the Ni-NTA matrix.

Next, the secondary structure of soluble PrP was analyzed by CD spectroscopy and compared to recombinant PrP that was folded from inclusion bodies following an established procedure. Both variants showed similar CD spectra with 2 minima at 208 and 222nm indicating predominantly α -helical proteins (Figure 7.32 F). Quantitative analysis indicates a similar percentage of α -helical structure elements in both PrP variants, typical for cellular PrP^C protein (Pan *et al.*, 1993; Riek *et al.*, 1997). The overall yield of soluble PrP protein from this strategy was 15 mg from 1 liter of *E. coli* culture (69% based on the amount of total PrP expressed), indicating the superior results obtained with this strategy when compared to another recently published soluble expression system for PrP (Abskharon *et al.*, 2012).

Furthermore, an aggregation experiment, based on Thioflavin T binding of fibrils, for soluble, refolded and denatured PrP variants was conducted to compare their biochemical characteristics. Soluble and refolded PrP exhibit a similar fibrillation behavior with an extended lag phase between 30 to 40 hrs, very different from that of denatured PrP with a lag-phase of ca. 10 hrs (Figure 7.34). In combination with the secondary structure analysis, this experiment emphasizes the similar properties in soluble and refolded PrP.

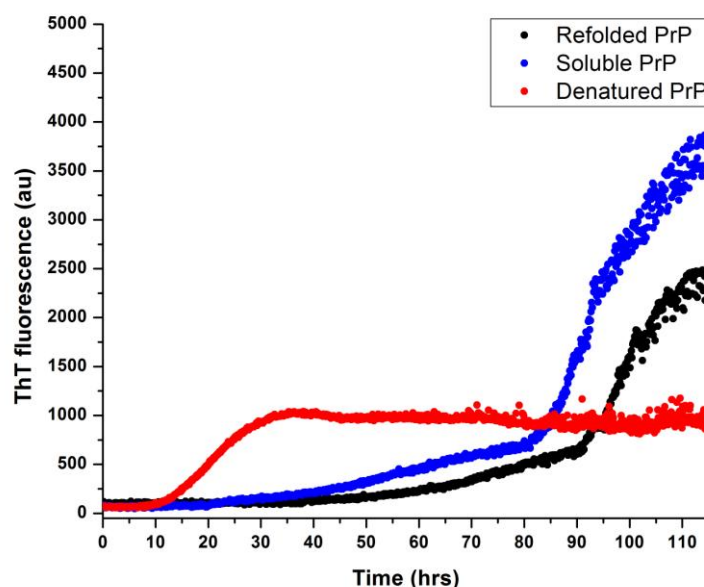


Figure 7.34 Aggregation kinetics of soluble PrP (blue), refolded PrP (black) and denatured PrP (red). A similar behavior of soluble and refolded PrP was observed in contrast to the fast aggregation of denatured PrP.

7.2.6 Synthesis of NBD-labeled peptide

Boc-based SPPS was used to synthesize NBD-labeled peptide (NBD peptide). This peptide contains an N-terminal cysteine for EPL, 6 histidine residues for advance application of Ni-NTA affinity purification to separate the ligation product from EPL reaction. Furthermore, NBD fluorophore was covalently coupled to lysine side chain for fluorescence applications. The NBD peptide was cleaved off from resin by HF, lyophilized and purified by HPLC using C8 column with a linear gradient of 5 to 45 % (v/v) of buffer B for 60 minutes. The purity of NBD peptide was analyzed by LC-MS (Waters AutoPurification HPLC/MS System), where monitoring wavelength at

465nm (excitation wavelength of NBD fluorophore) revealed a unique peak with the observed mass from ESI-MS analysis of 1350 Da, which is consistent with the calculated mass of NBD peptide 1348 Da (Figure 7.35).

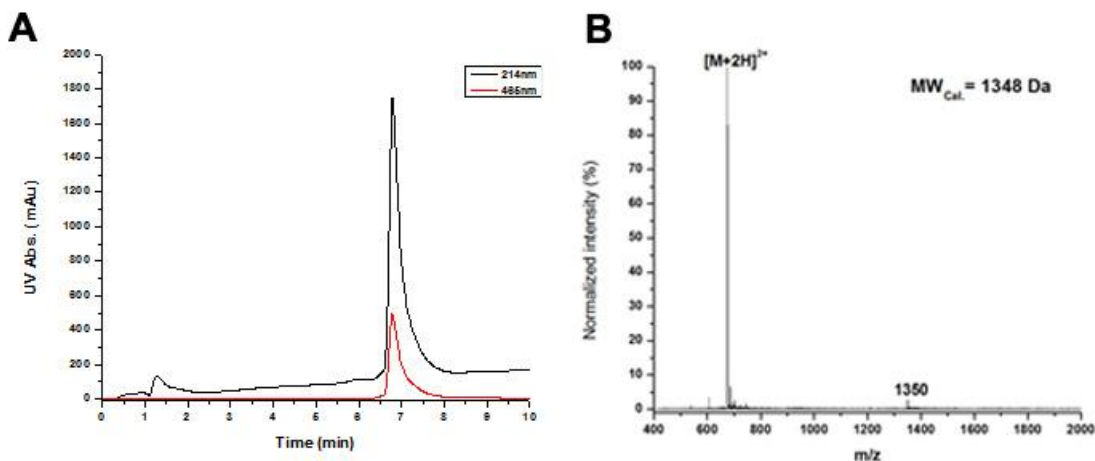


Figure 7.35 LC-MS analysis of purified NBD peptide including A) analytical HPLC chromatogram with an excitation wavelength (red) of NBD fluorophore and B) ESI-MS analysis of the peak corresponds to NBD peptide from HPLC chromatogram.

7.2.7 Preparation of soluble PrP containing a C-terminal α -thioester

The successful strategy for expression of large amounts of soluble T_PrP was extended to soluble expression of a T_PrP-intein construct. To this end, a C-terminal *Mxe* mini-intein-CBD tag was added to ASP. Soluble expression of this ASPM construct in *E. coli* BL21(DE3)RIL was confirmed by analysis of centrifugation fractions of lysed cells. ASPM accumulated mostly in the supernatant (Figure 7.36 A). Ni-NTA purification yielded ASPM that was subsequently immobilized on chitin beads via its C-terminal CBD (Figure 7.36 B). PrP expression was also confirmed by western blot analysis (Figure 7.33, lane 1). Addition of 250 mM MESNA led to cleavage of the *Mxe* mini-intein and to formation of an α -thioester group at the C-terminus of the ASP protein. The resulting ASP-SR was found in the supernatant (Figure 7.36 C) and further purified by SEC using a Superdex 75 (16/60) column to reach high purity (Figure 7.36 D). The presence of an α -thioester group at the C-terminus of ASP was confirmed by successful expressed protein ligation (EPL) with the NBD peptide containing an N-terminal cysteine residue (Figure 7. 30 C) (Muir, 2003). SDS-PAGE analysis in combination with a fluorescence scan of the gel prior

to coomassie staining clearly proved that the ASP protein was almost quantitatively linked to the NBD peptide (Figure 7.36 E). In a final step, the EPL reaction mix was incubated with SrtA in order to release soluble PrP carrying the NBD peptide. After incubation for 16 hrs the reaction mixture was centrifuged and the supernatant was again analyzed by SDS-PAGE (Figure 7.36 F). Almost quantitative ligation and subsequent complete removal of the ATPase domain make this strategy much more efficient than previously used systems based on refolded PrP and even split inteins (Olschewski *et al.*, 2007).

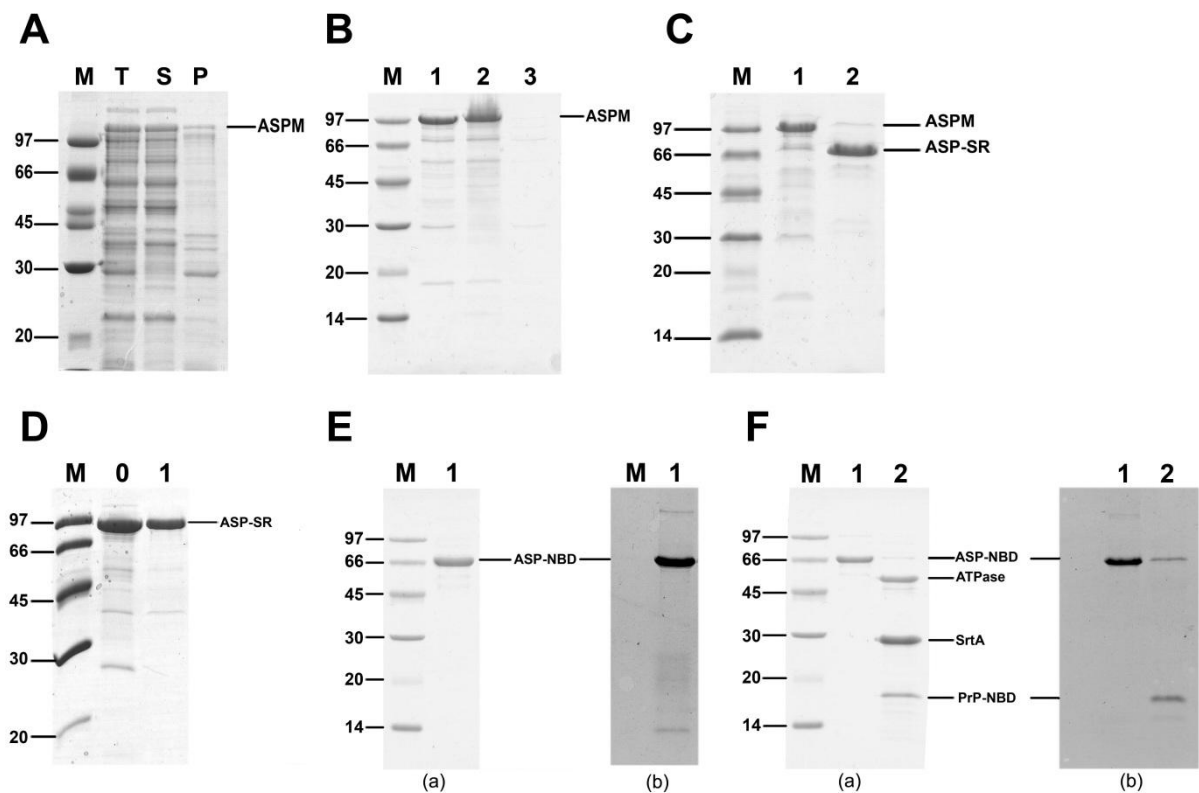


Figure 7.36 SDS-PAGE analysis of ASPM and ASP-SR in EPL reactions. **A)** ASPM expression, *T*: total cell extract, *S*: soluble fraction, *P*: pellet fraction of lysed cells. **B)** 1: Ni-NTA purifications of ASPM, 2: ASPM immobilized on chitin beads, 3: flow through. **C)** MESNA-induced cleavage of ASPM, 1: ASPM protein, 2: ASP-SR released from chitin beads. **D)** ASP-SR purification by SEC, 0: crude ASP-SR, 1: pure fraction. **E)** EPL reaction of ASP-SR with NBD peptide; (a) coomassie staining, (b) fluorescence scan. **F)** ASP-NBD after SrtA cleavage; (a) coomassie staining and (b) fluorescence scan.

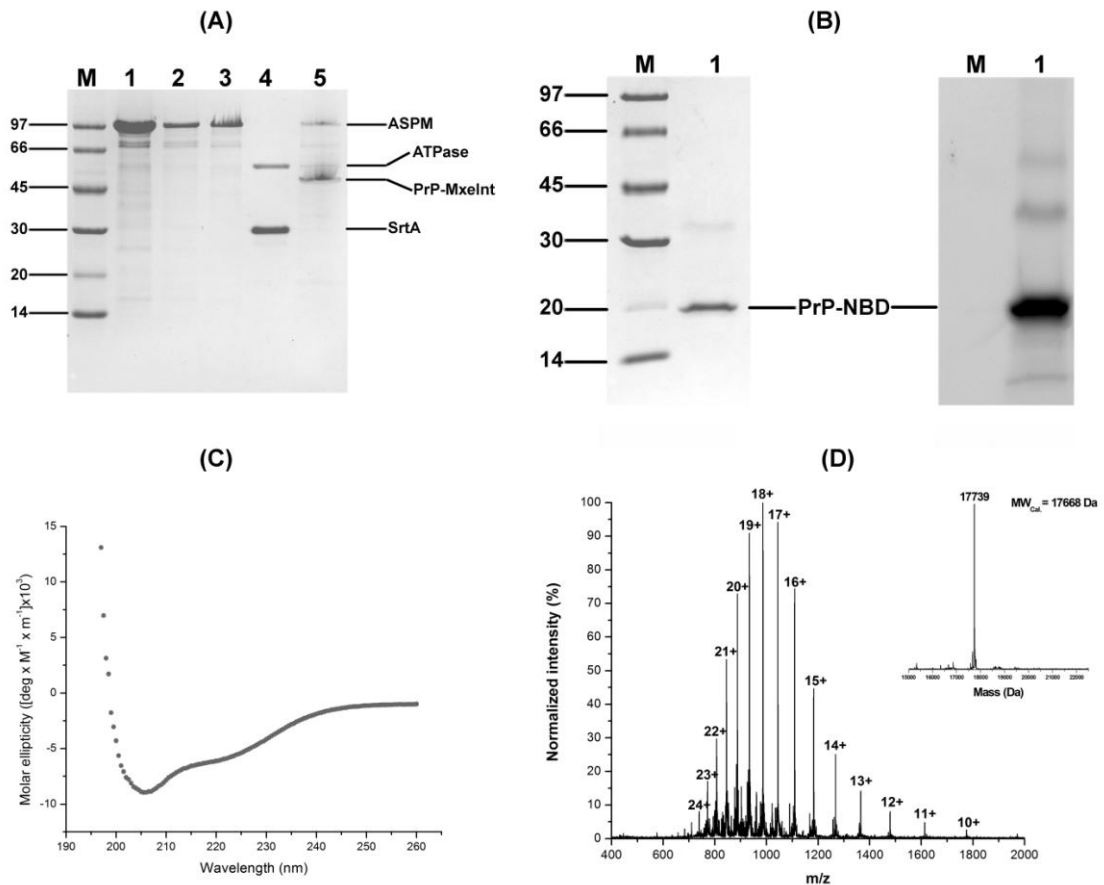


Figure 7.37 C-terminal modification of soluble PrP. A) SDS-PAGE of SrtA cleavage of immobilized ASPM protein. 1: ASPM used for loading chitin beads, 2: excess ASPM not bound to beads, 3: ASPM immobilized on chitin beads, 4: SrtA addition leads to release of ATPase domain, 5: PrP-intein bound to chitin beads. B) SDS-PAGE analysis of soluble PrP-NBD generated by *in situ* cleavage and EPL reaction with NBD peptide and subsequent purification by Ni-NTA chromatography. Coomassie staining (a) and fluorescence scan (b); C) CD spectrum of PrP-NBD; D) ESI-MS of soluble PrP-NBD.

To study the efficiency of the above described reaction in reverse order (Figure 7. 30 C, right), 4 mg of ASPM protein were immobilized on 2 ml of chitin beads and the ATPase domain was cleaved off by SrtA to produce PrP-intein on chitin beads (Figure 7.37 A). Immobilized PrP-intein was mixed with 100 μ M of NBD peptide and 50 mM MESNA in buffer containing 50 mM Tris-HCl at pH 8.0, 1 mM EDTA and 0.5 mM TCEP. The *in situ* cleavage and ligation reaction was carried out over 24 hrs with gentle shaking. The solution containing the ligation product PrP-NBD was centrifuged to remove chitin beads, dialyzed against buffer (50 mM Tris-HCl, pH

8.0) to remove excess NBD peptide and loaded on Ni-NTA resin to obtain purified PrP-NBD (Figure 7.37 B). Soluble PrP carrying a C-terminal NBD peptide was obtained with an overall yield of 250 μg from 4 mg of ASPM protein (32% based on the total amount of PrP that can theoretically be obtained from ASPM protein). Next, the secondary structure of soluble PrP-NBD was analyzed by CD spectroscopy, which showed the typical α -helical features of correctly folded cellular PrP (Figure 7.37 C). ESI-MS analysis of PrPNBD protein gave a molar mass of 17,739 Da (Figure 7.37 D), which deviates by +71 Da from the calculated mass of 17,668 Da. Such a difference was observed only when TCEP was added to the *in situ* cleavage and ligation reaction over extended periods of time at a concentration of 0.5 mM to prevent oxidation of the N-terminal cysteine residue of the NBD peptide. TCEP has long been recognized as a well-tolerated and widely used reducing agent that does not cause significant side reactions under many conditions (Hansen & Winther, 2009). However, here at pH 8.0 TCEP or an unidentified byproduct caused a defined modification of the PrP, which did not occur in the absence of TCEP.

7.2.8 Conclusion

The soluble expression of a recombinant PrP-Mxe intein fusion protein (ASPM) was developed to improve the efficiency of semisynthetic strategies for producing homogeneously posttranslationally modified PrP. We showed that PrP-Mxe intein protein N-terminally fused to the ATPase domain of HSP 70 DnaK overexpresses as a soluble protein in the cytoplasm of *E. coli*. Consequently, this fusion allowed a straightforward way to generate PrP-variants containing C-terminal modifications without the need for subsequent protein folding and disulfide bond formation. The latter step can be especially challenging when introducing additional cysteine residues, e.g. during EPL reactions that increase the probability of non-native disulfide bond formation. We further improved this strategy of soluble expression by minimizing the DnaK fusion partner down to the ATPase domain alone. This led to high quantities of soluble, cellular PrP even in the presence of a C-terminal intein fusion as well as preventing undesired strong interactions between the DnaK-SBD and PrP. Previous studies reported that neither coexpression with chaperones nor periplasmic expression in *E. coli* succeeded in producing soluble intact PrP proteins (Hornemann & Glockshuber, 1996; Kyratsous *et al.*, 2009). Thus, we believe that this strategy can be extensively applied for soluble expression of

other proteins containing disulfide bridges in fusion with intein for semisynthesis method.

7.3 Covalently linking the Tudor domain of SMN protein and its low affinity ligand sDMA for structural studies

7.3.1 Introduction

Survival motor neuron (SMN) protein is a 294-amino acid protein. Its assumed biochemical function is the formation of a large protein complex. The SMN complex is composed of SMN protein and 7 proteins named Gemin 2-8, and this complex regulates a strict specificity of the small nuclear ribonucleoprotein assembly process by binding both Sm proteins as well as small nuclear RNA (snRNA), and subsequently this binding results in the interaction of Sm proteins and snRNA (Figure 7.38 A) (Kolb *et al.*, 2007). SMN protein contains a central Tudor domain that facilitates the transient interactions of SMN and Sm proteins by its recognition and binding to symmetrically dimethylated arginine residues (sDMA) from the C-terminal tails of Sm proteins. The Tudor domain of SMN protein (SMN Tudor) contains approximately 60 amino acids consisting of a five-stranded β -sheet that forms a β -barrel structure (Figure 7.38 B). The binding pocket of the Tudor domain contains several aromatic residues forming a hydrophobic cage, which was found to interact with sDMA (Sprangers *et al.*, 2003). In addition, a mutation of E134K within the Tudor domain prevents Sm binding and consequently causes spinal muscular atrophy (Buhler *et al.*, 1999).

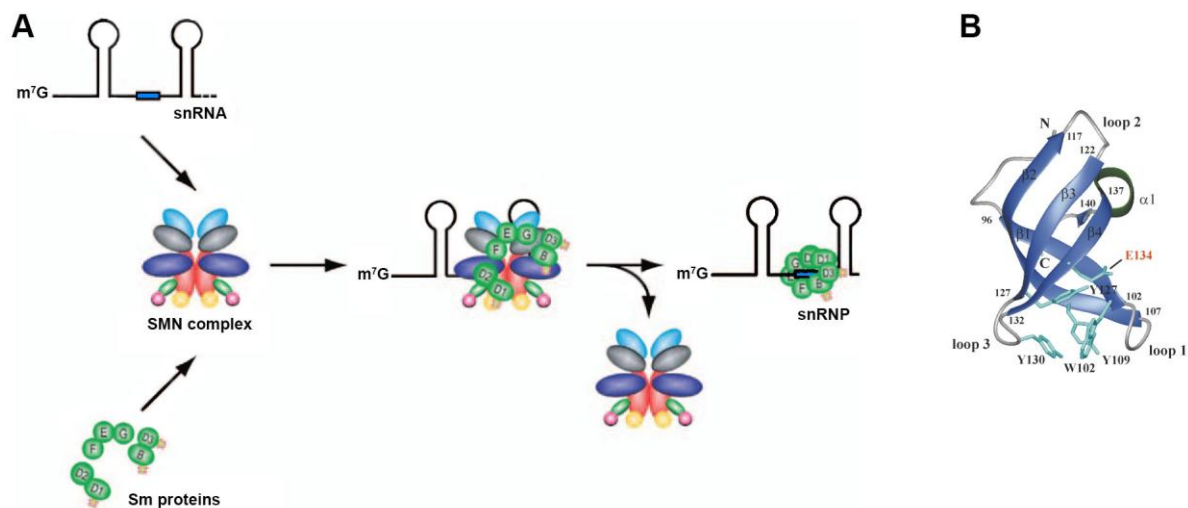


Figure 7.38 A) Schematic illustration of the function of SMN complex in the assembly of small nuclear ribonucleoprotein. The SMN complex binds to both Sm proteins and snRNA and drives the assembly of Sm proteins onto the Sm site of snRNA (blue) (Kolb *et al.*, 2007). B) NMR structure of the SMN Tudor with residues in the binding pocket are highlighted (Sprangers *et al.*, 2003).

Due to the weak binding of SMN Tudor to sDMA, previous structural studies of SMN Tudor bound to sDMA were forced to use a large excess of free sDMA to fully populate the complex and required high concentrations of both protein and ligand (mM range) (Tripsianes *et al.*, 2011). However, such condition is not always ideal for structural analyses of the weak interactions, in particular of proteins that can be aggregated at high concentration. Moreover, the transient interactions are weak and flexible that can challenge structural studies because the transient complex of protein-ligand can be difficult for crystallization or potentially induce detrimental exchange broadening in NMR spectra. To overcome these issues, covalently linking SMN Tudor to its ligand sDMA with glycine linkers of different length in between (as shown in Figure 7.39) was carried out.

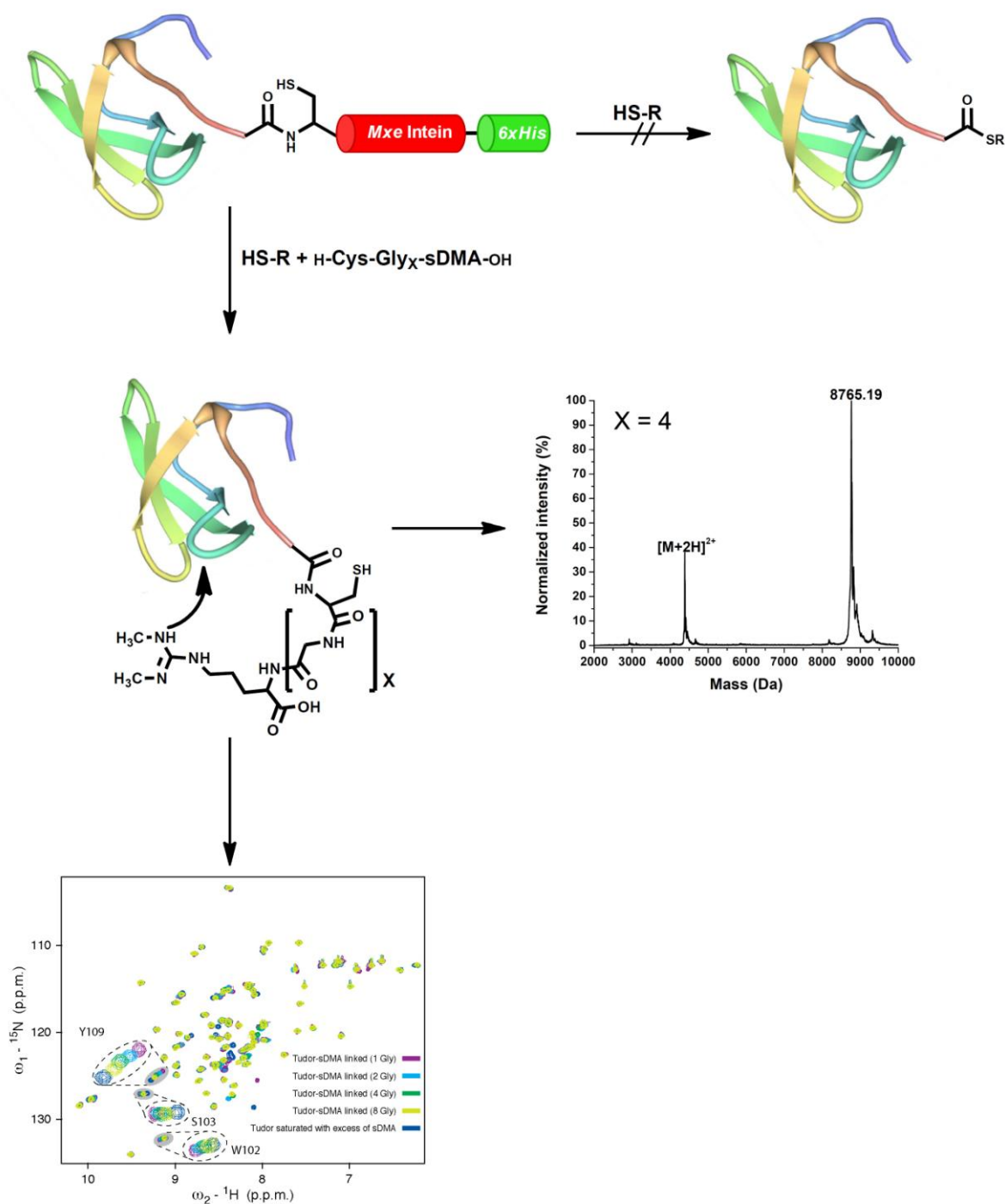


Figure 7.39 Semisynthesis strategy was used to produce SMN Tudor-sDMA proteins

7.3.2 Expression and purification of SMN Tudor-Mxe intein-6xHis

SMN Tudor was C-terminally fused to Mxe intein (section 6.5.1) to generate SMN Tudor containing a C-terminal α -thioester for EPL from an intein cleavage reaction (sections 7.1.2 and 7.2.7). SDS-PAGE analysis of the expression of SMN Tudor-Mxe intein revealed a soluble expression of this fusion protein in *E. coli* (Figure

7.40 A). The fusion protein was purified by affinity chromatography using Ni-NTA resin. The lower band in SDS-gel was assumed to be *Mxe* intein-6xHis, possibly generated by *in vivo* cleavage of the fusion protein during expression in *E. coli* (Southworth *et al.*, 1999).

In order to produce SMN Tudor protein for NMR analysis, the *E. coli* strain was grown in minimum medium containing ^{13}C -glucose and ^{15}N -ammonium chloride and the expression of SMN Tudor-*Mxe* intein fusion protein was induced. ^{13}C , ^{15}N -labeled SMN Tudor-*Mxe* intein fusion protein was purified using a similar procedure as described above.

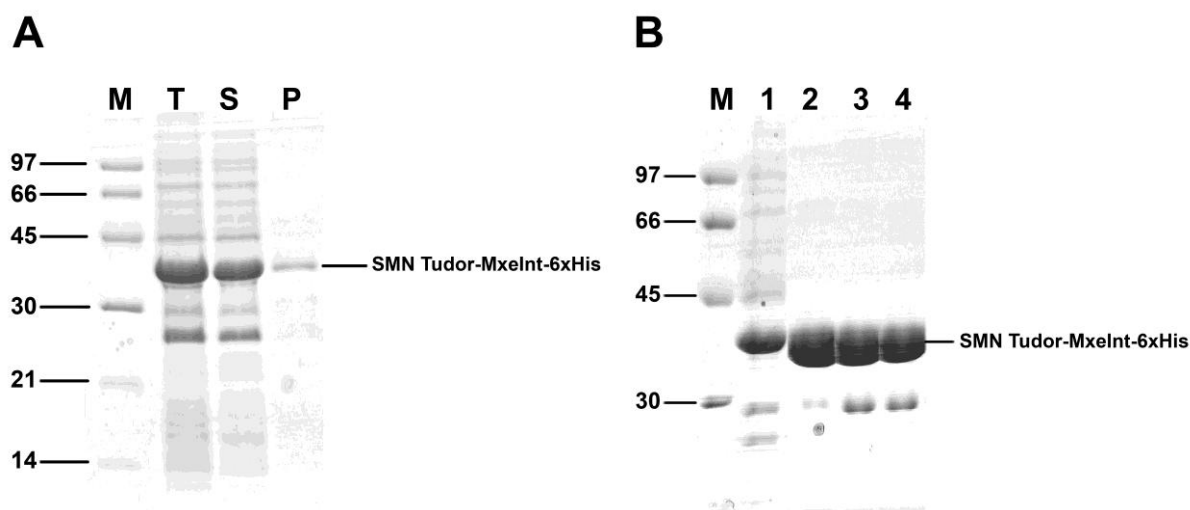


Figure 7.40 SDS-PAGE analysis of SMN Tudor-*Mxe* intein-6xHis fusion protein. A) Expression of the fusion protein in *E. coli* BL21(DE3)RIL, T: total cell extract, S: soluble fraction, P: pellet fraction. B) Affinity purification of the fusion protein by Ni-NTA resin (lane 1) followed by size exclusion chromatography with Superdex 75 (16/60) column (lanes 2, 3, 4).

7.3.3 Synthesis of sDMA peptides

Fmoc-based SPPS was used to synthesize the sDMA peptides (section 6.5.3). These peptides contain an N-terminal cysteine for EPL, the commercially available sDMA residue and variable glycine linkers consisting of 1, 2, 4 or 8 glycine residues. All peptides were purified by HPLC using RP-C8 column and the pure fractions were analyzed by ESI-MS. The observed masses of 1, 2 and 4 Gly sDMA peptides were in excellent agreement with calculated masses (Figure 7.41 A, B, C). Concerning the

synthesis of 8 Gly sDMA peptide, ESI-MS measurement showed two masses: 819.23 Da, which corresponds to the mass of 8 Gly sDMA peptide and another mass: 876.31 Da which deviates by + 57 Da from the mass of 8 Gly sDMA peptide (Figure 7.41 D). This mass deviation leads to one possible modification that is one more glycine was coupled to the peptide during the synthesis procedure and this additional coupling yielded the 9 Gly sDMA peptide. The separation of this peptide from 8 Gly sDMA peptide by HPLC is not possible for us due to their very similar chromatographic behavior.

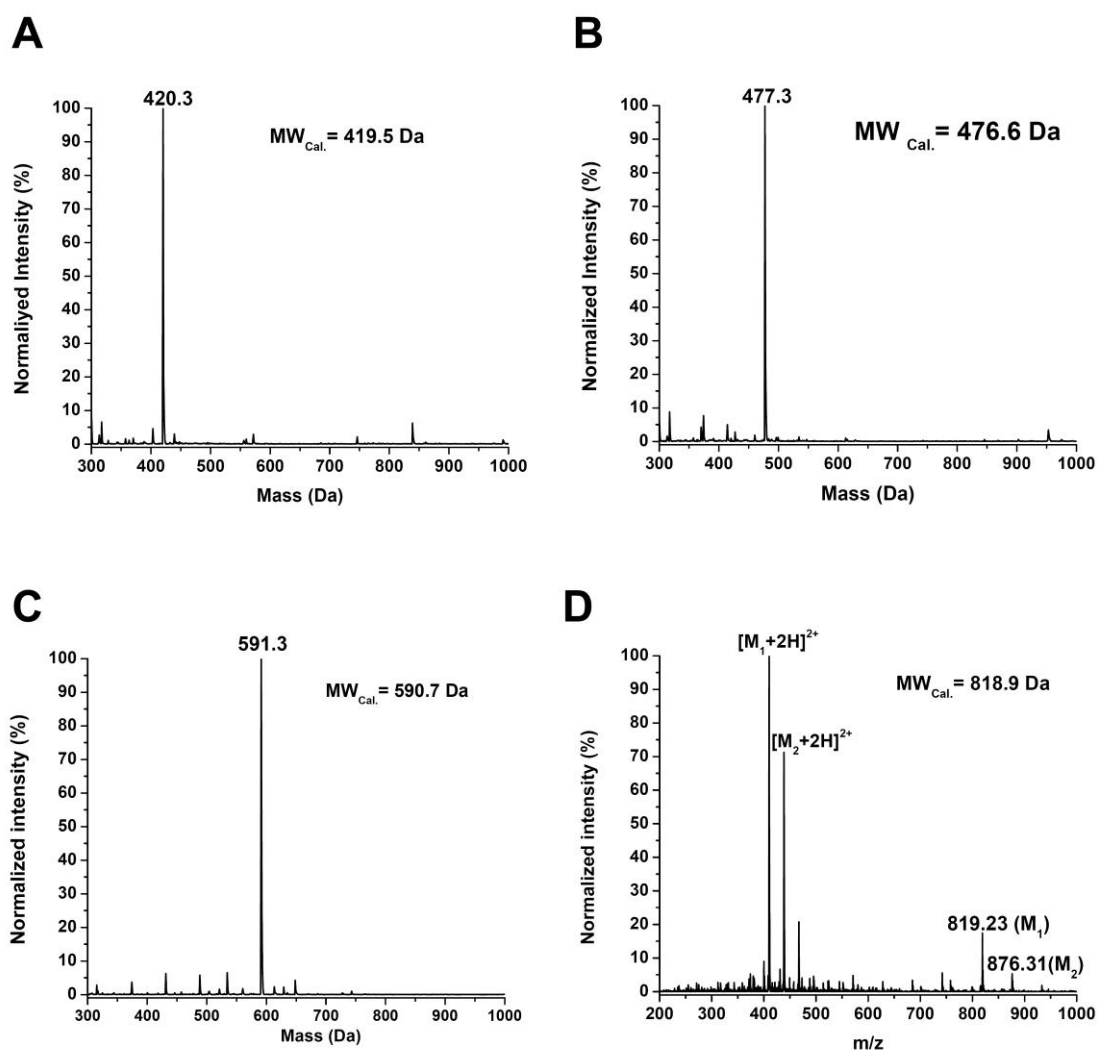


Figure 7.41 ESI-MS analysis of sDMA peptides with a flexible glycine linker: A) 01, B) 02, C) 04 and D) 08 glycine residues

7.3.4 Expressed protein ligation of SMN Tudor and sDMA peptides

7.3.4.1 Preparation of SMN Tudor containing a C-terminal α -thioester

Cleavage reactions of SMN Tudor-*Mxe* intein fusion protein were induced by adding an excess of MESNA. From the SDS-PAGE analysis, most of SMN Tudor was cleaved off from the SMN Tudor-*Mxe* intein fusion protein (Figure 7.42 A, lane 2) and successfully purified from the cleavage reaction by affinity purification with Ni-NTA resin. The resulting SMN Tudor thioester was collected in the flow through (Figure 7.42 A, lane 3) while remaining proteins: *Mxe* intein-6xHis and the uncleaved SMN Tudor-*Mxe* intein fusion protein were collected in elution fraction (Figure 7.42 A, lane 4). SMN Tudor was analyzed by MALDI-MS to unequivocally identify the protein and to confirm the presence of a MESNA-thioester. However, the observed masses of 7905 Da (minor) and 7763 Da (major) correspond to SMN Tudor with C-terminal α -thioester, and SMN Tudor without an α -thioester with an additional loss of 18 Da, respectively (Figure 7.42 B). The predominant generation of the latter species might be explained by an intramolecular reaction in which an intermediate MESNA-thioester was attacked by an internal cysteine thiol group to give an intramolecular thioester bond (thiolactone). Thiolactone formation involving an internal cysteine in synthetic peptide thioester segments for native chemical ligation has been reported and stability of these thiolactones seems to be highly sequence dependent (Banigan *et al.*, 2010; Durek *et al.*, 2007). Here we were not able to resolve the thiolactone by treatment of SMN Tudor with high concentrations thiol reagents such as MPAA, MESNA or ethanethiol (100 mM) in guanidine or TrisHCl containing buffers.

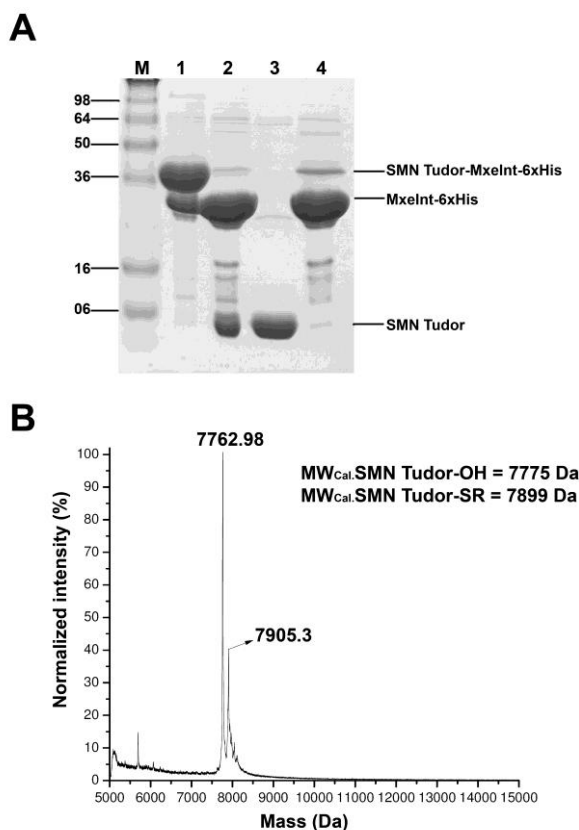


Figure 7.42 Preparation of SMN Tudor containing C-terminal α -thioester from cleavage reaction of SMN Tudor-Mxe intein. A) SDS-PAGE analysis of the cleavage reaction of SMN Tudor-Mxe intein and purification of SMN Tudor from this cleavage reaction. 1: SMN Tudor-Mxe intein fusion protein, 2: cleavage reaction of SMN Tudor-Mxe intein by addition of MESNA, 3: Flow through after loading the cleavage reaction on NiNTA-resin contains SMN Tudor without His tag, 4: Elution fraction from NiNTA-resin contains Mxe-6xHis and un-cleaved SMN Tudor-Mxe intein fusion protein. B) MALDI-MS analysis of the SMN Tudor with a mass deviation by +6 between observed and calculated masses.

7.3.4.2 One-pot EPL to produce SMN Tudor-sDMA proteins

To overcome the problem of thiolactone formation, a one-pot EPL strategy was developed, in which incubation of SMN Tudor-Mxe intein fusion protein with excess of the sDMA peptide was followed by addition of ethanethiol (section 6.5.4). The resulting SMN Tudor that was purified from this reaction by Ni-NTA affinity purification carried C-terminal covalently attached sDMA peptides. The observed mass of SMN Tudor-4 Gly sDMA was 8348.5 Da that is in very good agreement with

the calculated mass 8348.4 Da (Figure 7.43 A) and unligated SMN Tudor was not detected from the mass spectrometry analysis. In order to confirm that a covalent bond between SMN Tudor and the 4 Gly sDMA peptide was formed, the reaction product was incubated with 6 M guanidine chloride, 50 mM Tris-HCl, pH 8.0 and 10 mM BME at 37°C for 30 minutes followed by an LC-MS measurement. The LC-MS run revealed a unique peak corresponding to SMN Tudor-4 Gly sDMA protein (Figure 7.43 B). One possible explanation for this one-pot EPL is that the binding of the sDMA peptide to the binding pocket of SMN Tudor within SMN Tudor-*Mxe* intein fusion protein occurred during incubation of SMN Tudor-*Mxe* intein and sDMA peptide before addition of ethanethiol (Figure 7.39), thus the sDMA peptide was positioned in close proximity to C-terminus of SMN Tudor. Next, the fusion protein SMN Tudor-*Mxe* intein underwent thiolysis catalyzed by the thiol reagent to generate SMN Tudor α -thioester. The newly generated SMN Tudor α -thioester was immediately reacted with N-terminal cysteine of the sDMA peptide (Zhao *et al.*, 2008) to initiate the EPL reaction and prevent the thiolactone formation as found above from the cleavage of SMN Tudor-*Mxe* intein with MESNA (section 7.3.4.1).

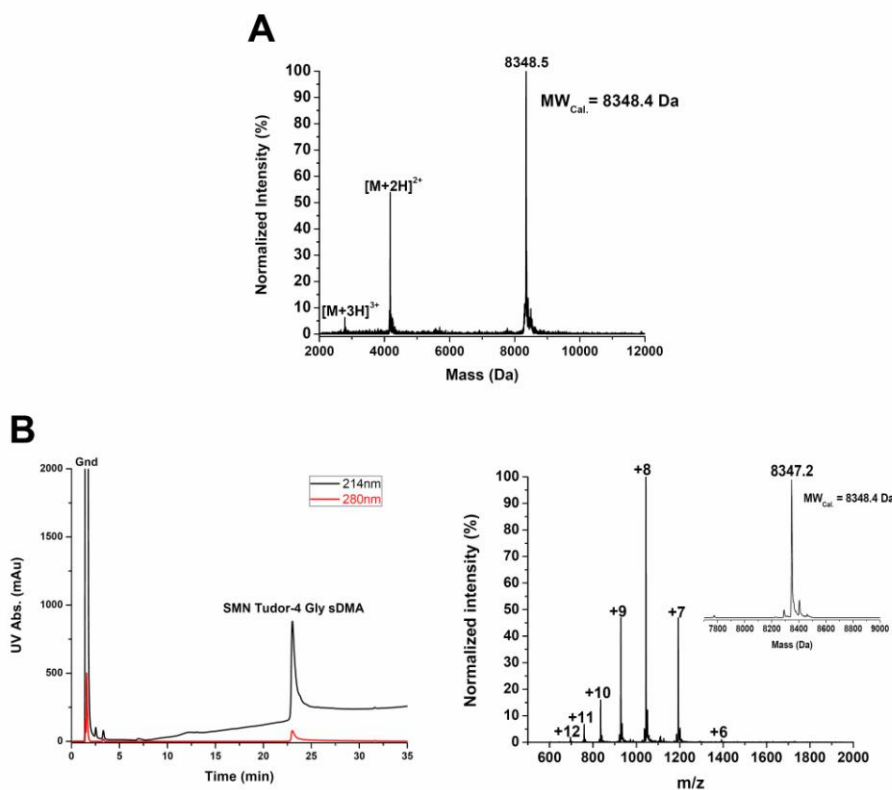


Figure 7.43 Mass spectrometry analysis of SMN Tudor-sDMA purified from one-pot EPL. A) MALDI-MS of SMN Tudor-4 Gly sDMA protein. B) LC-MS of SMN Tudor-4

Gly sDMA which was pretreated within buffer 6 M guanidine chloride, 50 mM Tris-HCl, pH 8.0 and 10 mM BME with HPLC chromatogram (left), Gnd: injection peak contains guanidine from pretreatment of protein, and ESI-MS of the peak corresponds SMN Tudor-4 gly sDMA protein from HPLC chromatogram (right).

Utilizing this successful one-pot EPL strategy, a variety of ^{15}N , ^{13}C -labeled SMN Tudor (CN_SMN Tudor) constructs with a C-terminal covalent link to sDMA peptides containing a flexible glycine linker with 1, 2, 4 and 8 glycine residues were generated (Figure 7.41 and section 7.3.3). Based on our assumption that pre-binding of sDMA peptide to SMN Tudor facilitates EPL, this strategy allowed us to rapidly identify the ideal linker length of sDMA peptides. Quantification of the ligation yields after 24 hrs by ESI-MS analysis showed that linkers with 4 or more glycine residues probably provide the necessary flexibility of sDMA to reach the binding pocket of the SMN Tudor as well as to ideally locate the Cysteine residue of the peptides close proximity with newly generated thioesters of SMN Tudor so that subsequently facilitate covalently linking the peptide to CN_SMN Tudor (Figure 7.44 D, E). Due to the additional 9 Gly sDMA peptide in synthesis of 8 Gly sDMA peptide, the ligation products were also generated two observed masses: 8999.63 Da and 9057.07 Da correspond to CN_SMN Tudor-8 Gly sDMA and CN_SMN Tudor-9 Gly sDMA, respectively (Figure 7.44 E). However, the presence of CN_SMN Tudor-9 Gly sDMA did not lead to any distinguished difference from CN_SMN Tudor-8 Gly sDMA in NMR analysis as showed below (Figure 7.45 A). In contrast, the linkers with 2 and 1 glycine residues led to generation of non-ligated CN_SMN Tudor proteins (Figure 7.44 B, C). The normalized intensities of MALDI analyses revealed that the 1 glycine linker resulted in much higher amount of non-ligated CN_SMN Tudor proteins were formed than the 2 glycine linker (Figure 7.44 B, C, M_2).

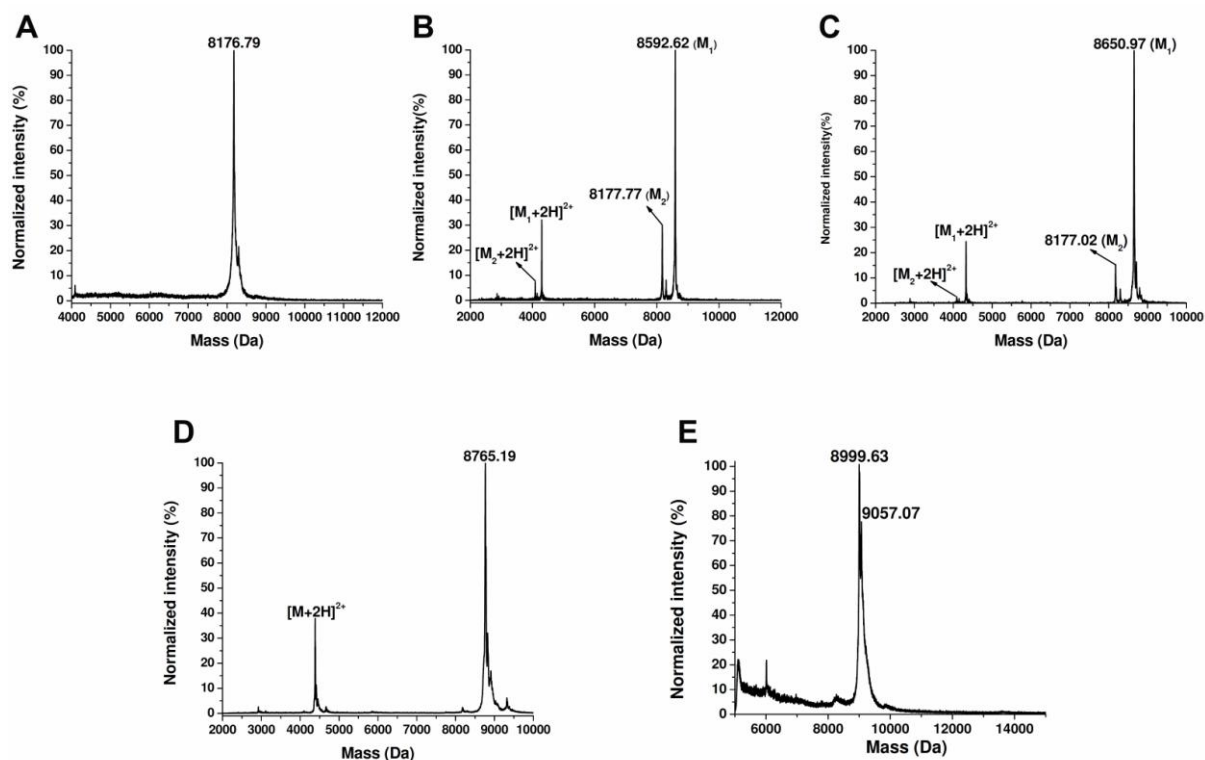


Figure 7.44 MALDI-MS analysis of CN_SMN Tudor purified from one-pot EPL reactions. A) CN_SMN Tudor alone; B, C, D and E) CN_SMN Tudor ligated to 1, 2, 4 and 8 Gly sDMA peptides, respectively.

7.3.5 Comparative NMR analysis of SMN Tudor-sDMA proteins and SMN Tudor that was fully saturated with high excess of free sDMA

$^{15}\text{N}, ^1\text{H}$ -HSQC spectra were recorded in collaboration with the group of M. Sattler for each of the 4 SMN Tudor-sDMA proteins and compared with the spectrum of SMN Tudor, which was fully saturated with free sDMA (sDMA-saturated SMN Tudor). The amide chemical shifts of all SMN Tudor-sDMA proteins are similar to the sDMA-saturated SMN Tudor (Figure 7.45 A and Figure 7.46). The latter interaction was found to occur in fast exchange regime on the NMR chemical shift time scale in agreement with the relatively weak binding, and five-fold molar excess of sDMA was required to analyze this interaction (Tripsianes *et al.*, 2011). A similar binding mode between all SMN Tudor-sDMA proteins and the sDMA-saturated SMN Tudor was observed. Since SMN Tudor-sDMA proteins contained a SMN Tudor/sDMA stoichiometry of 1:1, this observation presumably reflects that the binding of sDMA to SMN Tudor in CN_SMN Tudor-sDMA proteins has shifted to a slower exchange

regime than that of the sDMA-saturated SMN Tudor. Therefore, covalent linking of sDMA to C-terminus of SMN Tudor has significantly enhanced this interaction.

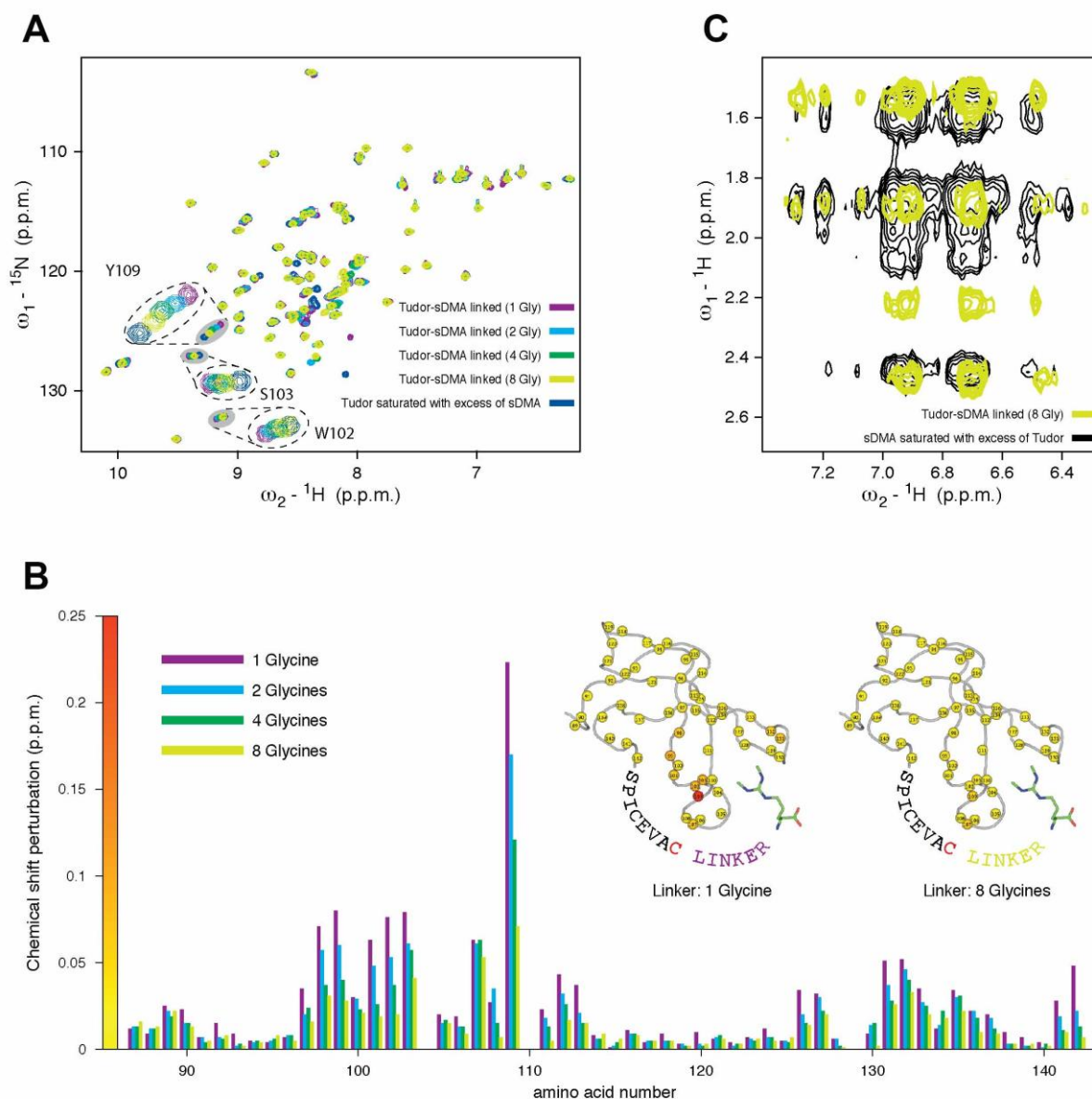


Figure 7.45 NMR analysis of SMN Tudor-sDMA interaction when covalently linked. A) Overlay of ^{15}N , ^1H HSQC spectra of SMN Tudor C-terminally ligated with sDMA peptides (linkers 1, 2, 4 or 8 glycine residues) and SMN Tudor saturated with excess of free sDMA. Some amides of SMN Tudor which have altered chemical shifts are highlighted. B) Amide chemical shift differences between SMN Tudor-sDMA proteins and fully bound SMN Tudor in excess of sDMA. Inset shows the SMN Tudor-sDMA structures with the C-terminal residues and linkers depicted. Nitrogen atoms are revealed as spheres, numbered and the colored according to the color gradient in the

vertical axis of the plot. Each panel maps the linker-induced perturbations on the SMN Tudor structure. C) Through space correlations between SMN Tudor (ω_2 , aromatic proton frequencies) and sDMA (ω_1 , proton frequencies) when SMN Tudor is linked via 8 glycine residues to sDMA or when sDMA is saturated with excess of SMN tudor.

Although a similar binding mode between all CN_SMN Tudor-sDMA proteins and the sDMA-saturated SMN Tudor was observed, a further analysis of the HSQC spectra revealed that the linker put a pressure on the SMN Tudor fold. Indeed, analysis of chemical shift perturbation showed the differences between ligated SMN Tudor proteins and the sDMA-saturated SMN Tudor, in particular of residues that shape the binding pocket (Figure 7.45 A, B). There is a linear relationship between local perturbations and linker length. A longer linker imposes less pressure on SMN Tudor fold. SMN Tudor-8 Gly sDMA protein showed the highest similarity to the sDMA-saturated SMN Tudor (Figure 7.46). This finding supports the information from analyzing the ligation yields of one-pot EPL by MS, which hinted toward the fact that the longer linker provides the required flexibility of sDMA to reach the binding pocket of SMN Tudor.

In order to prove that our ligation approach is suitable for structural analysis of weak protein-protein interactions such as the SMN Tudor-sDMA interaction, through-space correlations between ^{15}N , ^{13}C -labeled SMN Tudor and the unlabeled sDMA in SMN Tudor-8 Gly sDMA protein were recorded. Tripsianes and colleagues showed that this measurement was able to determine the fully bound form of unlabeled sDMA by using an excess of labeled SMN Tudor (Tripsianes *et al.*, 2011). The majority of correlations originate from proton frequencies of aromatic residues of SMN Tudor, which form the binding pocket and the proton frequencies of sDMA within the 8 Gly sDMA peptide were highly comparable to the ones corresponding to full bound state of sDMA that was saturated with excess of SMN Tudor (Figure 7.45 C). The NMR data demonstrate that a weak interaction such as SMN Tudor-sDMA is much more stable when two moieties are covalently linked.

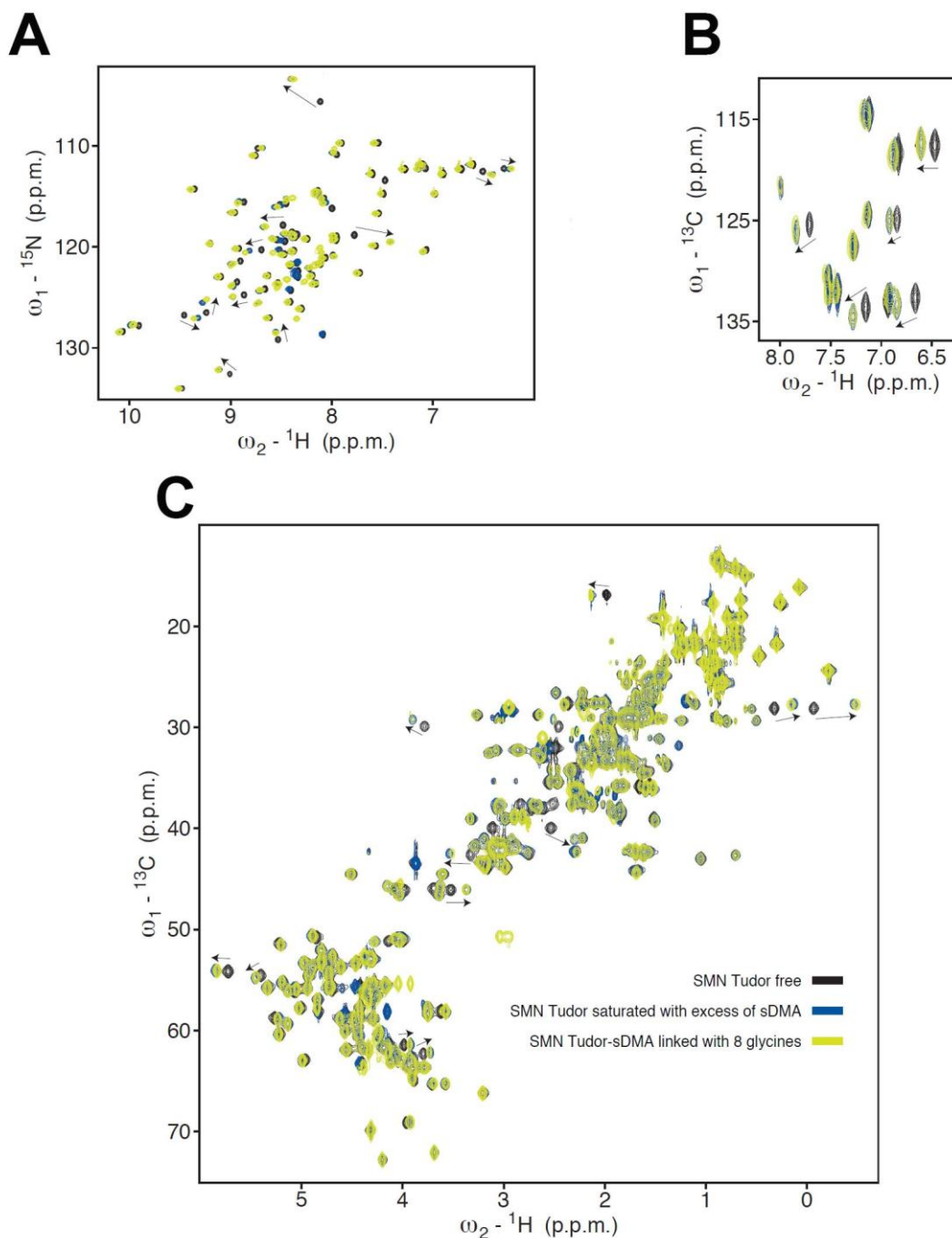


Figure 7.46 The chemical shifts of SMN Tudor ligated with 08 Gly sDMA peptide are highly comparable to the ones of SMN when saturated with excess of free sDMA, indicating similar binding mode. Each panel compares the HSQC spectra of free SMN (black), SMN saturated with excess of sDMA (blue), and SMN ligated with 08 Gly sDMA (lemon). A) ^1H , ^{15}N correlations, B) ^1H , ^{13}C correlations for aromatic protons, C) ^1H , ^{13}C correlations for aliphatic protons. In all spectra, chemical shift perturbations for some well-resolved peaks are indicated with arrows.

7.3.6 Conclusion

The obtained results suggest that the semisynthesis strategy described above is a useful tool to stabilize weak interactions such as SMN Tudor-sDMA for structural studies. This strategy allows a selective introduction of PTMs into the ligand by chemical synthesis to elucidate the role of PTMs in transient protein-protein interactions (section 4.4.1.4). Moreover, a fast quantification of the ligation yield from an established one-pot EPL in this strategy provides a crude but fast information to optimize the linker length so that covalently linking two moieties does not put high pressure on the protein fold. Additionally, by generating a covalent link between protein and ligand at a 1:1 stoichiometry, excess amount of the ligand bound to the protein in structural analysis of such weak interactions can be prevented. Another strategies to covalently stabilize the transient interactions are either utilizing chemical cross-linking (Singh *et al.*, 2010) or covalent attachment of the ligand into the selective amino acid side chain of protein (Krishnamurthy *et al.*, 2007). But potential effects of either cross-linking reagents or introduction of site directed point mutations on protein structure and function must be considered in these strategies. Therefore, we believe that this approach can be widely applied for structural studies of PTM-dependent weak interactions.

8. Abbreviations

ASP	: 6xHis-ATPase-SrtA-PrP
ASPM	: 6xHis-ATPase-SrtA-PrP/MxeIntein-6xHis-CBD
AU	: arbitrary unit
CBD	: chitin binding domain
CD	: circular dichroism
CJD	: Creutzfeldt-Jakob disease
Δ	: deletion
DNA	: deoxyribonucleic acid
DOPC	: 1,2-dioleoyl-sn-glycero-3-phosphocholine
DPPC	: 1,2-dipalmitoyl-sn-glycero-3-phosphocholine
EPL	: expressed protein ligation
eq.	: molar equivalents
ER	: endoplasmic reticulum
<i>E. coli</i>	: <i>Escherichia coli</i>
FTIR	: fourier transform infrared spectroscopy
GndHCl	: guanidine hydrochloride
GPI	: glycoposphatidylinositol
GSH	: reduced glutathione
GSSG	: oxidized glutathione
HDP	: 6xHis-DnaK-TEV-PrP
hr	: hour
HSQC	: Heteronuclear Single Quantum Correlation
IBs	: inclusion bodies
IPTG	: isopropyl-β-D-thiogalactopyranoside
kDa	: kilo-Dalton

K_{SV}	: Stern Volmer constant
MESNA	: sodium 2-mercaptoethanesulfonate
min	: minute
MLV	: multi-lamellar vesicle
<i>Mxe</i>	: <i>Mycobacterium xenopii</i>
NaOAc	: sodium acetate
NaPi	: sodium phosphate
NBD	: 4-chloro-7-nitrobenzofurazan
NCL	: native chemical ligation
NMR	: nuclear magnetic resonance
OD	: optical density
OG	: octyl- β -D-glucopyranoside
o/n	: overnight
PE	: phosphatidyl ethanolamine
PEG	: poly ethylene glycol
PI	: phosphoinositol
PK	: proteinase K
PMCA	: protein misfolding cyclic amplification
PMSF	: phenylmethylsulfonyl fluoride
POPG	: 1-palmitoyl-2-oleoyl- <i>sn</i> -glycero-3-phospho-(1'- <i>rac</i> -glycerol)
POPS	: 1-palmitoyl-2-oleoyl- <i>sn</i> -glycero-3-phospho-L-serine
PrP	: prion protein
PrP ^C	: cellular prion protein
PrP ^{Sc}	: prion protein scrapie (infectious and toxic)
PTM	: posttranslational modification
RML	: Rocky Mountain Laboratories
RT	: room temperature

SBD	: substrate binding domain
sDMA	: symmetrically dimethylated arginine
SDT	: sodium dithionite
SDS	: sodium dodecyl sulfate
SDS-PAGE	: sodium dodecyl sulfate polyacrylamide gel electrophoresis
SM	: sphingomyelin
SMN	: survival motor neuron protein
SMN Tudor	: the Tudor domain of SMN protein
SPPS	: solid phase peptide synthesis
SrtA	: Sortase A
SUVs	: small unilamellar vesicles
TCEP	: tris(2-carboxyethyl)phosphine
TEV	: tobacco etch virus
ThT	: thioflavin T
UV	: ultra violet

9. References

- Abskharon RN, Ramboarina S, El Hassan H, Gad W, Apostol MI, Giachin G, Legname G, Steyaert J, Messens J, Soror SH, Wohlkonig A (2012) A novel expression system for production of soluble prion proteins in *E. coli*. *Microbial cell factories* 11: 6
- Aguzzi A, Heppner FL (2000) Pathogenesis of prion diseases: a progress report. *Cell death and differentiation* 7: 889-902
- Alexandrov K, Heinemann I, Durek T, Sidorovitch V, Goody RS, Waldmann H (2002) Intein-mediated synthesis of geranylgeranylated Rab7 protein in vitro. *Journal of the American Chemical Society* 124: 5648-5649
- Alper T, Cramp WA, Haig DA, Clarke MC (1967) Does the agent of scrapie replicate without nucleic acid? *Nature* 214: 764-766
- Alper T, Haig DA, Clarke MC (1966) The exceptionally small size of the scrapie agent. *Biochemical and biophysical research communications* 22: 278-284
- Antos JM, Miller GM, Grotenbreg GM, Ploegh HL (2008) Lipid modification of proteins through sortase-catalyzed transpeptidation. *Journal of the American Chemical Society* 130: 16338-16343
- Arnold JE, Tipler C, Laszlo L, Hope J, Landon M, Mayer RJ (1995) The abnormal isoform of the prion protein accumulates in late-endosome-like organelles in scrapie-infected mouse brain. *The Journal of pathology* 176: 403-411
- Atarashi R, Moore RA, Sim VL, Hughson AG, Dorward DW, Onwubiko HA, Priola SA, Caughey B (2007) Ultrasensitive detection of scrapie prion protein using seeded conversion of recombinant prion protein. *Nature methods* 4: 645-650
- Banigan JR, Mandal K, Sawaya MR, Thammavongsa V, Hendrickx AP, Schneewind O, Yeates TO, Kent SB (2010) Determination of the X-ray structure of the snake venom protein omwaprין by total chemical synthesis and racemic protein crystallography. *Protein science : a publication of the Protein Society* 19: 1840-1849
- Barmada SJ, Harris DA (2005) Visualization of prion infection in transgenic mice expressing green fluorescent protein-tagged prion protein. *The Journal of neuroscience : the official journal of the Society for Neuroscience* 25: 5824-5832
- Baron GS, Caughey B (2003) Effect of glycosylphosphatidylinositol anchor-dependent and -independent prion protein association with model raft membranes on conversion to the protease-resistant isoform. *The Journal of biological chemistry* 278: 14883-14892
- Baron GS, Magalhaes AC, Prado MA, Caughey B (2006) Mouse-adapted scrapie infection of SN56 cells: greater efficiency with microsome-associated versus purified PrP-res. *Journal of virology* 80: 2106-2117
- Baron GS, Wehrly K, Dorward DW, Chesebro B, Caughey B (2002) Conversion of raft associated prion protein to the protease-resistant state requires insertion of PrP-res (PrP(Sc)) into contiguous membranes. *The EMBO journal* 21: 1031-1040

- Baskakov IV, Legname G, Baldwin MA, Prusiner SB, Cohen FE (2002) Pathway complexity of prion protein assembly into amyloid. *The Journal of biological chemistry* 277: 21140-21148
- Basler K, Oesch B, Scott M, Westaway D, Walchli M, Groth DF, McKinley MP, Prusiner SB, Weissmann C (1986) Scrapie and cellular PrP isoforms are encoded by the same chromosomal gene. *Cell* 46: 417-428
- Baumann F, Tolnay M, Brabeck C, Pahnke J, Kloz U, Niemann HH, Heikenwalder M, Rulicke T, Burkle A, Aguzzi A (2007) Lethal recessive myelin toxicity of prion protein lacking its central domain. *The EMBO journal* 26: 538-547
- Baybutt H, Manson J (1997) Characterisation of two promoters for prion protein (PrP) gene expression in neuronal cells. *Gene* 184: 125-131
- Becker CF, Hunter CL, Seidel R, Kent SB, Goody RS, Engelhard M (2003) Total chemical synthesis of a functional interacting protein pair: the protooncogene H-Ras and the Ras-binding domain of its effector c-Raf1. *Proceedings of the National Academy of Sciences of the United States of America* 100: 5075-5080
- Becker CF, Liu X, Olschewski D, Castelli R, Seidel R, Seeberger PH (2008) Semisynthesis of a glycosylphosphatidylinositol-anchored prion protein. *Angew Chem Int Ed Engl* 47: 8215-8219
- Becker CF, Oblatt-Montal M, Kochendoerfer GG, Montal M (2004) Chemical synthesis and single channel properties of tetrameric and pentameric TASP (template-assembled synthetic proteins) derived from the transmembrane domain of HIV virus protein u (Vpu). *The Journal of biological chemistry* 279: 17483-17489
- Bessette PH, Aslund F, Beckwith J, Georgiou G (1999) Efficient folding of proteins with multiple disulfide bonds in the Escherichia coli cytoplasm. *Proceedings of the National Academy of Sciences of the United States of America* 96: 13703-13708
- Biasini E, Turnbaugh JA, Unterberger U, Harris DA (2012) Prion protein at the crossroads of physiology and disease. *Trends in neurosciences* 35: 92-103
- Biasini E, Unterberger U, Solomon IH, Massignan T, Senatore A, Bian H, Voigtlaender T, Bowman FP, Bonetto V, Chiesa R, Luebke J, Toselli P, Harris DA (2013) A mutant prion protein sensitizes neurons to glutamate-induced excitotoxicity. *The Journal of neuroscience : the official journal of the Society for Neuroscience* 33: 2408-2418
- Bigay J, Antonny B (2005) Real-time assays for the assembly-disassembly cycle of COP coats on liposomes of defined size. *Methods in enzymology* 404: 95-107
- Borchelt DR, Taraboulos A, Prusiner SB (1992) Evidence for synthesis of scrapie prion proteins in the endocytic pathway. *The Journal of biological chemistry* 267: 16188-16199
- Borra R, Dong D, Elnagar AY, Woldemariam GA, Camarero JA (2012) In-cell fluorescence activation and labeling of proteins mediated by FRET-quenched split inteins. *Journal of the American Chemical Society* 134: 6344-6353
- Botti P, Carrasco MR, Kent SBH (2001) Native chemical ligation using removable N-alpha-(1-phenyl-2-mercaptoethyl) auxiliaries. *Tetrahedron letters* 42: 1831-1833

- Botto L, Masserini M, Cassetti A, Palestini P (2004) Immunoseparation of Prion protein-enriched domains from other detergent-resistant membrane fractions, isolated from neuronal cells. *FEBS letters* 557: 143-147
- Breydo L, Makarava N, Baskakov IV (2008) Methods for conversion of prion protein into amyloid fibrils. *Methods Mol Biol* 459: 105-115
- Brugger B, Graham C, Leibrecht I, Mombelli E, Jen A, Wieland F, Morris R (2004) The membrane domains occupied by glycosylphosphatidylinositol-anchored prion protein and Thy-1 differ in lipid composition. *The Journal of biological chemistry* 279: 7530-7536
- Brunsveld L, Kuhlmann J, Alexandrov K, Wittinghofer A, Goody RS, Waldmann H (2006) Lipidated ras and rab peptides and proteins--synthesis, structure, and function. *Angew Chem Int Ed Engl* 45: 6622-6646
- Bueler H, Fischer M, Lang Y, Bluethmann H, Lipp HP, DeArmond SJ, Prusiner SB, Aguet M, Weissmann C (1992) Normal development and behaviour of mice lacking the neuronal cell-surface PrP protein. *Nature* 356: 577-582
- Buhler D, Raker V, Luhrmann R, Fischer U (1999) Essential role for the tudor domain of SMN in spliceosomal U snRNP assembly: implications for spinal muscular atrophy. *Human molecular genetics* 8: 2351-2357
- Butko P, Huang F, Pusztai-Carey M, Surewicz WK (1996) Membrane permeabilization induced by cytolytic delta-endotoxin CytA from *Bacillus thuringiensis* var. israelensis. *Biochemistry* 35: 11355-11360
- Calzolari L, Lysek DA, Perez DR, Guntert P, Wuthrich K (2005) Prion protein NMR structures of chickens, turtles, and frogs. *Proceedings of the National Academy of Sciences of the United States of America* 102: 651-655
- Campana V, Sarnataro D, Zurzolo C (2005) The highways and byways of prion protein trafficking. *Trends in cell biology* 15: 102-111
- Castilla J, Saa P, Hetz C, Soto C (2005) In vitro generation of infectious scrapie prions. *Cell* 121: 195-206
- Caughey B, Baron GS (2006) Prions and their partners in crime. *Nature* 443: 803-810
- Caughey B, Raymond GJ (1991) The scrapie-associated form of PrP is made from a cell surface precursor that is both protease- and phospholipase-sensitive. *The Journal of biological chemistry* 266: 18217-18223
- Chan DI, Prenner EJ, Vogel HJ (2006) Tryptophan- and arginine-rich antimicrobial peptides: structures and mechanisms of action. *Biochimica et biophysica acta* 1758: 1184-1202
- Chesebro B, Race R, Wehrly K, Nishio J, Bloom M, Lechner D, Bergstrom S, Robbins K, Mayer L, Keith JM, *et al.* (1985) Identification of scrapie prion protein-specific mRNA in scrapie-infected and uninfected brain. *Nature* 315: 331-333

- Chesebro B, Trifilo M, Race R, Meade-White K, Teng C, LaCasse R, Raymond L, Favara C, Baron G, Priola S, Caughey B, Masliah E, Oldstone M (2005) Anchorless prion protein results in infectious amyloid disease without clinical scrapie. *Science* 308: 1435-1439
- Christiaens B, Symoens S, Verheyden S, Engelborghs Y, Joliot A, Prochiantz A, Vandekerckhove J, Rosseneu M, Vanloo B (2002) Tryptophan fluorescence study of the interaction of penetratin peptides with model membranes. *European journal of biochemistry / FEBS* 269: 2918-2926
- Cohen FE (1999) Protein misfolding and prion diseases. *Journal of molecular biology* 293: 313-320
- Cohen FE, Pan KM, Huang Z, Baldwin M, Fletterick RJ, Prusiner SB (1994) Structural clues to prion replication. *Science* 264: 530-531
- Colby DW, Prusiner SB (2011) De novo generation of prion strains. *Nature reviews Microbiology* 9: 771-777
- Colby DW, Wain R, Baskakov IV, Legname G, Palmer CG, Nguyen HO, Lemus A, Cohen FE, DeArmond SJ, Prusiner SB (2010) Protease-sensitive synthetic prions. *PLoS pathogens* 6: e1000736
- Crich D, Banerjee A (2007) Native chemical ligation at phenylalanine. *Journal of the American Chemical Society* 129: 10064-10065
- Critchley P, Kazlauskaitė J, Eason R, Pinheiro TJ (2004) Binding of prion proteins to lipid membranes. *Biochemical and biophysical research communications* 313: 559-567
- David R, Richter MP, Beck-Sickinger AG (2004) Expressed protein ligation. Method and applications. *European journal of biochemistry / FEBS* 271: 663-677
- Dawson PE, Muir TW, Clark-Lewis I, Kent SB (1994) Synthesis of proteins by native chemical ligation. *Science* 266: 776-779
- Deleault NR, Geoghegan JC, Nishina K, Kascsak R, Williamson RA, Supattapone S (2005) Protease-resistant prion protein amplification reconstituted with partially purified substrates and synthetic polyanions. *The Journal of biological chemistry* 280: 26873-26879
- Deleault NR, Harris BT, Rees JR, Supattapone S (2007) Formation of native prions from minimal components in vitro. *Proceedings of the National Academy of Sciences of the United States of America* 104: 9741-9746
- Deleault NR, Lucassen RW, Supattapone S (2003) RNA molecules stimulate prion protein conversion. *Nature* 425: 717-720
- Donne DG, Viles JH, Groth D, Mehlhorn I, James TL, Cohen FE, Prusiner SB, Wright PE, Dyson HJ (1997) Structure of the recombinant full-length hamster prion protein PrP(29-231): the N terminus is highly flexible. *Proceedings of the National Academy of Sciences of the United States of America* 94: 13452-13457

- Durek T, Torbeev VY, Kent SB (2007) Convergent chemical synthesis and high-resolution x-ray structure of human lysozyme. *Proceedings of the National Academy of Sciences of the United States of America* 104: 4846-4851
- Eberl H, Tittmann P, Glockshuber R (2004) Characterization of recombinant, membrane-attached full-length prion protein. *The Journal of biological chemistry* 279: 25058-25065
- Eftink MR (1991) Fluorescence techniques for studying protein structure. *Methods of biochemical analysis* 35: 127-205
- Garg P, Nemeč KN, Khaled AR, Tatulian SA (2012) Transmembrane pore formation by the carboxyl terminus of Bax protein. *Biochimica et biophysica acta* 1828: 732-742
- Gauczynski S, Peyrin JM, Haik S, Leucht C, Hundt C, Rieger R, Krasemann S, Deslys JP, Dormont D, Lasmezas CI, Weiss S (2001) The 37-kDa/67-kDa laminin receptor acts as the cell-surface receptor for the cellular prion protein. *The EMBO journal* 20: 5863-5875
- Geoghegan JC, Valdes PA, Orem NR, Deleault NR, Williamson RA, Harris BT, Supattapone S (2007) Selective incorporation of polyanionic molecules into hamster prions. *The Journal of biological chemistry* 282: 36341-36353
- Gerlach H, Laumann V, Martens S, Becker CF, Goody RS, Geyer M (2010) HIV-1 Nef membrane association depends on charge, curvature, composition and sequence. *Nature chemical biology* 6: 46-53
- Gilch S, Winklhofer KF, Groschup MH, Nunziante M, Lucassen R, Spielhauer C, Muranyi W, Riesner D, Tatzelt J, Schatzl HM (2001) Intracellular re-routing of prion protein prevents propagation of PrP(Sc) and delays onset of prion disease. *The EMBO journal* 20: 3957-3966
- Godsave SF, Wille H, Kujala P, Latawiec D, DeArmond SJ, Serban A, Prusiner SB, Peters PJ (2008) Cryo-immunogold electron microscopy for prions: toward identification of a conversion site. *The Journal of neuroscience : the official journal of the Society for Neuroscience* 28: 12489-12499
- Gogolin L, Schroeder H, Itzen A, Goody RS, Niemeyer CM, Becker CF (2013) Protein-DNA arrays as tools for detection of protein-protein interactions by mass spectrometry. *Chembiochem : a European journal of chemical biology* 14: 92-99
- Goold R, Rabbanian S, Sutton L, Andre R, Arora P, Moonga J, Clarke AR, Schiavo G, Jat P, Collinge J, Tabrizi SJ (2011) Rapid cell-surface prion protein conversion revealed using a novel cell system. *Nature communications* 2: 281
- Govaerts C, Wille H, Prusiner SB, Cohen FE (2004) Evidence for assembly of prions with left-handed beta-helices into trimers. *Proceedings of the National Academy of Sciences of the United States of America* 101: 8342-8347
- Griffith JS (1967) Self-replication and scrapie. *Nature* 215: 1043-1044
- Haase C, Rohde H, Seitz O (2008) Native chemical ligation at valine. *Angew Chem Int Ed Engl* 47: 6807-6810

- Hackenberger CP, Schwarzer D (2008) Chemoselective ligation and modification strategies for peptides and proteins. *Angew Chem Int Ed Engl* 47: 10030-10074
- Haginoya K, Kato T, Higuchi M, Shitomi Y, Asakura T, Hayakawa T, Mitsui T, Hori H (2005) Preparation of stable liposomes using sucrose density gradient centrifugation and their interaction with insecticidal Cry1A toxins of *Bacillus thuringiensis*. *Bulletin of the Faculty of Agriculture, Niigata University* 57: 115-120
- Haigh CL, Drew SC, Boland MP, Masters CL, Barnham KJ, Lawson VA, Collins SJ (2009) Dominant roles of the polybasic proline motif and copper in the PrP²³⁻⁸⁹-mediated stress protection response. *Journal of cell science* 122: 1518-1528
- Halevy R, Rozek A, Kolusheva S, Hancock RE, Jelinek R (2003) Membrane binding and permeation by indolicidin analogs studied by a biomimetic lipid/polydiacetylene vesicle assay. *Peptides* 24: 1753-1761
- Han S, Hill AF (2008) Analysis of PrP conformation using circular dichroism. *Methods Mol Biol* 459: 145-159
- Hansen RE, Winther JR (2009) An introduction to methods for analyzing thiols and disulfides: Reactions, reagents, and practical considerations. *Analytical biochemistry* 394: 147-158
- Harris DA (2003) Trafficking, turnover and membrane topology of PrP. *British medical bulletin* 66: 71-85
- Harris DA, Huber MT, van Dijken P, Shyng SL, Chait BT, Wang R (1993) Processing of a cellular prion protein: identification of N- and C-terminal cleavage sites. *Biochemistry* 32: 1009-1016
- Hauser PS, Raussens V, Yamamoto T, Abdullahi GE, Weers PMM, Sykes BD, Ryan RO (2009) Semisynthesis and segmental isotope labeling of the apoE3 N-terminal domain using expressed protein ligation. *J Lipid Res* 50: 1548-1555
- Hegde RS, Mastrianni JA, Scott MR, DeFea KA, Tremblay P, Torchia M, DeArmond SJ, Prusiner SB, Lingappa VR (1998) A transmembrane form of the prion protein in neurodegenerative disease. *Science* 279: 827-834
- Hicks MR, Gill AC, Bath IK, Rullay AK, Sylvester ID, Crout DH, Pinheiro TJ (2006) Synthesis and structural characterization of a mimetic membrane-anchored prion protein. *The FEBS journal* 273: 1285-1299
- Holm L, Ackland GL, Edwards MR, Breckenridge RA, Sim RB, Offer J (2012) Chemical labelling of active serum thioester proteins for quantification. *Immunobiology* 217: 256-264
- Hope J, Morton LJ, Farquhar CF, Multhaup G, Beyreuther K, Kimberlin RH (1986) The major polypeptide of scrapie-associated fibrils (SAF) has the same size, charge distribution and N-terminal protein sequence as predicted for the normal brain protein (PrP). *The EMBO journal* 5: 2591-2597
- Hornemann S, Glockshuber R (1996) Autonomous and reversible folding of a soluble amino-terminally truncated segment of the mouse prion protein. *Journal of molecular biology* 261: 614-619

Hornemann S, Korth C, Oesch B, Riek R, Wider G, Wuthrich K, Glockshuber R (1997) Recombinant full-length murine prion protein, mPrP(23-231): purification and spectroscopic characterization. *FEBS letters* 413: 277-281

Huang Z, Prusiner SB, Cohen FE (1995) Scrapie prions: a three-dimensional model of an infectious fragment. *Folding & design* 1: 13-19

James TL, Liu H, Ulyanov NB, Farr-Jones S, Zhang H, Donne DG, Kaneko K, Groth D, Mehlhorn I, Prusiner SB, Cohen FE (1997) Solution structure of a 142-residue recombinant prion protein corresponding to the infectious fragment of the scrapie isoform. *Proceedings of the National Academy of Sciences of the United States of America* 94: 10086-10091

Jeffrey M (2013) Review: Membrane-associated misfolded protein propagation in natural transmissible spongiform encephalopathies (TSEs), synthetic prion diseases and Alzheimer's disease. *Neuropathology and applied neurobiology* 39: 196-216

Jeffrey M, Goodsir CM, Bruce ME, McBride PA, Fraser JR (1997) In vivo toxicity of prion protein in murine scrapie: ultrastructural and immunogold studies. *Neuropathology and applied neurobiology* 23: 93-101

Kanaani J, Prusiner SB, Diacovo J, Baekkeskov S, Legname G (2005) Recombinant prion protein induces rapid polarization and development of synapses in embryonic rat hippocampal neurons in vitro. *Journal of neurochemistry* 95: 1373-1386

Kaneko K, Vey M, Scott M, Pilkuhn S, Cohen FE, Prusiner SB (1997) COOH-terminal sequence of the cellular prion protein directs subcellular trafficking and controls conversion into the scrapie isoform. *Proceedings of the National Academy of Sciences of the United States of America* 94: 2333-2338

Kawakami T, Aimoto S (2003) A photoremovable ligation auxiliary for use in polypeptide synthesis. *Tetrahedron letters* 44: 6059-6061

Kim BH, Lee HG, Choi JK, Kim JI, Choi EK, Carp RI, Kim YS (2004) The cellular prion protein (PrPC) prevents apoptotic neuronal cell death and mitochondrial dysfunction induced by serum deprivation. *Brain research Molecular brain research* 124: 40-50

Knaus KJ, Morillas M, Swietnicki W, Malone M, Surewicz WK, Yee VC (2001) Crystal structure of the human prion protein reveals a mechanism for oligomerization. *Nature structural biology* 8: 770-774

Kocisko DA, Come JH, Priola SA, Chesebro B, Raymond GJ, Lansbury PT, Caughey B (1994) Cell-free formation of protease-resistant prion protein. *Nature* 370: 471-474

Kolb SJ, Battle DJ, Dreyfuss G (2007) Molecular functions of the SMN complex. *Journal of child neurology* 22: 990-994

Kovacs GG, Trabattoni G, Hainfellner JA, Ironside JW, Knight RS, Budka H (2002) Mutations of the prion protein gene phenotypic spectrum. *Journal of neurology* 249: 1567-1582

Kretschmar HA, Prusiner SB, Stowring LE, DeArmond SJ (1986) Scrapie prion proteins are synthesized in neurons. *The American journal of pathology* 122: 1-5

- Krishnamurthy VM, Semetey V, Bracher PJ, Shen N, Whitesides GM (2007) Dependence of effective molarity on linker length for an intramolecular protein-ligand system. *Journal of the American Chemical Society* 129: 1312-1320
- Kyratsous CA, Silverstein SJ, DeLong CR, Panagiotidis CA (2009) Chaperone-fusion expression plasmid vectors for improved solubility of recombinant proteins in *Escherichia coli*. *Gene* 440: 9-15
- Langner M, Hui SW (1993) Dithionite penetration through phospholipid bilayers as a measure of defects in lipid molecular packing. *Chemistry and physics of lipids* 65: 23-30
- Lazzari C, Peggion C, Stella R, Massimino ML, Lim D, Bertoli A, Sorgato MC (2011) Cellular prion protein is implicated in the regulation of local Ca²⁺ movements in cerebellar granule neurons. *Journal of neurochemistry* 116: 881-890
- Lee KS, Magalhaes AC, Zanata SM, Brentani RR, Martins VR, Prado MA (2001) Internalization of mammalian fluorescent cellular prion protein and N-terminal deletion mutants in living cells. *Journal of neurochemistry* 79: 79-87
- Legname G, Baskakov IV, Nguyen HO, Riesner D, Cohen FE, DeArmond SJ, Prusiner SB (2004) Synthetic mammalian prions. *Science* 305: 673-676
- Li A, Christensen HM, Stewart LR, Roth KA, Chiesa R, Harris DA (2007) Neonatal lethality in transgenic mice expressing prion protein with a deletion of residues 105-125. *The EMBO journal* 26: 548-558
- Liemann S, Glockshuber R (1999) Influence of amino acid substitutions related to inherited human prion diseases on the thermodynamic stability of the cellular prion protein. *Biochemistry* 38: 3258-3267
- Linden R, Martins VR, Prado MA, Cammarota M, Izquierdo I, Brentani RR (2008) Physiology of the prion protein. *Physiological reviews* 88: 673-728
- Liu H, Farr-Jones S, Ulyanov NB, Llinas M, Marqusee S, Groth D, Cohen FE, Prusiner SB, James TL (1999) Solution structure of Syrian hamster prion protein rPrP(90-231). *Biochemistry* 38: 5362-5377
- Liu LP, Deber CM (1997) Anionic phospholipids modulate peptide insertion into membranes. *Biochemistry* 36: 5476-5482
- Locht C, Chesebro B, Race R, Keith JM (1986) Molecular cloning and complete sequence of prion protein cDNA from mouse brain infected with the scrapie agent. *Proceedings of the National Academy of Sciences of the United States of America* 83: 6372-6376
- Lopez Garcia F, Zahn R, Riek R, Wuthrich K (2000) NMR structure of the bovine prion protein. *Proceedings of the National Academy of Sciences of the United States of America* 97: 8334-8339
- Ludwig C, Schwarzer D, Zettler J, Garbe D, Janning P, Czeslik C, Mootz HD (2009) Semisynthesis of proteins using split inteins. *Methods in enzymology* 462: 77-96

- Lue RY, Chen GY, Hu Y, Zhu Q, Yao SQ (2004) Versatile protein biotinylation strategies for potential high-throughput proteomics. *Journal of the American Chemical Society* 126: 1055-1062
- Lysek DA, Schorn C, Nivon LG, Esteve-Moya V, Christen B, Calzolari L, von Schroetter C, Fiorito F, Herrmann T, Guntert P, Wuthrich K (2005) Prion protein NMR structures of cats, dogs, pigs, and sheep. *Proceedings of the National Academy of Sciences of the United States of America* 102: 640-645
- Macmillan D, Bertozzi CR (2004) Modular assembly of glycoproteins: towards the synthesis of GlyCAM-1 by using expressed protein ligation. *Angew Chem Int Ed Engl* 43: 1355-1359
- Magalhaes AC, Silva JA, Lee KS, Martins VR, Prado VF, Ferguson SS, Gomez MV, Brentani RR, Prado MA (2002) Endocytic intermediates involved with the intracellular trafficking of a fluorescent cellular prion protein. *The Journal of biological chemistry* 277: 33311-33318
- Maiti NR, Surewicz WK (2001) The role of disulfide bridge in the folding and stability of the recombinant human prion protein. *The Journal of biological chemistry* 276: 2427-2431
- Malaga-Trillo E, Solis GP, Schrock Y, Geiss C, Luncz L, Thomanetz V, Stuermer CA (2009) Regulation of embryonic cell adhesion by the prion protein. *PLoS biology* 7: e55
- Mandal K, Pentelute BL, Bang D, Gates ZP, Torbeev VY, Kent SB (2012) Design, total chemical synthesis, and X-ray structure of a protein having a novel linear-loop polypeptide chain topology. *Angew Chem Int Ed Engl* 51: 1481-1486
- Manson JC, Clarke AR, Hooper ML, Aitchison L, McConnell I, Hope J (1994) 129/Ola mice carrying a null mutation in PrP that abolishes mRNA production are developmentally normal. *Molecular neurobiology* 8: 121-127
- Marella M, Lehmann S, Grassi J, Chabry J (2002) Filipin prevents pathological prion protein accumulation by reducing endocytosis and inducing cellular PrP release. *The Journal of biological chemistry* 277: 25457-25464
- Marijanovic Z, Caputo A, Campana V, Zurzolo C (2009) Identification of an intracellular site of prion conversion. *PLoS pathogens* 5: e1000426
- Martin DD, Xu MQ, Evans TC, Jr. (2001) Characterization of a naturally occurring trans-splicing intein from *Synechocystis* sp. PCC6803. *Biochemistry* 40: 1393-1402
- Mayer MP, Rudiger S, Bukau B (2000) Molecular basis for interactions of the DnaK chaperone with substrates. *Biological chemistry* 381: 877-885
- McIntyre JC, Sleight RG (1991) Fluorescence assay for phospholipid membrane asymmetry. *Biochemistry* 30: 11819-11827
- Meyer RK, McKinley MP, Bowman KA, Braunfeld MB, Barry RA, Prusiner SB (1986) Separation and properties of cellular and scrapie prion proteins. *Proceedings of the National Academy of Sciences of the United States of America* 83: 2310-2314
- Milhavet O, Lehmann S (2002) Oxidative stress and the prion protein in transmissible spongiform encephalopathies. *Brain research Brain research reviews* 38: 328-339

Mingeot-Leclercq MP, Lins L, Bensliman M, Van Bambeke F, Van Der Smissen P, Peuvot J, Schanck A, Brasseur R (2002) Membrane destabilization induced by beta-amyloid peptide 29-42: importance of the amino-terminus. *Chemistry and physics of lipids* 120: 57-74

Morillas M, Swietnicki W, Gambetti P, Surewicz WK (1999) Membrane environment alters the conformational structure of the recombinant human prion protein. *The Journal of biological chemistry* 274: 36859-36865

Mouillet-Richard S, Ermonval M, Chebassier C, Laplanche JL, Lehmann S, Launay JM, Kellermann O (2000) Signal transduction through prion protein. *Science* 289: 1925-1928

Moya KL, Sales N, Hassig R, Creminon C, Grassi J, Di Giamberardino L (2000) Immunolocalization of the cellular prion protein in normal brain. *Microscopy research and technique* 50: 58-65

Muir TW (2003) Semisynthesis of proteins by expressed protein ligation. *Annual review of biochemistry* 72: 249-289

Muir TW, Sondhi D, Cole PA (1998) Expressed protein ligation: a general method for protein engineering. *Proceedings of the National Academy of Sciences of the United States of America* 95: 6705-6710

Naslavsky N, Stein R, Yanai A, Friedlander G, Taraboulos A (1997) Characterization of detergent-insoluble complexes containing the cellular prion protein and its scrapie isoform. *The Journal of biological chemistry* 272: 6324-6331

Nunziante M, Gilch S, Schatzl HM (2003) Essential role of the prion protein N terminus in subcellular trafficking and half-life of cellular prion protein. *The Journal of biological chemistry* 278: 3726-3734

Oesch B, Westaway D, Walchli M, McKinley MP, Kent SB, Aebersold R, Barry RA, Tempst P, Teplow DB, Hood LE, *et al.* (1985) A cellular gene encodes scrapie PrP 27-30 protein. *Cell* 40: 735-746

Olschewski D, Becker CF (2008) Chemical synthesis and semisynthesis of membrane proteins. *Molecular bioSystems* 4: 733-740

Olschewski D, Seidel R, Miesbauer M, Rambold AS, Oesterhelt D, Winklhofer KF, Tatzelt J, Engelhard M, Becker CF (2007) Semisynthetic murine prion protein equipped with a GPI anchor mimic incorporates into cellular membranes. *Chemistry & biology* 14: 994-1006

Pan KM, Baldwin M, Nguyen J, Gasset M, Serban A, Groth D, Mehlhorn I, Huang Z, Fletterick RJ, Cohen FE, *et al.* (1993) Conversion of alpha-helices into beta-sheets features in the formation of the scrapie prion proteins. *Proceedings of the National Academy of Sciences of the United States of America* 90: 10962-10966

Patil G, Rudolph R, Lange C (2008) In vitro-refolding of a single-chain Fv fragment in the presence of heteroaromatic thiols. *Journal of biotechnology* 134: 218-221

Paulick MG, Wise AR, Forstner MB, Groves JT, Bertozzi CR (2007) Synthetic analogues of glycosylphosphatidylinositol-anchored proteins and their behavior in supported lipid bilayers. *Journal of the American Chemical Society* 129: 11543-11550

- Paulus H (2000) Protein splicing and related forms of protein autoprocessing. *Annual review of biochemistry* 69: 447-496
- Pauly PC, Harris DA (1998) Copper stimulates endocytosis of the prion protein. *The Journal of biological chemistry* 273: 33107-33110
- Pavlicek A, Bednarova L, Holada K (2007) Production, purification and oxidative folding of the mouse recombinant prion protein. *Folia microbiologica* 52: 391-397
- Perez DR, Damberger FF, Wuthrich K (2010) Horse prion protein NMR structure and comparisons with related variants of the mouse prion protein. *Journal of molecular biology* 400: 121-128
- Perkins JR, Diboun I, Dessailly BH, Lees JG, Orengo C (2010) Transient protein-protein interactions: structural, functional, and network properties. *Structure* 18: 1233-1243
- Peters PJ, Mironov A, Jr., Peretz D, van Donselaar E, Leclerc E, Erpel S, DeArmond SJ, Burton DR, Williamson RA, Vey M, Prusiner SB (2003) Trafficking of prion proteins through a caveolae-mediated endosomal pathway. *The Journal of cell biology* 162: 703-717
- Phan J, Zdanov A, Evdokimov AG, Tropea JE, Peters HK, 3rd, Kapust RB, Li M, Wlodawer A, Waugh DS (2002) Structural basis for the substrate specificity of tobacco etch virus protease. *The Journal of biological chemistry* 277: 50564-50572
- Prado MA, Alves-Silva J, Magalhaes AC, Prado VF, Linden R, Martins VR, Brentani RR (2004) PrPc on the road: trafficking of the cellular prion protein. *Journal of neurochemistry* 88: 769-781
- Prusiner SB (1998) Prions. *Proceedings of the National Academy of Sciences of the United States of America* 95: 13363-13383
- Prusiner SB, Groth DF, Bolton DC, Kent SB, Hood LE (1984) Purification and structural studies of a major scrapie prion protein. *Cell* 38: 127-134
- Prusiner SB, Hadlow WJ, Eklund CM, Race RE (1977) Sedimentation properties of the scrapie agent. *Proceedings of the National Academy of Sciences of the United States of America* 74: 4656-4660
- Puckett C, Concannon P, Casey C, Hood L (1991) Genomic structure of the human prion protein gene. *American journal of human genetics* 49: 320-329
- Raja SM, Rawat SS, Chattopadhyay A, Lala AK (1999) Localization and environment of tryptophans in soluble and membrane-bound states of a pore-forming toxin from *Staphylococcus aureus*. *Biophysical journal* 76: 1469-1479
- Rial DV, Ceccarelli EA (2002) Removal of DnaK contamination during fusion protein purifications. *Protein expression and purification* 25: 503-507
- Riek R, Hornemann S, Wider G, Billeter M, Glockshuber R, Wuthrich K (1996) NMR structure of the mouse prion protein domain PrP(121-231). *Nature* 382: 180-182

- Riek R, Hornemann S, Wider G, Glockshuber R, Wuthrich K (1997) NMR characterization of the full-length recombinant murine prion protein, mPrP(23-231). *FEBS letters* 413: 282-288
- Riek R, Wider G, Billeter M, Hornemann S, Glockshuber R, Wuthrich K (1998) Prion protein NMR structure and familial human spongiform encephalopathies. *Proceedings of the National Academy of Sciences of the United States of America* 95: 11667-11672
- Robinson PJ, Pinheiro TJ (2010) Phospholipid composition of membranes directs prions down alternative aggregation pathways. *Biophysical journal* 98: 1520-1528
- Rodal SK, Skretting G, Garred O, Vilhardt F, van Deurs B, Sandvig K (1999) Extraction of cholesterol with methyl-beta-cyclodextrin perturbs formation of clathrin-coated endocytic vesicles. *Molecular biology of the cell* 10: 961-974
- Saborio GP, Permanne B, Soto C (2001) Sensitive detection of pathological prion protein by cyclic amplification of protein misfolding. *Nature* 411: 810-813
- Saeki K, Matsumoto Y, Onodera T (1996) Identification of a promoter region in the rat prion protein gene. *Biochemical and biophysical research communications* 219: 47-52
- Sanghera N, Correia BE, Correia JR, Ludwig C, Agarwal S, Nakamura HK, Kuwata K, Samain E, Gill AC, Bonev BB, Pinheiro TJ (2011) Deciphering the molecular details for the binding of the prion protein to main ganglioside GM1 of neuronal membranes. *Chemistry & biology* 18: 1422-1431
- Sanghera N, Pinheiro TJ (2002) Binding of prion protein to lipid membranes and implications for prion conversion. *Journal of molecular biology* 315: 1241-1256
- Sarnataro D, Campana V, Paladino S, Stornaiuolo M, Nitsch L, Zurzolo C (2004) PrP(C) association with lipid rafts in the early secretory pathway stabilizes its cellular conformation. *Molecular biology of the cell* 15: 4031-4042
- Savva CG, Fernandes da Costa SP, Bokori-Brown M, Naylor CE, Cole AR, Moss DS, Titball RW, Basak AK (2013) Molecular architecture and functional analysis of NetB, a pore-forming toxin from *Clostridium perfringens*. *The Journal of biological chemistry* 288: 3512-3522
- Schatzl HM, Da Costa M, Taylor L, Cohen FE, Prusiner SB (1995) Prion protein gene variation among primates. *Journal of molecular biology* 245: 362-374
- Shmerling D, Hegyi I, Fischer M, Blattler T, Brandner S, Gotz J, Rulicke T, Flechsig E, Cozzio A, von Mering C, Hangartner C, Aguzzi A, Weissmann C (1998) Expression of amino-terminally truncated PrP in the mouse leading to ataxia and specific cerebellar lesions. *Cell* 93: 203-214
- Shyng SL, Heuser JE, Harris DA (1994) A glycolipid-anchored prion protein is endocytosed via clathrin-coated pits. *The Journal of cell biology* 125: 1239-1250
- Shyu WC, Lin SZ, Chiang MF, Ding DC, Li KW, Chen SF, Yang HI, Li H (2005) Overexpression of PrPC by adenovirus-mediated gene targeting reduces ischemic injury in a stroke rat model. *The Journal of neuroscience : the official journal of the Society for Neuroscience* 25: 8967-8977

- Singh P, Panchaud A, Goodlett DR (2010) Chemical cross-linking and mass spectrometry as a low-resolution protein structure determination technique. *Analytical chemistry* 82: 2636-2642
- Solomon IH, Huettner JE, Harris DA (2010) Neurotoxic mutants of the prion protein induce spontaneous ionic currents in cultured cells. *The Journal of biological chemistry* 285: 26719-26726
- Solomon IH, Khatri N, Biasini E, Massignan T, Huettner JE, Harris DA (2011) An N-terminal polybasic domain and cell surface localization are required for mutant prion protein toxicity. *The Journal of biological chemistry* 286: 14724-14736
- Southworth MW, Amaya K, Evans TC, Xu MQ, Perler FB (1999) Purification of proteins fused to either the amino or carboxy terminus of the Mycobacterium xenopi gyrase A intein. *BioTechniques* 27: 110-114, 116, 118-120
- Sprangers R, Groves MR, Sinning I, Sattler M (2003) High-resolution X-ray and NMR structures of the SMN Tudor domain: conformational variation in the binding site for symmetrically dimethylated arginine residues. *Journal of molecular biology* 327: 507-520
- Stahl N, Baldwin MA, Hecker R, Pan KM, Burlingame AL, Prusiner SB (1992) Glycosylinositol phospholipid anchors of the scrapie and cellular prion proteins contain sialic acid. *Biochemistry* 31: 5043-5053
- Stahl N, Baldwin MA, Teplow DB, Hood L, Gibson BW, Burlingame AL, Prusiner SB (1993) Structural studies of the scrapie prion protein using mass spectrometry and amino acid sequencing. *Biochemistry* 32: 1991-2002
- Stahl N, Borchelt DR, Prusiner SB (1990) Differential release of cellular and scrapie prion proteins from cellular membranes by phosphatidylinositol-specific phospholipase C. *Biochemistry* 29: 5405-5412
- Stern O and Volmer M (1919) On the quenching time of fluorescence. *Physikalische Zeitschrift* 20: 183-188
- Stewart JC (1980) Colorimetric determination of phospholipids with ammonium ferrothiocyanate. *Analytical biochemistry* 104: 10-14
- Stockel J, Safar J, Wallace AC, Cohen FE, Prusiner SB (1998) Prion protein selectively binds copper(II) ions. *Biochemistry* 37: 7185-7193
- Subtil A, Gaidarov I, Kobylarz K, Lampson MA, Keen JH, McGraw TE (1999) Acute cholesterol depletion inhibits clathrin-coated pit budding. *Proceedings of the National Academy of Sciences of the United States of America* 96: 6775-6780
- Sunyach C, Jen A, Deng J, Fitzgerald KT, Frobert Y, Grassi J, McCaffrey MW, Morris R (2003) The mechanism of internalization of glycosylphosphatidylinositol-anchored prion protein. *The EMBO journal* 22: 3591-3601
- Supattapone S (2010) Biochemistry. What makes a prion infectious? *Science* 327: 1091-1092

- Swietnicki W, Petersen RB, Gambetti P, Surewicz WK (1998) Familial mutations and the thermodynamic stability of the recombinant human prion protein. *The Journal of biological chemistry* 273: 31048-31052
- Tanaka T, Yamamoto T, Tsukiji S, Nagamune T (2008) Site-specific protein modification on living cells catalyzed by Sortase. *Chembiochem : a European journal of chemical biology* 9: 802-807
- Taraboulos A, Raeber AJ, Borchelt DR, Serban D, Prusiner SB (1992) Synthesis and trafficking of prion proteins in cultured cells. *Molecular biology of the cell* 3: 851-863
- Taraboulos A, Scott M, Semenov A, Avrahami D, Laszlo L, Prusiner SB (1995) Cholesterol depletion and modification of COOH-terminal targeting sequence of the prion protein inhibit formation of the scrapie isoform. *The Journal of cell biology* 129: 121-132
- Ton-That H, Liu G, Mazmanian SK, Faull KF, Schneewind O (1999) Purification and characterization of sortase, the transpeptidase that cleaves surface proteins of *Staphylococcus aureus* at the LPXTG motif. *Proceedings of the National Academy of Sciences of the United States of America* 96: 12424-12429
- Tripsianes K, Madl T, Machyna M, Fessas D, Englbrecht C, Fischer U, Neugebauer KM, Sattler M (2011) Structural basis for dimethylarginine recognition by the Tudor domains of human SMN and SPF30 proteins. *Nature structural & molecular biology* 18: 1414-1420
- Tsukiji S, Nagamune T (2009) Sortase-mediated ligation: a gift from Gram-positive bacteria to protein engineering. *Chembiochem : a European journal of chemical biology* 10: 787-798
- Turnbaugh JA, Unterberger U, Saa P, Massignan T, Fluharty BR, Bowman FP, Miller MB, Supattapone S, Biasini E, Harris DA (2012) The N-terminal, polybasic region of PrP(C) dictates the efficiency of prion propagation by binding to PrP(Sc). *The Journal of neuroscience : the official journal of the Society for Neuroscience* 32: 8817-8830
- Vey M, Pilkuhn S, Wille H, Nixon R, DeArmond SJ, Smart EJ, Anderson RG, Taraboulos A, Prusiner SB (1996) Subcellular colocalization of the cellular and scrapie prion proteins in caveolae-like membranous domains. *Proceedings of the National Academy of Sciences of the United States of America* 93: 14945-14949
- Vila-Perello M, Muir TW (2010) Biological applications of protein splicing. *Cell* 143: 191-200
- Viles JH, Cohen FE, Prusiner SB, Goodin DB, Wright PE, Dyson HJ (1999) Copper binding to the prion protein: structural implications of four identical cooperative binding sites. *Proceedings of the National Academy of Sciences of the United States of America* 96: 2042-2047
- Vogt TC, Bechinger B (1999) The interactions of histidine-containing amphipathic helical peptide antibiotics with lipid bilayers. The effects of charges and pH. *The Journal of biological chemistry* 274: 29115-29121
- Walsh CT, Garneau-Tsodikova S, Gatto GJ, Jr. (2005) Protein posttranslational modifications: the chemistry of proteome diversifications. *Angew Chem Int Ed Engl* 44: 7342-7372

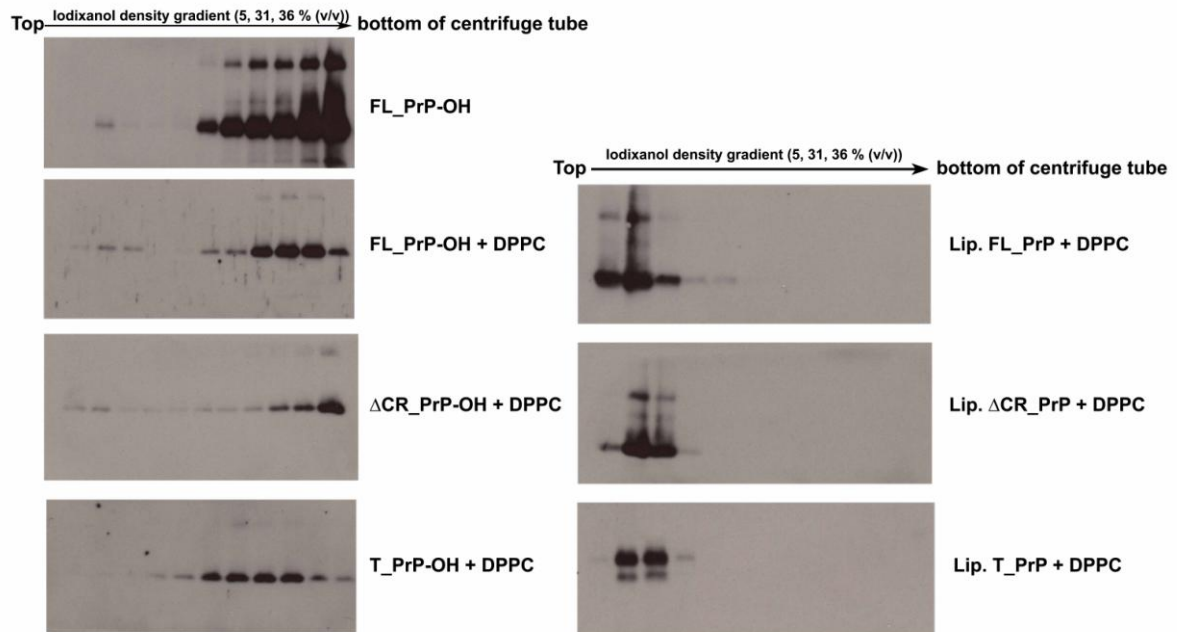
- Wang F, Wang X, Yuan CG, Ma J (2010a) Generating a prion with bacterially expressed recombinant prion protein. *Science* 327: 1132-1135
- Wang F, Yang F, Hu Y, Wang X, Jin C, Ma J (2007) Lipid interaction converts prion protein to a PrP^{Sc}-like proteinase K-resistant conformation under physiological conditions. *Biochemistry* 46: 7045-7053
- Wang F, Yin S, Wang X, Zha L, Sy MS, Ma J (2010b) Role of the highly conserved middle region of prion protein (PrP) in PrP-lipid interaction. *Biochemistry* 49: 8169-8176
- Watt NT, Hooper NM (2003) The prion protein and neuronal zinc homeostasis. *Trends in biochemical sciences* 28: 406-410
- Weissmann C (1994) Molecular biology of prion diseases. *Trends in cell biology* 4: 10-14
- Winklhofer KF, Heller U, Reintjes A, Tatzelt J (2003) Inhibition of complex glycosylation increases the formation of PrP^{Sc}. *Traffic* 4: 313-322
- Wong C, Xiong LW, Horiuchi M, Raymond L, Wehrly K, Chesebro B, Caughey B (2001) Sulfated glycans and elevated temperature stimulate PrP(Sc)-dependent cell-free formation of protease-resistant prion protein. *The EMBO journal* 20: 377-386
- Wopfner F, Weidenhofer G, Schneider R, von Brunn A, Gilch S, Schwarz TF, Werner T, Schatzl HM (1999) Analysis of 27 mammalian and 9 avian PrPs reveals high conservation of flexible regions of the prion protein. *Journal of molecular biology* 289: 1163-1178
- Wu H, Hu Z, Liu XQ (1998) Protein trans-splicing by a split intein encoded in a split DnaE gene of *Synechocystis* sp. PCC6803. *Proceedings of the National Academy of Sciences of the United States of America* 95: 9226-9231
- Wu YW, Oesterlin LK, Tan KT, Waldmann H, Alexandrov K, Goody RS (2010) Membrane targeting mechanism of Rab GTPases elucidated by semisynthetic protein probes. *Nature chemical biology* 6: 534-540
- Xu R, Ayers B, Cowburn D, Muir TW (1999) Chemical ligation of folded recombinant proteins: segmental isotopic labeling of domains for NMR studies. *Proceedings of the National Academy of Sciences of the United States of America* 96: 388-393
- Yan LZ, Dawson PE (2001) Synthesis of peptides and proteins without cysteine residues by native chemical ligation combined with desulfurization. *Journal of the American Chemical Society* 123: 526-533
- Yau WM, Wimley WC, Gawrisch K, White SH (1998) The preference of tryptophan for membrane interfaces. *Biochemistry* 37: 14713-14718
- Yoneyama F, Imura Y, Ohno K, Zendo T, Nakayama J, Matsuzaki K, Sonomoto K (2009) Peptide-lipid huge toroidal pore, a new antimicrobial mechanism mediated by a lactococcal bacteriocin, lacticin Q. *Antimicrobial agents and chemotherapy* 53: 3211-3217
- Zahn R, Liu A, Luhrs T, Riek R, von Schroetter C, Lopez Garcia F, Billeter M, Calzolari L, Wider G, Wuthrich K (2000) NMR solution structure of the human prion protein. *Proceedings of the National Academy of Sciences of the United States of America* 97: 145-150

Zanata SM, Lopes MH, Mercadante AF, Hajj GN, Chiarini LB, Nomizo R, Freitas AR, Cabral AL, Lee KS, Juliano MA, de Oliveira E, Jachieri SG, Burlingame A, Huang L, Linden R, Brentani RR, Martins VR (2002) Stress-inducible protein 1 is a cell surface ligand for cellular prion that triggers neuroprotection. *The EMBO journal* 21: 3307-3316

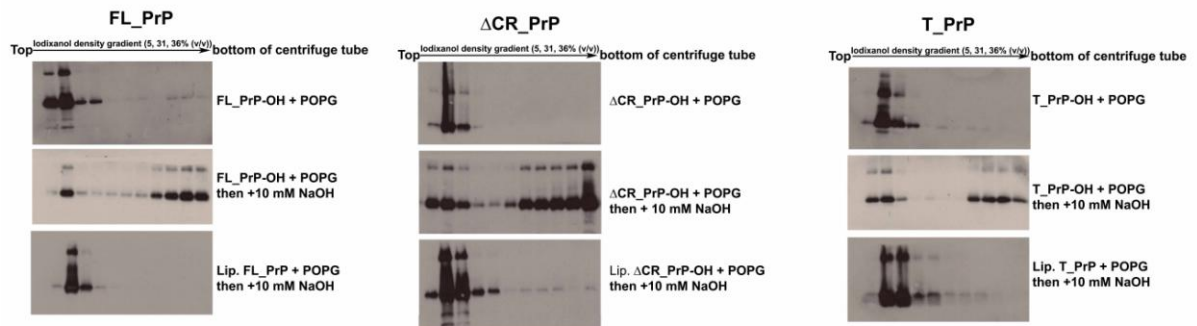
Zhang Y, Swietnicki W, Zagorski MG, Surewicz WK, Sonnichsen FD (2000) Solution structure of the E200K variant of human prion protein. Implications for the mechanism of pathogenesis in familial prion diseases. *The Journal of biological chemistry* 275: 33650-33654

Zhao W, Zhang Y, Cui C, Li Q, Wang J (2008) An efficient on-column expressed protein ligation strategy: application to segmental triple labeling of human apolipoprotein E3. *Protein science : a publication of the Protein Society* 17: 736-747

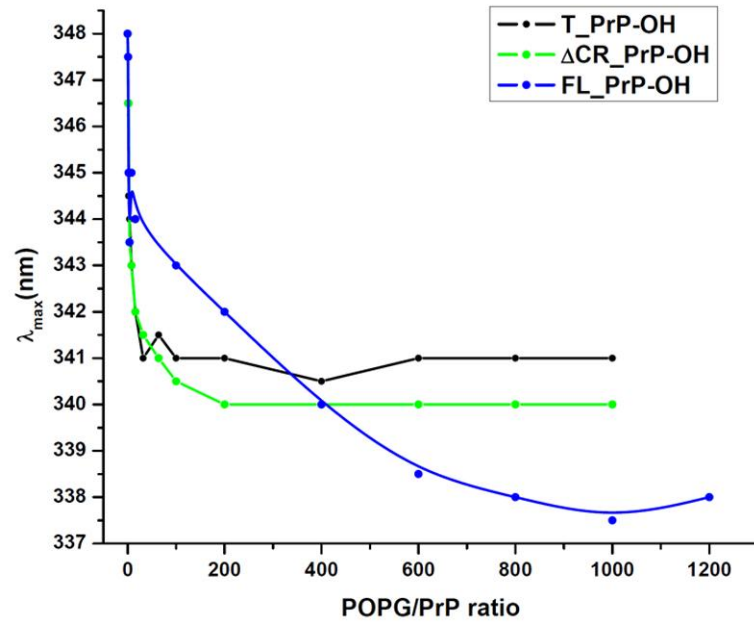
10. Appendix



Appendix 1. Western blots for floatation assays of the interactions of non-charged DPPC vesicles with non-lipidated and lipidated PrP variants.



Appendix 2. Western blots for floatation assays of the interactions of anionic POPG vesicles with non-lipidated and lipidated PrP variants and NaOH extraction to evaluate the strength of PrPs' binding to POPG vesicles.



Appendix 3. The tryptophan fluorescence peak wavelengths of non-lipidated FL_PrP (blue), Δ CR_PrP (green) and T_PrP (black) mixed with POPG vesicles.

Declaration

I, Nam Ky Chu, hereby declare that this thesis was prepared by me independently and using only the references and resources stated here. The work has so far not been submitted to any audit commission. Parts of this work have been published in scientific journals.

Hiermit erkläre ich, Nam Ky Chu, dass ich die vorliegende Arbeit selbständig verfasst und keine anderen als die angegebenen Quellen und Hilfsmittel verwendet habe. Die Arbeit wurde bisher keiner Prüfungskommission vorgelegt. Teile dieser Arbeit wurde in wissenschaftlichen Journalen veröffentlicht.

Nam Ky Chu

Publications

1. Chu K.N., Becker C.F. (2009) "Semisynthesis of membrane-attached prion proteins". *Methods in Enzymology*, 462: 177-193.
2. Chu K.N., Olschewski D., Seidel R., Winklhofer K.F., Tatzelt J., Engelhard M., Becker C.F. (2010) "Protein immobilization on liposomes and lipid-coated nanoparticles by protein trans-splicing". *Journal of Peptide Science*, 16: 582–588.
3. Chu K.N., Becker C.F. (2010) "Semisynthesis of membrane-associated full length prion proteins". 10th German Peptide Symposium, Berlin, Short poster presentation, No. 13.
4. Chu K.N., Araman M.C., Becker C.F. (2012) "The effect of C-terminal membrane anchor on prion protein interactions with membranes". Prion conference, Amsterdam, The Netherlands. *Prion*, 6, supplement: 117.
5. Araman M.C, Chu K.N, Becker C.F. (2012) "Semisynthesis of posttranslationally modified PrP variants". 2nd Austrian Peptide Symposium, Vienna.
6. Chu K.N., Becker C.F. (2013) "Recombinant expression of soluble murine prion protein for C-terminal modification". *FEBS Letters*, 587, 430-435.

Curriculum vitae

Name:	Nam Ky Chu
Birthplace:	Hochiminh city, Vietnam
Date of birth:	31-07-1981
Nationality:	Vietnamese
Education	
1987-1992	Primary school in Hochiminh city, Vietnam
1992-1996	Secondary school in Hochiminh city, Vietnam
1996-1999	High school in Hochiminh city, Vietnam
July 1999	Entrance examination for National higher education
1999-2003	Bachelor of Biotechnology at University of Science, Hochiminh city, Vietnam with thesis: "Cloning and expression of envelope protein VP281 of white spot syndrome virus (WSSV) in <i>E. coli</i> " with Prof. Dr. Linh Thuoc Tran
2004-2007	Master of Microbiology at University of Science, Hochiminh city, Vietnam with thesis: "Production of human insulin from recombinant mini-proinsulin" with Prof. Dr. Linh Thuoc Tran
Sep. 2005–Jan. 2006	Collaboration work at Institute of Genetics, University of Bayreuth, Germany with project: "Display the cellulase on the surface of <i>Bacillus subtilis</i> " with Prof. Dr. Wolfgang Schumann
Sep. 2007–Apr. 2008	Exchange student (internship) at Department of Physical Biochemistry, Max Planck Institute for Molecular Physiology, Dortmund, Germany with Dr. Kirill Alexandrov with projects: "Biophysical analysis of the interaction of Rab6a GTPase with its effector p150" (JBC, 2009, 284: 2628-2635), and "Construction of protein expression system for protozoon <i>Leishmania tarentolae</i> "
June 2008	Start of Ph.D. project at Department of Chemistry, Technische Universität München, Germany under supervision of Prof. Dr. Christian F.W. Becker
Dec. 2011	Continuation of Ph.D. at the Institute of Biological Chemistry, Faculty of Chemistry, University of Vienna, Austria with Prof. Dr. Christian F.W. Becker

Acknowledgements

First and foremost I would like to express my gratitude to my supervisor, Prof. Dr. Christian Becker for giving me a good opportunity to work in his group and for his continuous support in my PhD study. His understanding, patience and encouragement helped me to overcome the challenges in my work.

I warmly thank Ms. Katja Baeuml, Dr. Manuel Brehs, Dr. Martin Haslbeck, Dr. Aleksandr Kravchuk and Dr. Diana Olschewski for their kind help and assistance throughout my PhD study.

I sincerely thank Dr. Anders Friberg, Dr. Guenter Resch, Prof. Dr. Michael Sattler and Dr. Konstantinos Tripsianes for great collaboration works and insightful discussions.

I also would like to thank all the members in Prof. Becker's group for their kind help and stimulating discussions.

Finally but importantly, I must deeply thank my parents, my wife and my sisters for their constant support, encouragement, help, sacrifice and love to me throughout the years.